Peptide Nanoparticles As CXCR4 Chemokine Receptor Antagonists

BY

YOUNGSHIM LEE
M.S., Konkuk University, Korea 2006
B.S., Konkuk University, Korea 2004

THESIS
Submitted as a partial fulfillment of the requirements
for the degree of Doctor of Philosophy in
Biochemistry and Molecular Genetics
in the Graduate College of the
University of Illinois at Chicago, 2012

Chicago, Illinois

Defense Committee:

Vadim Gaponenko, Chair and Advisor
Michael Caffrey
Xiubei Liao
Sojin Shikano
Michael E. Johnson, Medicinal Chemistry and Pharmacognosy

ACKNOWLEDGEMENTS

I would like to thank my advisor, Dr. Vadim Gaponenko, who gave me the opportunity to learn various techniques and the way how to think scientifically. This dissertation would not have been possible without the guidance and the help of him.

I would like to thank my committee members: Dr. Michael Caffrey, Dr. Xiubei Liao, Dr. Michael E. Johnson, and Dr. Sojin Shikano, for their supports and the insights they have shared.

Dr. Nadya I. Tarasova, Head of the Synthetic Biologics Core, National Cancer Institution, who is collaborator had provided samples and shared her ideas about the project.

Dr. Benjamin Ramirez helped with scheduling and maintaining the NMR facility.

Dr. Tomoyoshi Kobayashi, Research Associate Professor in the Department of Physiology and Biophysics provided actin, tropomyosin, and the troponin I inhibitory peptide.

I thank Erika Guererro, Tanmay Chavan, and Dr. Minae Kobayashi who are lab mates for their help and friendship.

I also would like to thank my family, Youngdae Yoon, Brian, and Emma for their support. I am also grateful to my parents and parents-in-law who encourage me always.

TABLE OF CONTENTS

CHAPTER **PAGE**

TABLE OF CONTENTS (continued)

CHAPTER **PAGE**

LIST OF TABLES

TABLE **PAGE**

LIST OF FIGURES

FIGURE **PAGE**

LIST OF FIGURES (continued)

FIGURE **PAGE**

LIST OF ABBREVIATIONS

ABC	ATP-binding cassette
AIDS	Acquired immune deficiency syndrom
BRET	Bioluminescence resonance energy transfer
BSA	Bovine serum albumin
cAMP	cyclic adenosine monophosphate
CAC	Critical aggregation concentration
CD	Circular dichroism
CD184	Cluster differentiation 184
CXCR4	C-X-C receptor type 4
CXCR7	C-X-C receptor type 7
DLS	Dynamic light scattering
DMSO	Dimethyl sulfoxide
DPC	Dodecylphosphocholine
DTT	Dithiothreitol
ER	Endoplasmic reticulum
EPR	Enhanced permeability and retention
FBS	Fetal bovine serum
GPCR	G-protein coupled receptor
GRP	Gastrin-releasing peptide
IC_{50}	Half maximal inhibitory concentration
HIFs	Hypoxia-inducible factors
HIV	Human immunodeficiency virus
HOBt	Hydroxybenzotriazole
HPLC	High performance liquid chromatogram

LIST OF ABBREVIATIONS (continued)

HSQC	Heteronuclear single quantum correlation
MTT	3-(4,5-Dimethylthiazol-2-yl)-2,5-diphenyltetrazolium bromide
NMP	*N*-Methyl-2-pyrrolidone
NMR	Nuclear magnetic resonance
NOE	Nuclear Overhauser effect
NOESY	Nuclear Overhauser effect spectroscopy
PBS	Phosphate buffered saline
PEG	Polyethylene glycol
PI3K	Phosphoinositide 3 kinase
PLC	Phospholipase C
PMSF	Pheylmethanesulfonyl fluoride
RMSD	Root mean square deviation
SDF-1	Stromal derived factor 1
siRNA	Small interference
TEM	Transmission electron microscopy
TFA	Trifluoroacetic acid
ThT	Thioflavin T
TIS	triisopropylsilane
TM	Transmembrane
TOCSY	Total correlation spectroscopy
TROSY	Transverse relaxation optimized spectroscopy
UV	Ultra violet
VEGF	Vascular endothelial growth factor

SUMMARY

CXCR4 is a chemokine receptor that induces cell migration upon binding its ligand CXCL12 that is also known as the stromal derived factor 1 (SDF1α). Recent studies show that CXCR4 is highly expressed in many kinds of cancer including breast cancer, prostate cancer, and lung cancer. Also, cancer cells expressing CXCR4 exhibit highly invasive and migratory behavior at the sites containing high concentration of SDF-1α. Interaction between CXCR4 and SDF-1α is crucial during metastasis. Therefore, it is possible that inhibition of this interaction may reduce metastasis.

We developed a peptide antagonist X4-2-6 against CXCR4 function. The peptide antagonist is able to bind specifically to its target CXCR4 and to prolong survival in a mouse breast cancer dissipation model. This suggests that the peptide does not only have an anti-cancer therapeutic effect but also possesses low toxicity. The X4-2-6 peptide antagonist requires SDF-1α to inhibit CXCR4 downstream signal transduction. This requirement is expected to reduce toxicity further because the peptide interacts only with CXCR4 that is activated by SDF-1α. Moreover X4-2-6 peptide is able to form spherical nanoparticles that have high proteolytic stability due to strong intermolecular interactions within nanoparticles. Thus, X4-2-6 nanoparticles can be targeted to and accumulated in the tumor tissue passively mainly due to the long half-life time of the peptide antagonist and the enhanced permeability and retention effect (EPR) of solid tumors. We observed that nude mice developed metastatic cancer by injection of MDA-MB-231 breast cancer cells and died rapidly. However, the animals that were treated with X4-2-6 nanoparticles survived much longer. *In vivo* mice experiments proved that X4-2-6 nanoparticles have potential to be used as therapeutics for the cancer treatment.

We also found an interesting mechanism of peptide self-assembly by studying the monomer structure of X4-2-6 peptide derivatives. The X4-2-9 peptide has identical primary structure to that of X4-2-6 except the first two leucine residues. However, the X4-2-9 peptide is assembled into fibrils. In order to understand mechanism, we determined monomer structure of both peptides by NMR techniques and found that the initial intermolecular contacts between monomers of different topology are important for self-assembly. We found that monomer structure of X4-2-1, nonPEGylated form of X4-2-6 adopts a conical shape of hairpin-like structure while X4-2-9 is cylindrical hairpin-like structure. The difference in overall shape of monomers may be the reason for the preference in the final morphology. We suggest that the conical shape of monomeric subunits defines the preference for assembly of spherical nanoparticles and cylindrical monomers assemble into fibers.

Furthermore, I used the reductive methylation technique to study the extremely large size of protein complex, which consists of actin, tropomyosin, and the inhibitory peptide derived from the inhibitory subunit of cardiac troponin. The reductively methylated lysines on actin filaments are detectable by NMR due reduced order parameters of lysine side chains and make it possible to observe conformational changes upon addition of tropomyosin and/or the inhibitory peptide. The reductive methylation followed by NMR is a good tool to study protein-protein interactions regardless of molecular weight of proteins.

CHAPTER 1.

PEPTIDE NANOPARTICLES AS CXCR4 CHEMOKINE RECEPTOR ANTAGONISTS

I. INTRODUCTION AND BACKGROUND

1.1. CXCR4 chemokine receptor and SDF-1

C-X-C chemokine receptor type 4 (CXCR4) also known as fusin or CD184 (cluster of differentiation 184) is a receptor specific for stromal derived factor 1 (SDF-1 or also called CXCL12). Although most chemokine receptors interact with more than one chemokine and chemokines tend to bind to multiple receptors, it is known that the CXCL12 binds to the CXCR4 and CXCR7 (*1-3*). SDF-1, ligand of CXCR4 is known to be crucial in hematopoietic stem cell homing to the bone marrow. SDF-1 has two isoforms, SDF-1α and SDF-1β formed by alternate splicing of the same gene (*4*). Full lenth of SDF-1α (residues 1-68) is cleaved to produce functional SDF-1α (residues 3-67) while SDF-1β (residues 1-72) is modified to generate SDF-1β (residues 3-72) by proteolytic processing in the serum. The modified SDF-1β has additional five residues in the C-terminal as compared to SDF-1α. SDF-1α is the predominant and ubiquitously expressed splicing variant. SDF-1 is constitutively expressed in several organs including lung, liver, skeletal muscle, brain, kidney, heart, skin, and bone marrow (*5-8*). CXCR4 is widely expressed on hematopoietic cells including T-lymphocytes, B-lymphocytes, monocytes and macrophages, and neutrophils. CXCR4 expression is also found in brain, lung, colon, heart, kidney, and liver. The cells expressed functional CXCR4 migrate toward SDF-1 gradients. The binding of SDF-1 to CXCR4 initiates divergent signaling pathways downstream of ligand binding which can result in a variety of responses such as cell migration, cell survival and proliferation, increase intracellular calcium, and gene transcription. CXCR4 is coupled to heterotrimeric G-protein for signal transduction. It is known that primarily $G\alpha_i$ is coupled to CXCR4 resulting in inhibition of adenylyl cyclase and intracellular calcium flux is increased upon CXCR4 activation by ligand stimulation. This calcium flux can be readily measured and is

frequently used as a measure of chemokine activity. CXCR4 activation by interaction with SDF-1 induces phosphoinositide 3 kinase (PI3K) and phospholipase C (PLC) through $G_{\beta\gamma}$ subunits leading to Rac and Rho activation that regulate actin cytoskeletal organization (*9*). PI3K also can activate serine-threonine kinase Akt, which plays a key role in tumor cell survival, and possibly proliferation (*9*). It has been reported that the chemokine receptors including CXCR4 are constitutively hetero- or homodimerized (*10-12*). It also has been published that small antagonist of CXCR4, AMD3100 decrease bioluminescence resonance energy transfer (BRET) signal of CXCR4 homodimer (*13*). Although the functional importance of dimerization is not characterized completely, a considerable amount of data suggests that it is important in vivo pharmacological effects (*14, 15*).

Initial investigations of CXCR4 receptor focused on its role in pathogenesis of human immune deficiency virus (HIV) infection. CXCR4 acts as a co-receptor with CD4 to allow HIV to infect host cells (*16*). Although most of the HIV strains use CCR5 macrophage tropic chemokine receptor for cell entry, more virulent mutant strains instead utilize the CXCR4 receptor (*17, 18*). The discovery of the CXCR4 portal for HIV infection generated a great interest in developing CXCR4 antagonists as anti-AIDS pharmaceutical agents. Despite considerable effort to discover small molecule inhibitors of CXCR4 the progress has been slow in this area presumably because of the lack sufficient knowledge about the interactions between the receptor and its ligand. However, several promising CXCR4 antagonists have been developed. AMD3100 is a bicyclam compound that is a potent inhibitor of CXCR4. AMD3100 was found to be effective against HIV-1 and HIV-2 viral replication (*19*).

Recently, much research was performed to show that CXCR4 is the most common chemokine receptor expressed in diverse human cancers including breast cancer, colon cancer,

lung cancer, and prostate cancer (*20-24*). In tumor tissue, hypoxia-inducible factors (HIFs) induce CXCR4 expression and cancer cell invasion (*25-27*). The CXCL12/CXCR4 axis is involved in several aspects of tumor progression including angiogenesis, metastasis, and survival (*28-30*). In addition, it is shown that CXCR4 is expressed by breast cancer cells in a nonrandom manner and neutralization of CXCR4 by its antibodies inhibits metastasis in an animal model [6]. Anti-metastatic activity of AMD3100 and a 14-amino acid long peptide inhibitor of CXCR4 T140 has been demonstrated in cancer cell lines as well as in animal models (*31-34*). Other CXCR4 antagonists (18-amino acid long peptide T22, T134, and ALX40-4C) have been investigated for anti-HIV activity (*35-38*). Anti-CXCR4 monoclonal antibodies abate proliferation of non-Hodgkin's lymphoma cells, and metastasis of breast cancer cells (*6, 39*). Inhibition of CXCR4 by small interference RNA (siRNA) prevents metastasis of grafted breast cancer cells in a mouse model and reduces glioma and breast cancer cell invasion in *in vitro* assays (*40, 41*). Although CXCR4 is an excellent drug target, inhibition of this chemokine receptor may cause long-term immune system side effects. The use of functionalized nanoparticles capable of targeting of CXCR4 inhibitors to tumor cells can alleviate this potential problem.

1.2. Nanotechnology and cancer research

Nanotechnology has shown promising applications from diagnosis to treatment of various types of diseases including cancer (*42*). As the drug delivery system, nano-sized materials such as liposomes and polymer-based particles have been approved by the US Food and Drug Administration. For examples, Abraxane is an albumin bound chemotherapy drug paclitaxel and Doxil is made of liposome and encapsulated strong anticancer drug doxorubicin (*43-46*). Many more nano-sized materials are undergoing clinical trials. Compared to using a small drug by

itself, drug bound or conjugated to a nanoscale delivery system has some significant advantages. Nano-sized materials diffuse and accumulate at specific sites in the body showing excessively leaky microvasculature. Particularly, solid tumor tissues usually show enhanced permeability and retention (EPR) effects due to active angiogenesis (*47*). The EPR effects allow macromolecules and other large molecules which are not penetrating normal endothelial cells to selectively increase their transport from the blood vessels to the tumor tissues. The ability of targeting specific tissues is increased by incorporation of a ligand specific for the receptor or epitope of the target tissue to the surface of nano-sized carrier (*48, 49*). Another advantage of nanoscale drug carriers is in their low toxicity because of specific targeting and biocompatibility of nanoparticles. Nano-sized drug carriers increase the time of circulation in the bloodstream whereas small size drugs are easily excreted through the renal filtration system (*50, 51*). The liposomal formulation of doxorubicin resulted in significantly increased circulation half-life of doxorubicin from 10 miniutes to 50 hours (*52*). The controlled release of drugs is possible because of the stable structure of the nanoparticles. Moreover, high concentrations of drug molecules can be encapsulated or incorporated into nanoparticles. However, it has been challenging to design nanoparticles with desirable size and morphology. Although there are many attempts to understand mechanism of assembly, there has been little success so far.

1.3. Peptide nanoparticles

Peptide therapeutics has several attractive features for anticancer treatments compared to current small drug molecules. Since peptides provide high specificity, nonspecific binding to molecular structures is reduced resulting in lower toxicity. An important disadvantage is that most peptides are quickly degraded and cleared from the body and need to be re-injected. In recent years several attempts have been made to increase the bioavailability of peptides by

modifications such as glycosylation or attachment of polyethylene glycol (PEG) (*53, 54*), and encapsulation into liposomes or nanoparticles (*55-57*). Another way to overcome disadvantages of peptide drugs is designing self-assembled nanoparticles using the peptides that have an active function because peptides offer chemical and biological diversity. There are many reports showing that a variety of nanostructures may be designed from peptide building blocks such as hydrogels, fibers, vesicles, and nanotubes (*56, 58, 59*). It is possible that nanoparticles made of peptides will have better protection from the proteolysis attack due to less solvent exposure and strong interactions between peptide building blocks.

II. SELF-ASSEMBLY OF NANOPARTICLES

2.1. Introduction

Nanoscale technologies are changing the methods of diagnostics and treatment of human disease (*60, 61*). Among known nanoscale devices, peptide-based nanoparticles represent an emerging group of therapeutic agents, drug delivery vehicles, tissue-engineering materials, and nanowires. The advantages of peptide-based nanostructures include biodegradability, versatility of design, and ease of synthetic functionalization. Despite the growing interest in peptide-based nanostructures, there are no guidelines for their design and optimization.

One intriguing property of peptide-based nanoparticles is their ability to self-assemble. Complex structures can be built out of many simple units with minimal manufacturing interference. For pharmaceutical applications nanoparticles that are uniform in size are more desirable, especially if they are designed for drug delivery where uniform loading of the nanoshells with medication is important. Conversely, fibrous peptide assemblies may be employed for tissue engineering.

We recently discovered that peptides corresponding to transmembrane helices assemble into nanoparticles in aqueous solutions (*62*). In the case of CXCR4 chemokine receptor, peptides derived from the second transmembrane helix, X4-2-6 form uniform spherical nanoparticles that have intrinsic biological activity that will be discussed in the next section under the title **III. BIOLOGICAL ACTIVITY OF X4-2-6 NAOPARTICLES**. Surprisingly, a peptide just two amino acid residues shorter than X4-2-6, X4-2-9 assembles into nanofibers. The differences in the shape of nanoparticles formed by X4-2-6 and X4-2-9 peptides are confirmed by transmission electron microscopy and dynamic light scattering in solution. In order to

investigate molecular mechanisms that define the ability of these peptides to form such different molecular assemblies, we undertook structural and biophysical comparison of the two peptides. We find that although X4-2-6 and X4-2-9 have almost identical amino acid sequences, their monomeric structures of the peptide region differ significantly. While X4-2-1, the non-PEGylated form of X4-2-6, exhibits a conical topology, the X4-2-9 peptide has a cylindrical structure. It is known that conical lipids assemble into micelles, while cylindrical lipids form bilayers (*63*). Our results suggest that peptide nanoassembly may follow similar rules to those governing aggregation of lipids. In addition, we address the question of differential stability of spherical and fibrous peptide assemblies against proteolytic degradation. Due to more extensive intermolecular interactions the spherical X4-2-6 nanoparticles are less susceptible to proteolysis than X4-2-9 fibers. Proteolysis in the blood stream commonly prevents development of peptides into therapeutic agents. Therefore, knowledge of which peptide assembly is more efficient in abating proteolytic degradation is highly desirable.

2.2. Materials and methods

2.2.1. Peptide synthesis

Peptide were synthesized by solid phase peptide synthesis on 433A Applied Biosystems Peptide Synthesizer equipped with conductivity monitoring unit utilizing Fmoc amino acid derivatives. Since all peptides contain Asp residues that are prompt to aspartamide formation upon piperidine treatment during deprotection, the synthesizer was reprogrammed to use 50 % piperidine in *N*-Methyl-2-pyrrolidone (NMP) containing 0.25 M hydroxybenzotriazole (HOBt). Solvent delivery times were calibrated to achieve final concentration of HOBt of 0.1 M during deprotection. Addition of HOBt completely prevented aspartimide formation that is usually

accompanied by appearance of products with -18 and +60 (piperidine additive) molecular masses on mass spectra. Peptides were cleaved from the resin with 87.5 % trifluoroacetic acid containing 5 % water, 5 % thioanisol and 2.5 % triisopropylsilane (TIS), precipitated with cold diethyl ether, washed five times with ether and dried in vacuum overnight. Peptides dissolved in dimethylformamide were purified by high-performance liquid chromatography (HPLC) on a preparative (19 x 250 mm) Atlantis C3 reverse phase column (Agilent, Palo Alto, CA) in a gradient of 0.05 % trifluoroacetic acid in water and acetonitril containing 0.05 % trifluoroacetic acid. Only fractions containing more than 95 % pure product were combined and freeze-dried. The purity and structure were further confirmed by ion-spray LC/MS with separation on Zorbax C3 analytical column.

2.2.2. Dynamic Light Scattering (DLS)

The peptide solutions in phosphate buffered saline (PBS), pH 7.2, were prepared from 32 mg⁄ml stock solutions of peptides in dimethyl sulfoxide (DMSO). The final concentration of DMSO in all samples was 1.25 % (v⁄v). The solutions were sonicated for 10 min and left at ambient temperature overnight. The samples were spun at 9740 × g for 10 min and analyzed by dynamic light scattering (DLS) on a DynaPro Titan instrument equipped with Temperature-Controlled Micro-Sampler (Wyatt Technology Corp.) at a laser wavelength of 830 nm. To obtain the hydrodynamic radii, the intensity autocorrelation functions were analyzed by "Dynamics 6.7.7.9." software (Wyatt). For data analysis, viscosity, and refractive index values for a solution of 1.25% DMSO in water (v⁄v) were calculated using data from Nieto-Draghi *et al*. (*64*) and Viggiano *et al*. (*65*).

2.2.3. Transmission Electron Microscopy (TEM)

The peptides were dissolved in DMSO at concentration of 50 mg/ml and diluted into PBS (pH 7.2) to yield 1.25 mg/ml solution. The solutions were vortexed at maximum speed and sonicated at maximum intensity for 10 min. The samples were incubated at room temperature overnight. 2 µl of a sample was applied directly on a microscopy grid, air-dried, stained with 0.5 % (w/v) uranyl acetate, and visualized using either a Tecnai 12 transmission electron microscope (FEI Company, OR) or a Hitachi H-7000 electron microscope equipped with a digital camera system (Gatan, Inc.).

2.2.4. Nuclear Magnetic Resonance (NMR) experiments

The ^{1}H-^{13}C heteronuclear single quantum correlation (HSQC) NMR experiments were performed on 600 and 800 MHz Bruker Avance spectrometers equipped with cryogenic probes. All experiments were carried out at 25 ºC. The peptides were dissolved in DMSO-d_6. The peptide resonance assignments were performed using homonuclear total correlation spectroscopy (TOCSY) and nuclear Overhauser effect spectroscopy (NOESY) experiments with mixing times of 70 ms and 500 ms, respectively. The zero-filling and sine-bell window function was applied to both direct and indirect dimensions prior to Fourier transformation. A linear prediction was applied to the data in the indirect dimension. All data were processed and analyzed using NMRPipe and Sparky, respectively (*66*).

2.2.5. Peptide structure calculations

NOEs and dihedral angles were used for structure calculations. NOEs were classified as strong, medium, or weak corresponding to distance restraints of 1.8-2.5, 1.8-3.5, 1.8-6.0, and 1.8-7.0 Å (for methyl NOEs), respectively. The distance restraints were derived from cross-peak volumes calibrated against the H_{ε}-H_{ζ} interproton distance (2.45Å) of Trp18. Dihedral angle

restraints were acquired from the analysis of chemical shift index for $^{13}C_{\alpha}$ and $^{13}C_{\beta}$ using TALOS software (*67*). The initial 100 structures were generated using CNS 1.1 (*68*). Twenty structures with the lowest energy, showing the least violation of restraints, were selected among initial structures. The structure analysis was carried out using MOLMOL to identify violations of NOE and dihedral angle restraints and to superimpose structures and measure RMSD (*69*).

2.2.6. Determination of β-sheet formation in assemblies of X4-2-6 and X4-2-9

The environmental-sensitive fluorescence dye Thioflavin T (ThT) was used to determine the appearance of β-sheet structure upon assembly of X4-2-6 and X4-2-9. ThT was dissolved in hot PBS to make 28.14 μM stock solutions. The 0.8 mg/ml solutions of X4-2-6 and X4-2-9 peptide were diluted with PBS to vary the concentration of nanoparticles. The peptide solutions were mixed with the ThT stock solution resulting in a final ThT concentration for all solutions was 13.69 μM determined by UV-vis. Fluorescence measurements were performed on a steady-state fluorescence spectroscopy instrument. The fluorescence emission and excitation spectra were recorded at 25 ^{o}C on a single photon counting spectrofluorometer FluoroMax-2 from Jobin Yvon HORIBA – SPEX (Edison, NJ) using a 1 mm path quartz cell. The excitation and emission monochromator slits were set to 7 and 10 nm band width. The values of ThT fluorescence intensity were obtained by performing emission scans from 455 to 600 nm when excited at 440 nm and excitation scans from 350 to 470 nm for fixed emission at 482 nm. An extinction coefficient: E^{mM} = 26.6 at 412 nm in PBS was used to determine the concentration of the dye in the final probe.

2.2.7. Determination of peptide stability against proteolytic degradation

We incubated 2 mg/ml X4-2-6 nanospheres and X4-2-9 fibrils with equal volume of bovine serum (Invitrogen, Carlsbad, CA) at 37°C. During the incubation, 50 µl aliquots were taken every hour. All samples were assayed on a coupled Xcalibur HPLC-MS system. The peptide molecular weight was determined using mass spectrometry, while the A280 absorbance was measured by an HPLC UV detector. The extinction coefficients for X4-2-6 and X4-2-9 are identical.

2.2.8. Peptide degradation by proteinase K

The 2 mg/ml X4-2-6 and X4-2-9 peptide nanoparticles were incubated with 0.4 mg/ml proteinase K at a molar ratio of 1:1000 (proteinase K: peptide nanoparticles) at 37˚C. The 50 µl aliquots were taken at various time points from 0 to 3 hours and phenylmethanesulphonyl fluoride (PMSF) was added to a final concentration of 5 mM to quench the proteinase K activity. All samples were stored on dry ice until further analysis by HPLC.

2.2.9. HPLC analysis

A Shimadzu Prominence HPLC system with UV/vis photodiode array detector was used for analysis of peptide degradation. A Shimadzu C18 reverse-phase column (50 mm × 4.5 mm) was equilibrated with 0.1 % of trifluoroacetic acid (TFA). The sample injection volume was 5 µl. The peptide was eluted with a linear gradient of 90% acetonitrile containing 0.1 % TFA. The amount of non-degraded peptide was estimated by measuring peak area at 280 nm.

2.2.10. Determination of critical aggregation concentration

To determine the critical aggregation concentration (CAC) a fluorescence probe pyrene was used. Pyrene was dissolved in 100% ethanol to make 2 mM stock solution because of its

low solubility in water. The 4 mg/ml solutions of X4-2-6 and X4-2-9 peptide nanoparticles were diluted with PBS to vary the concentration of nanoparticles. The peptide solutions were mixed with the pyrene stock solution resulting in a final pyrene concentration of 1 μM. The mixtures were incubated overnight at room temperature. Fluorescence measurements were performed on a PTI Quantamaster instrument at 25 °C. All experiments were carried out in quartz cuvettes using 1200 μl of peptide and pyrene mixture. The excitation profile was scanned from 315 to 360 nm when the emission was set to 390 nm. The slits for excitation and emission set to 2 nm and 2.5 nm, respectively.

2.3 Results

2.3.1. Nomenclature and self-assembling ability of synthetic peptides

Earlier studies have shown analogs of the second transmembrane helix of chemokine receptors to have potent and selective antagonistic effects on the corresponding receptor (*70*). Several peptides were selected for detailed studies of peptide self-assembly (TABLE I). TEM studies revealed assembly of transmembrane peptides, X4-2-1, into uniform round nanoparticles. The particles, however, tend to aggregate, forming string-like structures (Figure 1A). To prevent this nanoparticle superaggregation, the original X4-2-1 sequence was augmented with polyethyleneglycol (PEG) extensions of different lengths at the C-terminus. Addition of 27 monomeric units of PEG (X4-2-6, TABLE I) was sufficient to prevent superaggregation without interfering with self-assembly (Figure 1 D and E). To investigate the structural requirements for nanoparticle assembly, variants of the X4-2-6-1 peptide were synthesized and tested by DLS and TEM for their ability to form nanoparticles. Substitution of two C-terminal negatively charged

TABLE I

THE NOMENCLATURE OF CXCR4 TM2 DERIVED PEPTIDES AND THEIR SEQUENCES

Peptide	Primary structure
X4-2-1	LLFVITLPFWAVDAVANWYFGNDD-OH
X4-2-2	LLFVITLPFWAVDAVANWYFGNKK-NH_2
X4-2-3	LLFVITLPFWAVDAVANWYFGN-OH
X4-2-4	LLFVITLPFWAVDAVANWYFGNDD-$(CH_2CH_2O)_{11}$-NH_2
X4-2-5	LLFVITLPFWAVDAVANWYFGN-$(CH_2CH_2O)_{27}$-NH_2
X4-2-6	LLFVITLPFWAVDAVANWYFGNDD-$(CH_2CH_2O)_{27}$-NH_2
X4-2-8	AAVANWYFGNDD-$(CH_2CH_2O)_{11}$-NH_2
X4-2-9	FVITLPFWAVDAVANWYFGNDD-$(CH_2CH_2O)_{11}$-NH_2
X4-2-11	LLFVITLPFWAVDAVANWYFGNDD-$(CH_2CH_2O)_{27}$-CO-NH- $(CH_2CH_2O)_{11}$-NH_2

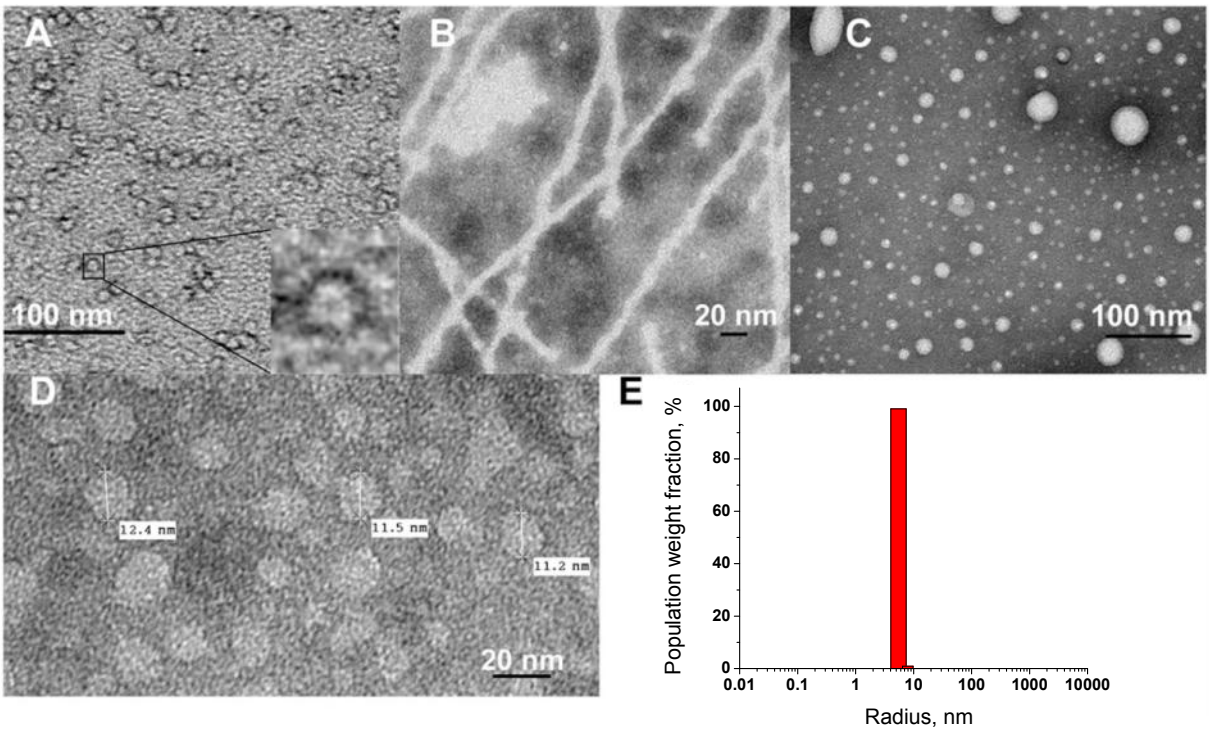

Figure 1. Self-assembly of analogs of the CXCR4 second transmembrane helix.
(A) Transmission electron microscopy of self-assembled X4-2-1 (LLFVITLPFWAVDAVANW-YFGNDD). (B) X4-2-9 (FVITLPFWAVDAVANWYFGNDD-$(CH_2CH_2O)_{27}$-NH_2), just two residues shorter than X4-2-6, self-assembles into fibrils. (C) X4-2-2 (LLFVITLPFWA-VDAVANWYFGNKK) assembled into nonuniform nanostructures. (D) Transmission electron microscopy of X4-2-6 (LLFVITLPFWAVDAVANWYFGNDD-PEG_{27}). (E) Dynamic light scattering of X4-2-6, 0.4 mg⁄ml in PBS reveals remarkable size homogeneity. These experiments were done by a collaborator, Nadya I. Tarasova.

aspartates of X4-2-1 with two positively charged lysine residues (X4-2-2, TABLE I) resulted in aggregates that were very heterogeneous in size (Figure 1C). X4-2-1 analog without two C-terminal aspartates (X4-2-3) had poor solubility and showed strong tendency to form super aggregates (TABLE I). X4-2-3 derivative with PEG-27 on the C-terminus, X4-2-5 (TABLE I) did form nanoparticles. However, they were more heterogeneous than the ones formed by the peptides with negative charges, X4-2-6. To test the importance of the N-terminal residues for nanoparticle assembly, N-terminal truncation mutants of the X4-2-6 peptide (X4-2-8, X4-2-9, and X4-2-10) were constructed (TABLE I). Unexpectedly, removal of two N-terminal leucine residues (X4-2-9) resulted in the formation of fibrils instead of round particles (Figure 1B), suggesting that these particular residues may be instrumental in nanoparticle assembly. Truncation of the peptide by twelve amino acids (X4-2-8) produced a peptide that did not self-assemble at concentrations as high as 10 mg⁄ml. CXCR4 TM2 analogs with additions of 27 or more monomeric units of PEG showed remarkable size homogeneity (Figure 1 D and E). The size of the particles showed no dependence on peptide concentration in 0.05–0.4 mg⁄ml concentration range (Figure 2). DLS revealed that nanoparticles formed by both peptides had unchanged apparent radii and dispersity for 21 d when stored at room temperature. Interestingly, peptide elongated with an additional PEG block consisting of 11 monomeric units (38 units in total), X4-2-11 (TABLE 1) started aggregating much sooner, just in 8 days (Figure 3). When kept at 37 °C, self-assembled X4-2-6 showed no changes for at least 48 hours (Figure 3), suggesting that nanoparticles remain intact at temperature conditions of biological assays.

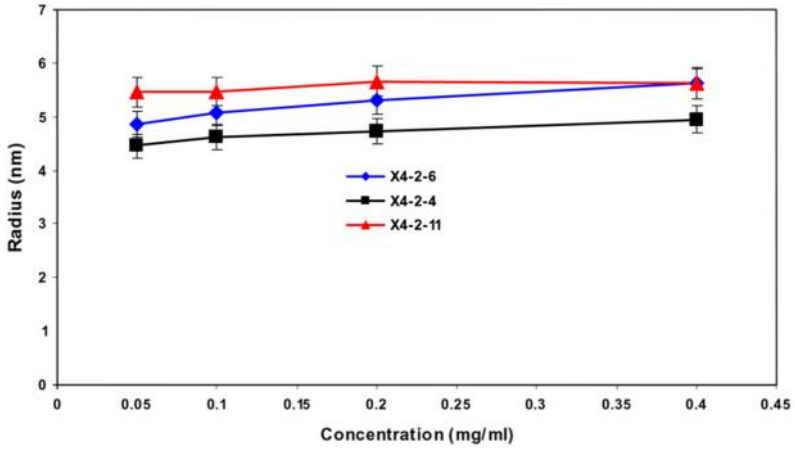

Figure 2. The size of the nanoparticles in different peptide concentration.
The radii were determined by dynamic light scattering. The size of the X4-2-6, X4-2-4 and X4-2-11 nanoparticles was independent of peptide concentration in 0.05–0.4 mg⁄ml range. The experiments were done by Nadya I. Tarasova.

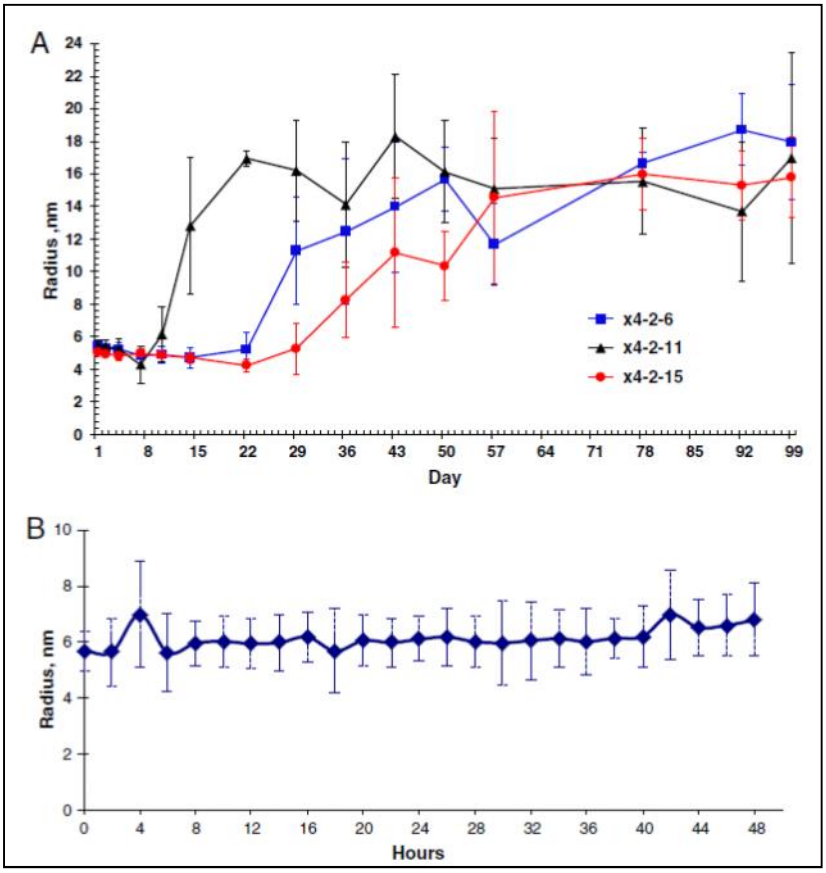

Figure 3. Structural stability of nanoparticles as a function of time.
The radii and size distributions were determined by dynamic light scattering for 0.4 mg⁄ml solutions of peptides in PBS containing 1.25 % (v⁄v) DMSO (A) Stability upon incubation at room temperature; (B) Stability of X4-2-6 nanoparticles at 37 °C. The experiments were done by Nadya I. Tarasova.

2.3.2. Proteolytic stability of nanoparticles

Since the X4-2-6 and X4-2-9 peptides may have therapeutic value as inhibitors of CXCR4, it is important to determine if the type of peptide assembly correlates with the degree of protection against proteolysis by serum proteases. The half-life of self-assembled X4-2-6 in bovine serum was 9 h (Figure 4). Truncated version of X4-2-6 that forms fibrils, X4-2-9 is less stable in serum and has a half-life of less than 2.5 h (Figure 4). Increased degradation rates correlate with reduced stability of X4-2-9 self-assembling structure. By studying X4-2-6 and X4-2-9 stability in bovine serum we were able to uncover significant differences in protection from proteolysis in these peptides. However, since serum contains a mixture of proteases and the tested peptides do not have identical amino acid sequences, the possible differences in half-life values for the two peptides may also be interpreted in terms of preferential recognition of X4-2-6 and X4-2-9 by distinct proteases that differ in abundance in serum. To address this potential issue we performed a peptide degradation assay with 2 mg/ml of either X4-2-6 or X4-2-9 and purified proteinase K. The results of this experiment are shown in Figure 5. The results of the peptide degradation assay demonstrate that X4-2-6 peptide within spherical nanospheres with the half-life time of 11.8 ± 1.8 min is significantly more protected against proteolysis by proteinase K than the X4-2-9 peptide within fibrils (2.9 ± 1.2 min).

2.3.3. Structure determination of X4-2-1 and X4-2-9 peptide monomers

The amino acid sequences of X4-2-1, X4-2-6 and X4-2-9 peptides shown in Figure 6A are very similar. X4-2-6 and X4-2-9 peptides have identical primary structures, except the two N-terminal leucines are lacking in the structure of X4-2-9. Interestingly, X4-2-1 and X4-2-6 peptides self-assemble into nanospheres 10 nm in diameter, while the truncated version of the

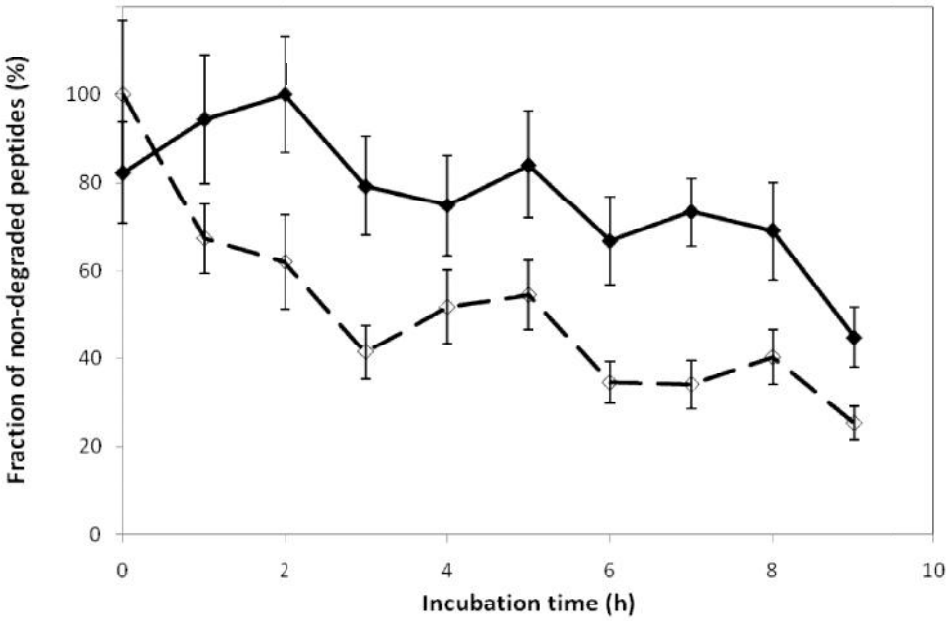

Figure 4. Proteolytic stability of X4-2-6 and X4-2-9 peptides in fetal bovine serum.
The fractions of not degraded X4-2-6 (♦, filled diamonds) and x4-2-9 (◊, open diamonds) were determined by HPLC-MS and plotted versus time of the experiment. The errors were determined by analysis of three peaks representing differentially charged peptides.

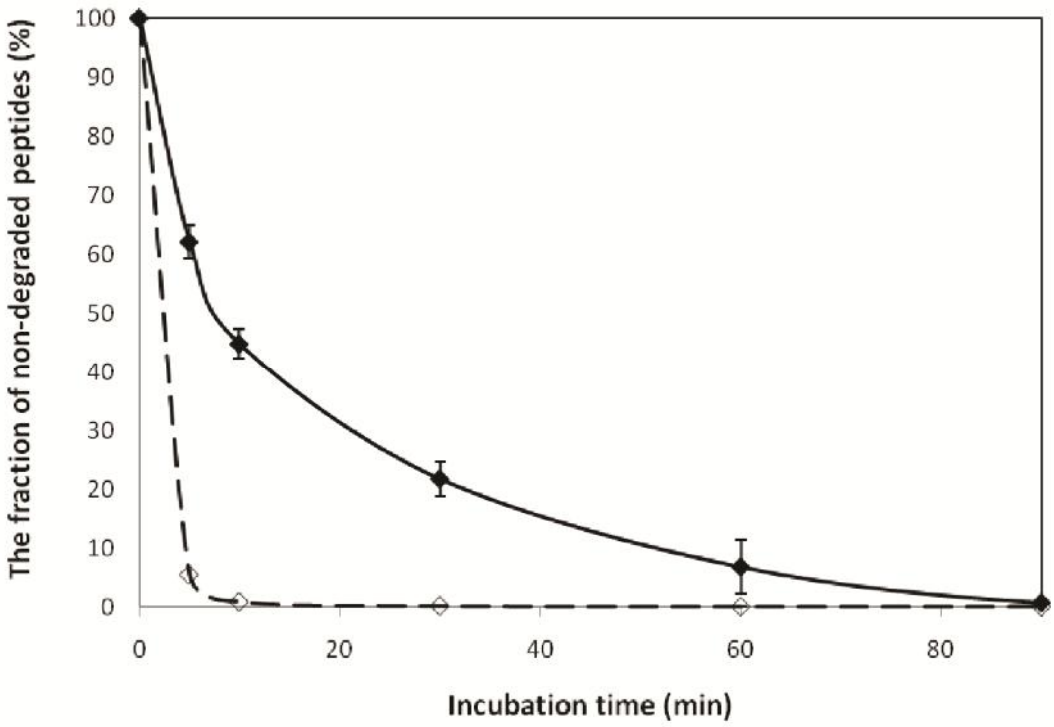

Figure 5. Time course of 2 mg/ml of X4-2-6 (♦, filled diamonds) and X4-2-9 (◊, open diamonds) peptide degradation in PBS, pH 7.1 by proteinase K.

The reaction was stopped after defined time intervals by addition of 5 mM PMSF (proteinase K inhibitor) after incubation. All experiments were carried out at 37 °C and repeated three times for statistical analysis. Spherical nanoparticles (X4-2-6) showed better protection from proteolysis than fibrils (X4-2-9).

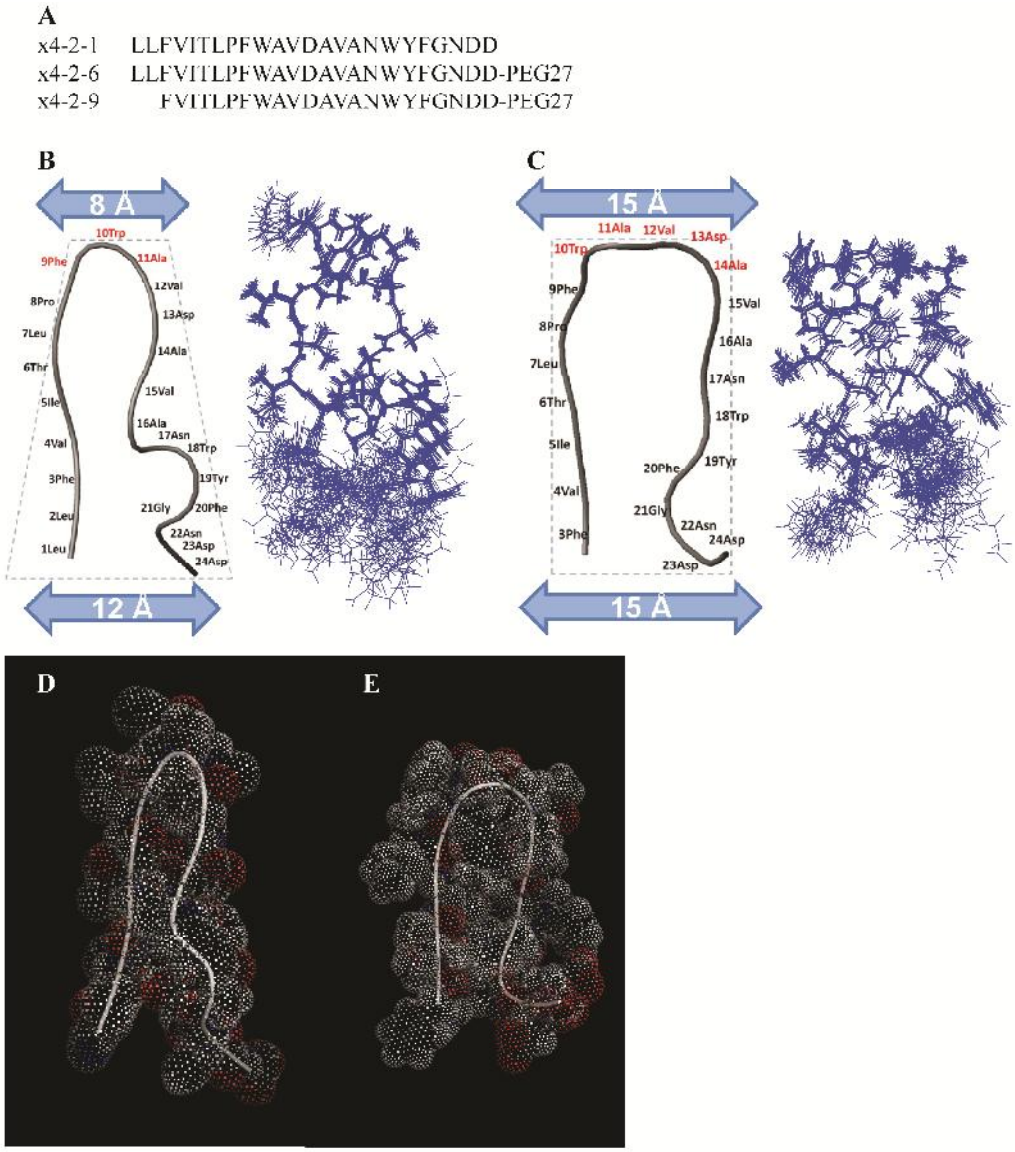

Figure 6. Structural characterization of X4-2-1, X4-2-6, and X4-2-9 peptides.
(A) Amino acid sequences of X4-2-6 and X4-2-9 peptides differ by only two N-terminal residues. Comparison of average structures of X4-2-1 (B) and X4-2-9 (C) shows differences in the overall topology of peptide monomers. The width of the head and the base of the hairpin structures were measured. Residues involved in the head region are shown in red. The dotted outline shows the conical shape of X4-2-1 structure and the cylindrical shape of X4-2-9 structure. The blue bars represent the widths of the head and the base of X4-2-1 and X4-2-9 hairpins. The space filling models of average X4-2-1 and X4-2-9 structures is shown in (D) and (E), respectively.

peptide lacking two N-terminal Leu residues, X4-2-9 forms fibrils using TEM and DLS (*62*). To better understand the mechanisms defining the architecture of the self-assembled aggregates we studied structures of X4-2-1, X4-2-6 and X4-2-9 monomers in DMSO-d_6 by NMR. DMSO is known to interfere with peptide aggregation without disrupting its tertiary structure (*71*). DMSO is relevant to our studies because the assembly of X4-2-1, X4-2-6, and X4-2-9 is initiated in a highly concentrated DMSO solution phase, since dissolving solid peptides directly in an aqueous buffer produces amorphous aggregates instead of ordered assemblies. We initially solved the structure of X4-2-1 without the C-terminal PEG moiety that is present in X4-2-6. The PEG extension was added to prevent superaggregation in the aqueous solution. We recorded a ^{1}H-^{13}C HSQC spectrum of X4-2-6 peptide and compared it to the ^{1}H-^{13}C HSQC spectrum of X4-2-1 (Figure 7 and 8). The only changes in chemical shifts were observed in the vicinity of the PEG moiety. Since no significant changes in chemical shifts were observed in the rest of the peptide molecule, we assumed that the peptide structure with PEG is similar to the structure without PEG.

NMR chemical shift assignment for the X4-2-1 peptide was completed. The assignment is shown in TABLE II. The peptide sequence was confirmed by sequential NOEs between α protons of *i* and amide protons of *i+1*. For the structure calculations, 167 NOE restraints including 25 long-range NOEs and 33 dihedral angle restraints were used. The structural topology of monomeric X4-2-1 is a hairpin with two tight helix-like turns in the C-terminus (Figure 6B). Most of the residues in the hairpin structure (71%) exhibit a β-strand conformation, as evidenced by analysis of the distribution of ψ-dihedral angels in the Ramachandran plot (Figure 9). The backbone and heavy atom root mean square deviation (RMSD) values calculated

TABLE II

CHEMICAL SHIFT ASSIGNMENT OF X4-2-1

	HN	$H(C)_{\alpha}$		$H(C)_{\beta}$		$H(C)_{others}$
1L	n.o.	3.483	(51.47)	1.367/1.347	(41.57)	γ:1.5725(23.83); δ1:0.831(23.02); δ2:0.802(21.73)
2L	8.278	4.287	(50.93)	1.365	(41.21)	γ:1.503(24.08); δ1:0.83(23.05); δ2:0.800(21.73)
3F	8.093	4.555	(53.5)	2.784/2.988	(37.07)	δ:7.168(129.01); ε:7.193(128.0); ζ:7.14(126.2)
4V	7.871	4.191	(57.68)	1.922	(30.77)	γ1:0.773(18.01); γ2:0.785(19.19)
5I	7.972	4.232	(56.92)	1.715	(36.41)	γ3:1.057(24.35); γ2:1.4(23.84); δ:0.773(10.98)
6T	7.785	4.202	(57.71)	3.932	(66.61)	γ:0.9666(19.7)
7L	7.753	4.494	(48.84)	1.313/1.391	(40.09)	γ:1.58(23.83); δ1:0.794(29.25); δ2:0.798(21.71)
8P	-	4.213	(59.49)	1.578/1.836	(28.74)	γ:1.712(24.42); δ3.527/3.363(46.84)
9F	7.876	4.319	(54.37)	2.781/2.921	(36.98)	δ:7.113(129.09); ε:7.193(128.0); ζ:7.14(126.2)
10W	7.865	4.509	(53.26)	2.988/3.106	(27.46)	δ:7.115(123.48); ε:7.52(118.33); ζ2:7.304(111.2); ζ3:6.944(118.27); η2:7.036(120.82)
11A	8.043	4.308	(48.48)	1.163	(17.63)	-
12V	7.714	4.153	(57.7)	1.929	(30.61)	γ1:0.788(15.3); γ2:0.777(17.88)
13D	8.11	4.496	(49.91)	2.495/2.549	(37.07)	-
14A	8.171	4.201	(48.98)	1.215	(17.71)	-
15V	7.959	3.985	(58.79)	2.025	(29.89)	γ1:0.805(18.52); γ2:0.796(19.19)
16A	8.187	4.094	(49.01)	1.155	(17.24)	-
17N	8.000	4.477	(50.18)	2.476	(36.75)	δ:7.579
18W	8.029	4.316	(54.28)	2.847/3.0	(27.1)	δ:7.024(123.42); ε:7.409(118.0); ζ2:7.289(111.2); ζ3:76.90(118.22); η2:7.008(120.75)
19Y	7.933	4.251	(55.02)	2.611/2.755	(36.38)	δ:6.917(130.094); ε:6.593(116.764)
20F	7.958	4.443	(54.29)	2.808/3.051	(37.22)	δ:7.212(129.09); ε:7.193(128.0); ζ:7.14(126.2)
21G	7.981	3.696	(42.09)	-	-	-
22N	8.091	4.552	(49.69)	2.394/2.551	(37.01)	δ:7.385
23D	7.695	4.129	(48.9)	2.37/2.521	(39.39)	-
24D	n.o.	4.131	(48.98)	2.37/2.521	(39.39)	-

n.o. means not observed.

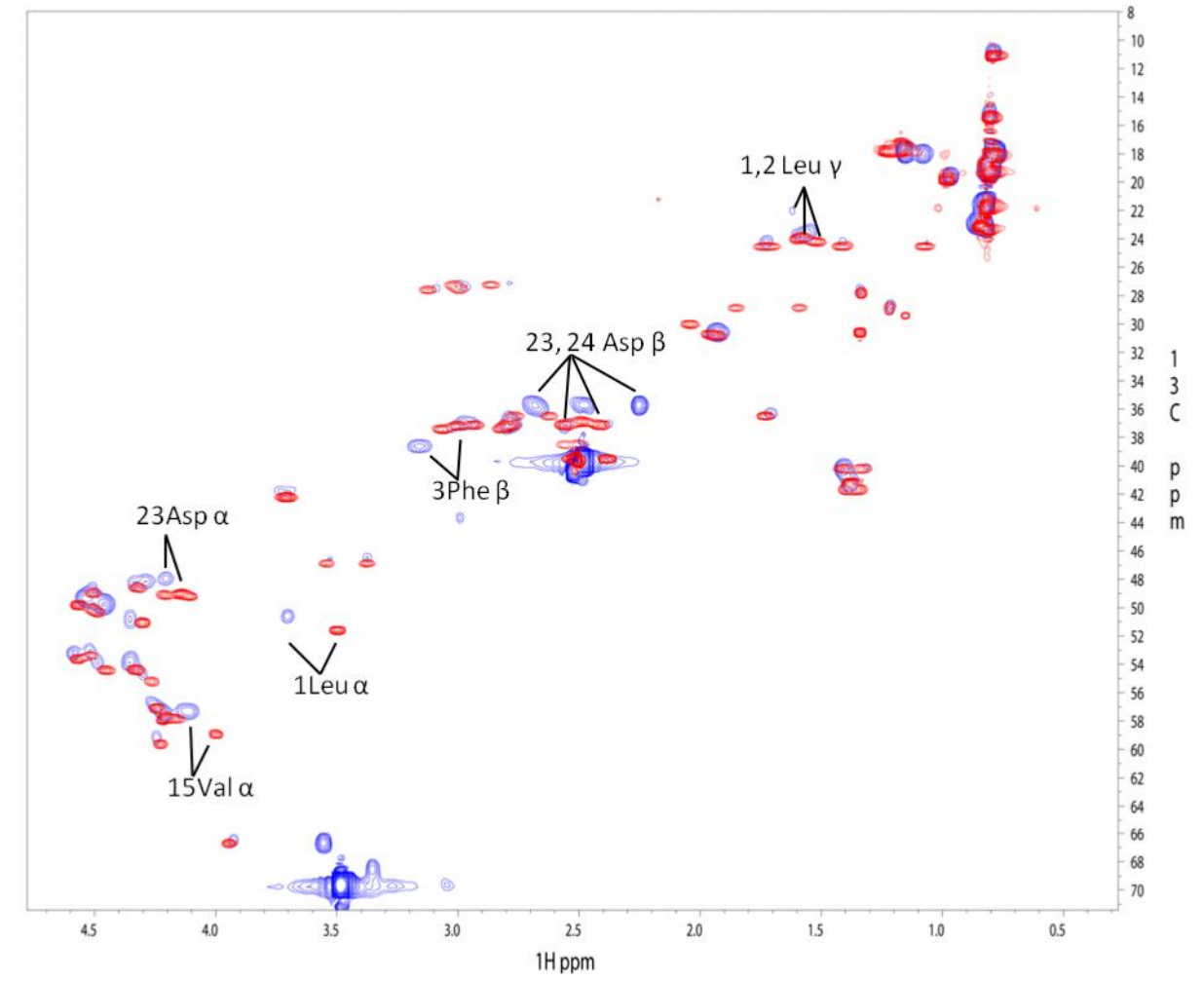

Figure 7. The overlay of ^{1}H-^{13}C HSQC spectra of X4-2-1 (red) and X4-2-6 (blue).
The labeled residues showing perturbations in chemical shifts are located in both the N- and C-termini of the peptide, which are in close proximity to the C-terminally attached PEG.

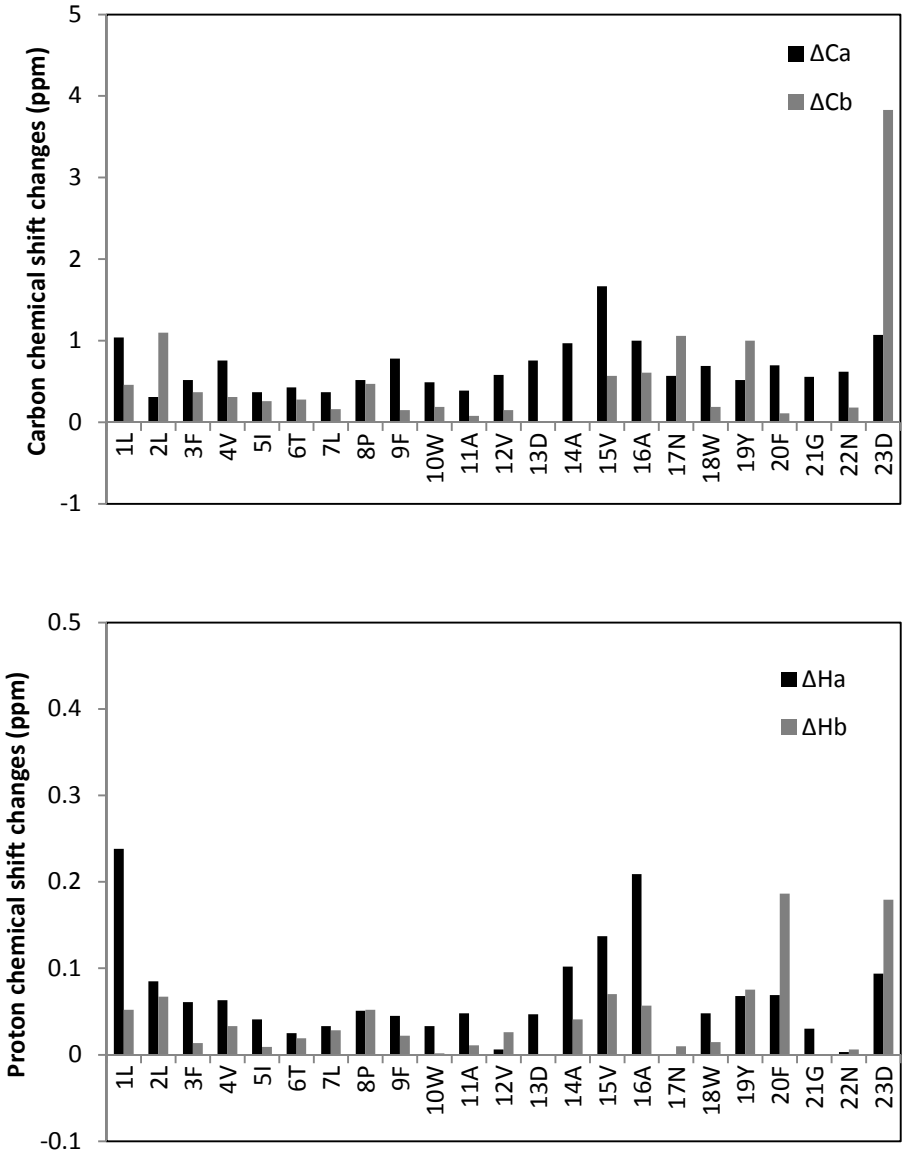

Figure 8. The carbon and proton chemical shift changes between X4-2-1 and X4-2-6. Alpha carbon and proton chemical shift differences are shown in black bars and beta carbon and proton chemical shift differences are shown in gray bars. The chemical shift differences are calculated by this equation.

The chemical shift changes = |(Chemical shift of x4-2-6) – (chemical shift of x4-2-1)|

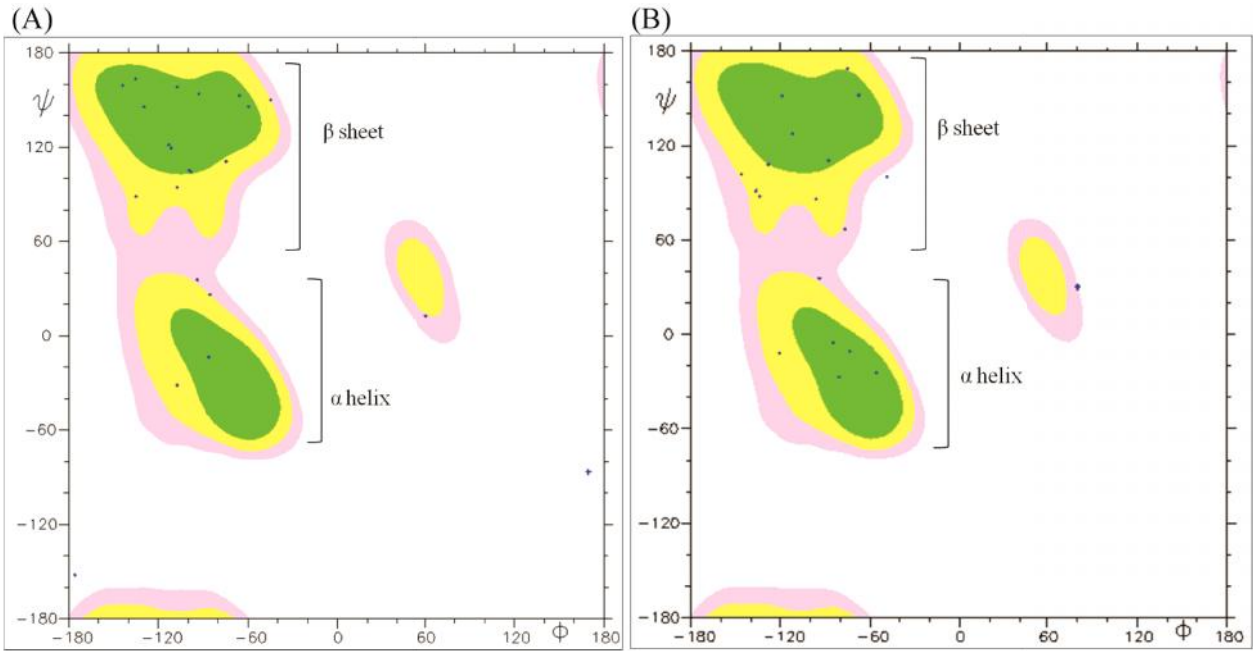

Figure 9. The ramachandran plot of average conformations for twenty X4-2-1 and X4-2-9 structures determined by NMR.

The MOLMOL 2K.1 software was used for analysis. Phi (φ) and psi (ψ) angles of most residues in both X4-2-1 (A) and X4-2-9 (B) structures are positioned in the β-sheet region, except those for residues involved in hairpin bending and the C-terminal helix. This plot shows that monomers of X4-2-1 and X4-2-9 adopt a β-hairpin conformation in the DMSO.

for residues 4-20 are 0.37 ± 0.16 Å and 1.18 ± 0.28 Å, respectively. The amino acids responsible for stabilization of the hairpin structure include Val^{4}, Thr^{6}, Pro^{8}, Asp^{13}, and Ala^{14}. The hydrogen bonds between two strands, such as the side-chain of Thr^{6} to the amide backbone hydrogen of Val^{15} and the nitrogen of Val^{4} to the δ proton of Asn^{17} may be present. The hydrophobic interactions between Pro^{8} and Val^{12}, and Val^{4} and Ala^{16} stabilize the hairpin-like structure. The negative charges provided by C-terminal aspartates further stabilize the hairpin conformation of X4-2-1 by interacting with the positively charged N-terminus. This structural arrangement allows close packing and subsequent stabilization of the N-terminal turns by the C-terminal strand. The hairpin conformation of the X4-2-1 structure and C-terminal turns define a conical overall shape of X4-2-1. This is consistent with our hypothesis that the conical shape of the X4-2-1 peptide may facilitate assembly into spherical nanoparticles.

The NMR chemical shift assignment of X4-2-9 is shown in TABLE III. The structure calculations were carried out with 217 NOE and 31 dihedral angle restraints. NOE restraints include 16 long range NOEs. X4-2-9 structures in DMSO-d_6 were calculated with the RMSD of 0.53 ± 0.34 Å for backbone and 1.13 ± 0.39 Å for heavy atoms for superimposed 20 structures over residues Val^{4} to Phe^{20}. The average structure of X4-2-9 is shown in Figure 6C. The PEG moiety was unstructured and therefore is not shown in the Figure 6. The residues involved in stabilization of the hairpin structure are Ile^{5}, Thr^{6}, Ann^{17}, and Tyr^{19} through H-bonds. Helical turns are absent in the structure of X4-2-9. This observation reveals that the structural significance of Leu^{1} and Leu^{2} is to stabilize the helical turns in the C-terminus of X4-2-1. Without the stabilizing effect of the two leucine residues the N-terminal strand packs loosely next to the C-terminal strand yielding a cylinder-like topology of X4-2-9. In addition, the number of amino acids in the β-strand conformation in X4-2-9 (50 %) is significantly reduced, as

TABLE III

CHEMICAL SHIFT ASSIGNMENT OF X4-2-9

	HN	$H(C)_{\alpha}$		$H(C)_{\beta}$		$H(C)_{others}$
3F	8.066	4.151	(52.68)	3.049/2.934	(36.69)	δ:7.236(128.2); ε:7.293(128.1); ζ:7.274(127.1)
4V	8.535	4.33	(57.23)	1.94	(30.73)	γ1:0.848(17.95); γ2:0.85(18.86)
5I	8.158	4.293	(56.65)	1.734	(35.96)	γ3:1.108(24.11); γ2:1.455(24.12); δ:0.815(10.66)
6T	7.838	4.233	(57.4)	3.968	(66.26)	γ1:4.756; γ2:0.987(19.46)
7L	7.715	4.543	(48.3)	1.341/1.424	(39.92)	γ:1.631(23.52); δ1:0.839(22.98); δ2:0.837(21.15)
8P	-	4.267	(58.96)	1.669/1.863	(28.4)	γ:1.753(24.02); δ3.547/3.395(46.315)
9F	7.844	4.386	(53.64)	2.783/2.959	(36.83)	δ:7.168(127.7); ε:7.2(129.1); ζ:7.131(129.1)
10W	7.947	4.54	(52.79)	3.114/2.985	(27.3)	δ1:7.132(123.3); ε1: 10.788; ε3:7.558(118.4); ζ2:7.316(111.0); ζ3:6.96(117.9); η2:7.048(120.5)
11A	8.097	4.366	(47.98)	1.187	(17.46)	-
12V	7.725	4.161	(57.1)	1.968	(30.48)	γ1:0.833(14.97); γ2:0.811(18.91)
13D	8.254	4.55	(49.12)	2.501/2.699	(35.45)	-
14A	7.793	4.313	(47.96)	1.178	(17.85)	-
15V	7.75	4.128	(57.13)	1.951	(30.3)	γ1:0.809(17.54); γ2:0.786(17.71)
16A	7.949	4.235	(47.72)	1.1	(17.86)	-
17N	8.032	4.54	(49.07)	2.399/2.562	(36.89)	δ21:7.493; δ22:7.054
18W	8.113	4.366	(53.56)	2.808/3.01	(26.9)	δ1:7.034(123.1); ε1:10.728; ε3:7.473(117.9); ζ2:7.302(111.0); ζ3:6.941(117.9); η2:7.034(120.6)
19Y	8.025	4.325	(54.53)	2.665/2.815	(35.99)	δ:6.971(129.8); ε:6.623(114.6); η:9.143
20F	7.891	4.509	(53.69)	2.823/3.057	(30.2)	δ:7.244(129.1); ε:7.162(127.7); ζ:n.o.
21G	8.031	3.691/3.756	(41.59)	-	-	-
22N	8.15	4.577	(49.14)	2.453/2.592	(37.1)	δ21:7.509; δ22:7.028
23D	8.53	4.464	(49.96)	2.518/2.715	(35.53)	-
24D	8.17	4.503	(49.45)	2.518/2.715	(35.53)	-

n.o. means not observed

compared to X4-2-1 (Figure 8). Further comparison of X4-2-1 and X4-2-9 structures revealed that five residues from Trp10 to Ala14 are involved in the head region of the X4-2-9 hairpin, whereas only three residues from Phe^{9} to Ala^{11} form the head of the X4-2-1 hairpin (Figure 6). This implies that the X4-2-1 hairpin has a much narrower head (8 Å) than the base (12 Å). This feature may be responsible for the cone-like topology of this peptide. On the contrary, both widths of the head and the base of X4-2-9 are approximately 15 Å giving rise to the cylindrical shape of X4-2-9. This result is again consistent with our hypothesis that the cylinder-like peptides may assemble into fibrils, while conical peptides form spherical nanoparticles.

The overall structures of X4-2-1 and X4-2-9 with space-filling method support that peptides which have similar amino acid sequence show different structures as conical and cylinder-like shape (Figure 6D and E). Several long range NOE signals between two strands indicate hairpin-like structure of X4-2-1 and X4-2-9. However, the set of NOEs in X4-2-1 structure that support hair-pin conformation was different from the set of those in X4-2-9 structure. For instance, long range NOEs between Thr^{6} Hγ2 and Ala^{14} Hα and Val^{15} Hα in X4-2-1 NOESY spectrum were absent in NOESY spectrum of X4-2-9. Based on the analysis of NOESY spectrum of X4-2-9, Hα of Ile^{5} and Thr^{6} are close to Asn^{17} Hδ2 which were missing in NOESY spectrum of X4-2-1 (Figure 10). Therefore, the X4-2-9 peptide adopts a different conformation from the structure of X4-2-1. This observation allows us to conclude that final morphology of nanoparticles may depend on the structure of monomer.

2.3.4. Structure information of X4-2-1 nanoparticles

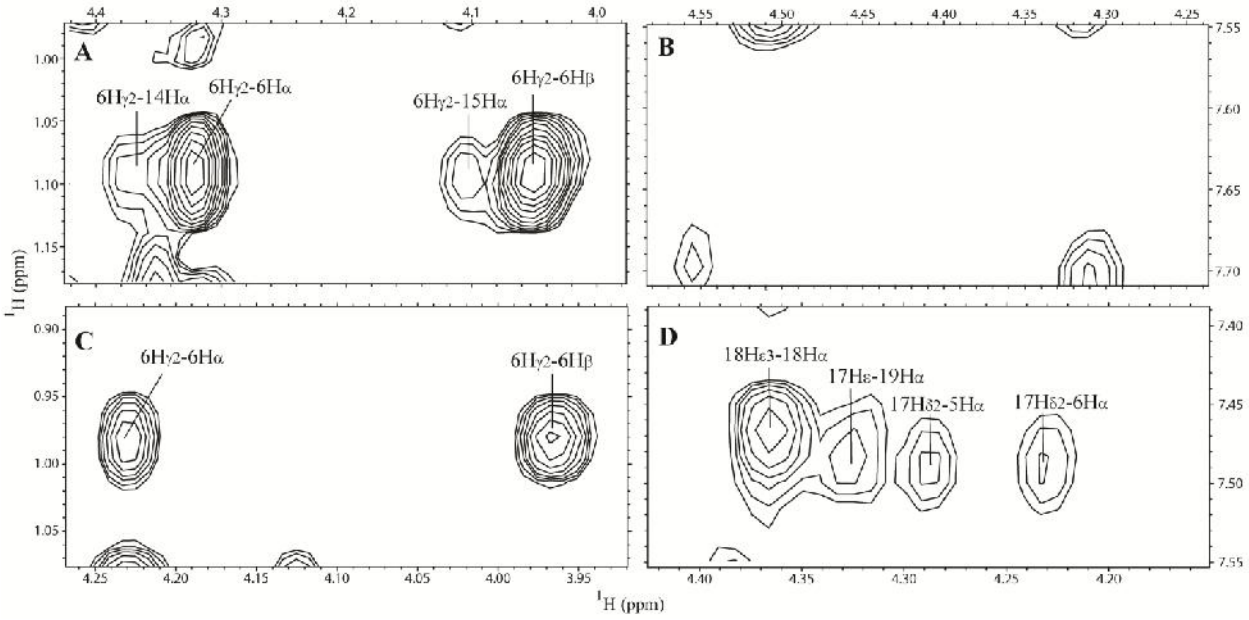

Figure 10. Partial NOESY spectra of X4-2-1 and X4-2-9.
The partial NOESY spectra of X4-2-1 (A and B) and X4-2-9 (C and D) suggest that X4-2-1 and X4-2-9 peptides do not share the same long range NOEs supporting the hypothesis that the structures of these peptides are different.

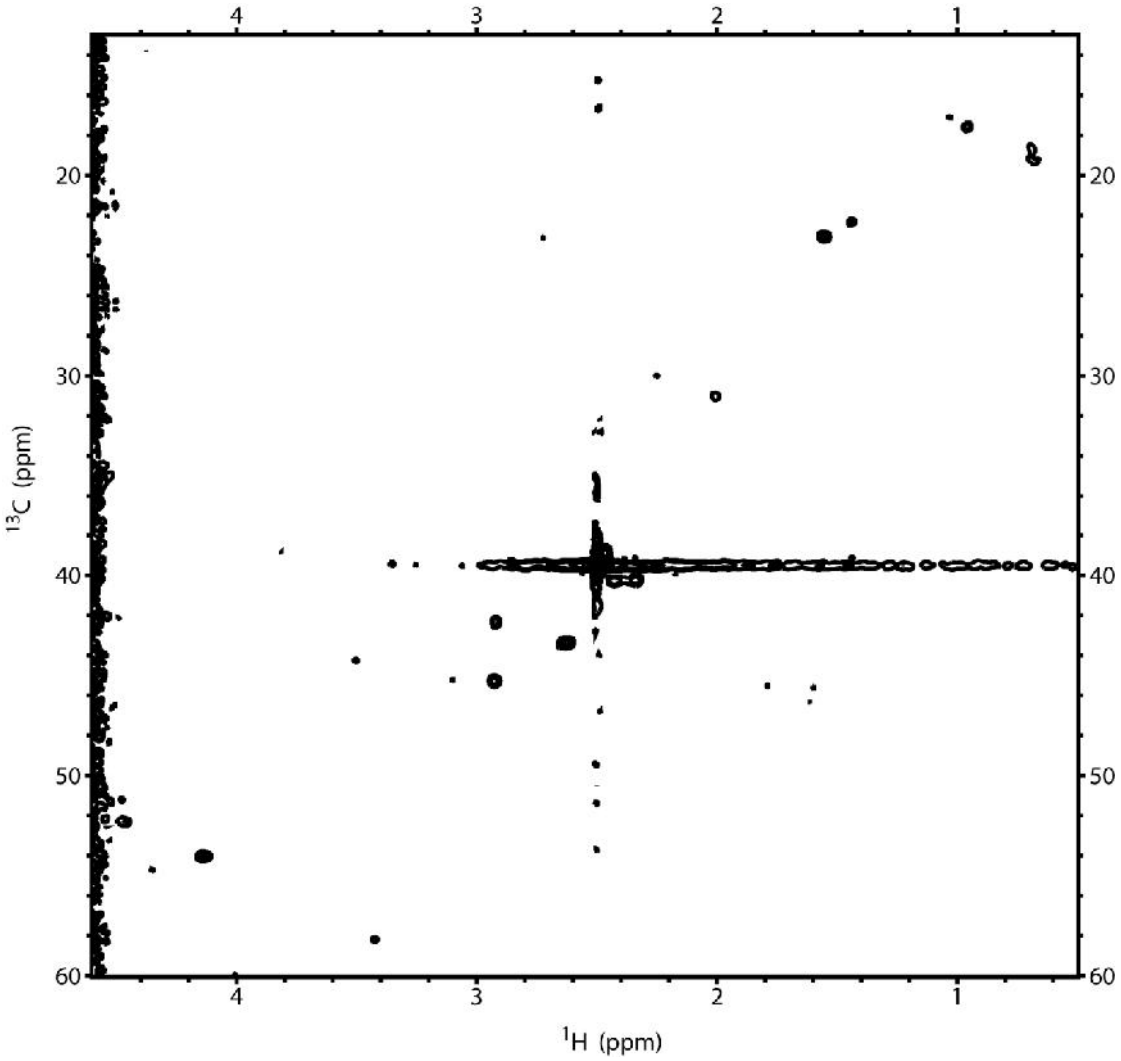

Figure 11. ^{1}H-^{13}C HSQC spectrum of X4-2-1 in PBS, pH7.4.
The X4-2-1 peptide is assembled into nanoparticles resulting in high molecular weight. Because of large molecular weight, most of signals were disappeared and few signals were observable.

In order to determine the nanoparticle structure of X4-2-1, the ^{1}H-^{13}C HSQC experiment of X4-2-1 in the PBS, pH 7.4 was carried out. Only few signals, however, were observed because nanoparticle formation results in increasing molecular weight (Figure 11). Those signals from the HSQC spectrum could not be assigned. To assign the signals shown in the HSQC spectrum of X4-2-1 in PBS, DMSO was titrated from 0 % to 100% and ^{1}H-^{13}C HSQC was carried out with all samples having different concentration of DMSO. Segments of the ^{1}H-^{13}C HSQC spectra of the methyl region from of the nanoparticle sample and the peptide in 50% and 100% DMSO are shown in Figure 12. All of the methyl resonances observed in the monomeric peptide in DMSO are also present in the spectrum of the nanoparticles with 50% DMSO. Significant line-broadening in the nanoparticle in the aqueous solution spectrum is indicative of a longer tumbling time and thus a higher molecular weight assembly (Figure 12C). Only few methyl resonances are observed in the spectrum of nanoparticles in the aqueous solution. Resonance assignments for the methyl signals are not possible under these experimental conditions due to severe line-broadening. However, all of the methyl signals are observed in the spectrum with 50% DMSO in the buffering solution (Figure 12B). The spectrum at 50% DMSO indicates that under these experimental conditions the peptide exists as a mixture of disassembled and intact nanoparticles. Under these conditions of exchange between assembled and disassembled peptides observation of signals involved in nanoparticle assembly is possible. In the spectrum of X4-2-1 in 50% DMSO two types of exchange regime are observed, slow exchange manifested in additional signals (representing the assembled nanoparticles because these signals are also seen in the spectrum of nanoparticles) compared to the spectrum in 100% DMSO and intermediate exchange manifested in increased linewidths of certain resonances. Although the extra signals due to slow exchange are not observed in the heteronuclear

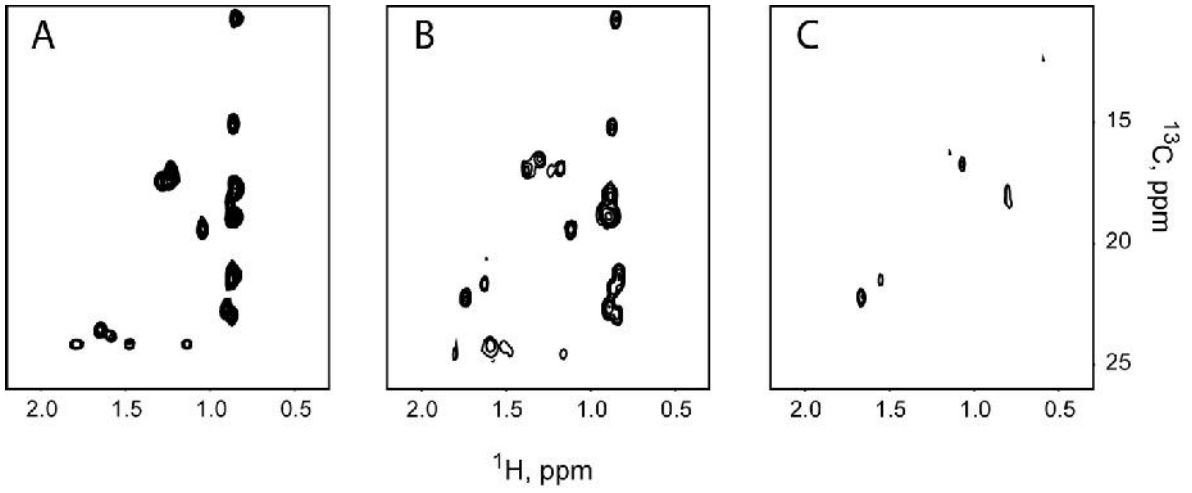

Figure 12. ^{1}H-^{13}C HSQC spectra showing the methyl regions of X4-2-1 in (A) 100% DMSO, (B) 50% DMSO, (C) aqueous solution.
Black arrows in (B) mark resonances in slow exchange and red arrows mark T6 and L7 resonances in intermediate exchange.

correlation spectra at 100% DMSO because of the sensitivity issues, we were able to identify them in homonuclear TOCSY experiments. Assignment of these signals is currently under way. Comparison of linewidths corrected for solvent viscosity in the spectra in 50% DMSO with the spectra at 100% DMSO (Figure 12A) allowed identification of signals undergoing intermediate exchange and possibly reporting on intermolecular contacts mediating nanoparticle assembly. These signals belong to T6 and L7.

2.3.5. Identification of β-sheet structure of nanoparticles

To gain insight into the possible mechanism of peptide assembly we utilized a fluorescent dye ThT that is widely used for selectively staining and identifying β-sheet structure in amyloid fibrils both *in vivo* and *in vitro* (*72*). The changes in fluorescent properties of ThT upon binding amyloids include a shift in its excitation spectrum and an increase in quantum yield (*73*). ThT absorbs at 340 nm with an emission maximum at 445 nm. Upon binding to self-assembled X4-2-6 and X4-2-9 peptides a peak at 440 nm became dominant in excitation spectra with the fluorescent emission maximum shifting to 480 nm. This was accompanied by a strong enhancement of fluorescence (Figure 13). Spectral changes of this type are broadly accepted as defining characteristics for the presence of β-sheets and thus suggest that the structural organization of self-assembled CXCR4 antagonists occurs *via* β-sheet formation from β-strands in the peptide hairpins. If the appearance of β-sheets marks formation of nanostructures then the range of CAC for the peptides may be determined by measuring absorbance of particle-bound ThT at 482 nm. Using this approach we found that CAC is much lower for the conical X4-2-6 peptide (between 0.004 to 0.01 mg/ml) than for the cylindrical X4-2-9 peptide (between 0.035 to 0.08 mg/ml).

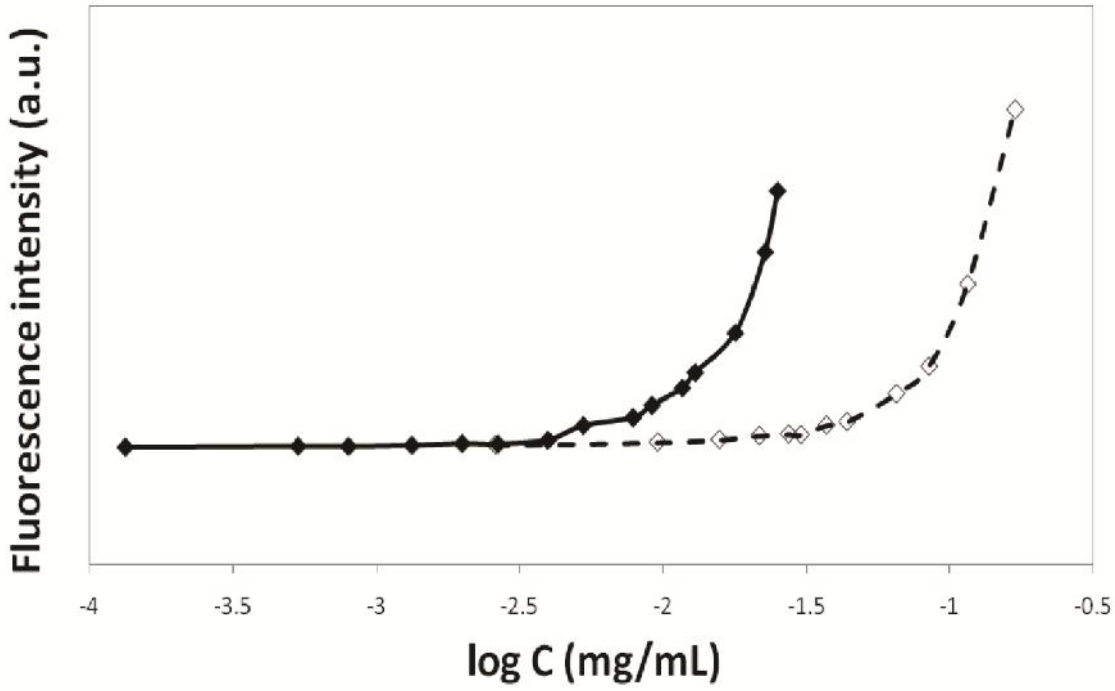

Figure 13. The fluorescence of ThT incorporated into X4-2-6 or X4-2-9 nanoparticles. Peptide concentration dependence of ThT fluorescence intensity at 482 nm allowed to determine that the critical aggregation concentration is much lower for X4-2-6 (♦, filled diamonds) than for X4-2-9 (◊, open diamonds).

2.3.6. Critical aggregation concentration determination

Next, we wished to address the question of significance of the shape of peptide assemblies. Previous stability studies of spherical and fibril nanoparticles showed that spherical X4-2-6 peptide nanoparticles have longer half-life time than that of X4-2-9 fibrils. The reason for enhanced protection against proteolysis of peptides assembled into nanospheres *versus* fibrils may be (i) minimized surface exposure within nanospheres compared to fibrils and/or (ii) a difference in strength of intermolecular interactions in nanospheres and in fibrils leading to different rates of their disassembly. These explanations may not necessarily be mutually exclusive. Although the role of the difference in surface exposure in proteolytic degradation of peptides is challenging to demonstrate, the strength of intermolecular contacts in peptide assemblies may be readily assessed by studying the peptide CAC.

Pyrene is a small molecule that changes its fluorescence upon transitioning from the aqueous to the micellar phase. This property of pyrene has been extensively used to measure CAC of polymers (*74, 75*). The CAC marks the onset of polymer aggregation when the first aggregates are observed. We incubated pyrene with varying concentrations of X4-2-6 and X4-2-9 and recorded pyrene excitation spectra at 390 nm of emission. As the peptide concentration increased, we observed an increase in total fluorescence intensity and a red shift indicating that pyrene incorporated into hydrophobic core structure of nanoparticles. The CAC was determined using the fluorescence intensity ratio I_{337}/I_{334} of pyrene from excitation spectra (*76*). The results of our analysis are shown in Figure 14. The error in measurements was estimated based on taking double points at several peptide concentrations. The measured CAC values of 0.02 mg/ml and 0.1 mg/ml for the X4-2-6 and X4-2-9 peptides, respectively are in agreement with the CAC determination using ThT fluorescence. The CAC measurements suggest that stronger

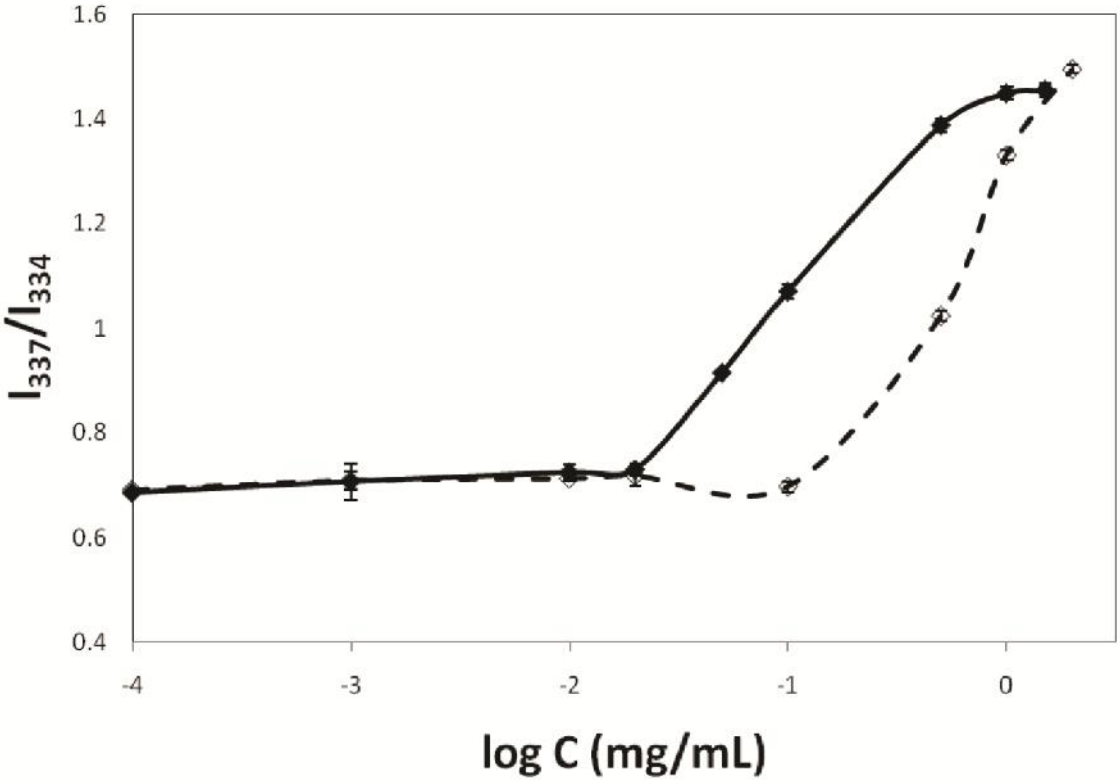

Figure 14. The plot of fluorescence intensity ratio (I_{337}/I_{334}) from pyrene excitation spectra as a function of concentration of x4-2-6 or x4-2-9 nanoparticles.
The CAC value for x4-2-6 (♦, filled diamonds) and x4-2-9 (◊, open diamonds) was 0.02 mg/ml and 0.1 mg/ml, respectively. The experiments were repeated for statistical analysis.

intermolecular interactions must exist within spherical nanoparticles than in fibrils. This observation implies that the spherical peptide nanoparticles disassemble at a slower rate than peptide fibrils allowing enhanced protection against proteases.

2.4. Discussion

There are a number of literature reports describing peptide-based spherical assemblies (*77-79*). There is also abundant literature on peptide aggregation into amyloid fibrils (*80*). These data suggest that common rules governing peptide assembly into higher order structures may exist. In this article we do not address the generality of mechanisms of peptide assembly. However, it is possible that the requirements for peptide monomeric structure delineated in this report apply to other peptides.

The mechanism of peptide aggregation into amyloid fibrils is still under investigation. However, it is already clear that it involves interactions of linear β-structures (*81*). The β-strands and β-hairpins assembling into amyloid fibrils would satisfy the cylindrical shape requirement for fibril formation. The initial cones and cylinders may not directly assemble into macrostructures. Intermediate assembly states may be necessary for the final architectures. However, the clear differences in the structure of the monomeric building blocks may dictate the assembly pathways.

There have been many attempts to create diverse higher order assemblies using inorganic and organic materials as building blocks (*82-84*). However, the mechanism of self-assembly into nanostructrures is not clearly understood. Self-assembly of inorganic molecules is currently better studied than self-assembly of organic materials, such as proteins and peptides. This is mostly due to the lack of well developed techniques to study nanoassembly of proteins and

peptides. The current knowledge of assembly mechanisms has been recently reviewed (*85-87*). The consensus is that the shape of the nanostructures is mostly defined by the nature of intermolecular interactions between the monomer building blocks. The driving force for self-assembly events is largely due to desolvation, collapse, and intermolecular association of hydrophobic molecular interfaces. It is possible that electrostatics and hydrogen bonding also contribute to the assembly process. This general conclusion seems to hold for both inorganic and organic materials. The importance of the overall topology of monomeric structures for definition of the shape of nanostructures has been recognized to a much lesser extent. The monomeric structure tends to be viewed as way to create amphiphilic molecules by polarizing charged and hydrophobic surfaces rather than to limit the possibilities for intermolecular interactions through steric interference. A model reflecting this idea has been recently described for peptides assembling into rods, tubes, and spheres (*58*). A modification of this hypothesis suggests that conical amphiphilic peptides containing terminal bulky aromatic residues or amphiphilic tree-like peptides may also form spherical nanoparticles based on steric compatibility (*88, 89*).

By studying peptide molecules of almost identical amino acid composition but very different in their topology we propose that the three-dimensional structure of peptide monomeric components may function as a determinant of the final shape of nanoassembly. Unlike in protein molecules that are much larger than peptides, small changes in the amino acid composition may have a drastic effect on three-dimensional structure. For example, the X4-2-6 peptide that differs only by two N-terminal amino acids from the X4-2-9 peptide displays a cone-shaped conformation, while the X4-2-9 peptide is cylindrical in shape (Figure 6B and C).

Based on the reports that structure of nanoparticles depends on the shape of monomeric building blocks and based on our structural characterization of X4-2-1 and X4-2-9 peptides

assembling into spherical nanoparticles and fibrils, we propose that the conical structures of monomeric components are required for spherical assemblies, while cylindrical shapes produce fibrils. This principle is schematically illustrated in Figure 15. Although our data suggests that the PEG moiety does not significantly interfere with the monomeric structures of peptides in DMSO, undoubtedly it affects the structure of the final nanoassembly. Many literature reports testify to this assumption (*89-91*). However, in this report by comparing the architectures of X4-2-6 and X4-2-9 we uncover the role of the structure of peptide monomers in the assembly mechanism. Since both peptides are PEGylated, the structure of the peptide part clearly dominates over the influence of PEG as the determining factor of the topology of resulting nanoparticles.

The conical X4-2-6 peptide engages in more significant intermolecular interactions than the cylindrical X4-2-9 peptide as evidenced by differences in CAC (Figure 14). These differences in intermolecular binding and perhaps differences in surface accessibility result in enhanced protection of peptides within spherical nanoparticles *versus* the peptides in fibrils against proteolytic degradation (Figure 5).

Proteolytic stability of peptide molecules in the blood stream is an important parameter in development of their therapeutic applications. In addition, well-defined structures are important for drug delivery. The spherical shapes are necessary for encapsulation of drug molecules. Fibrils may also have value for tissue repair (*92, 93*). Conversely, random aggregates may be neurotoxic (*94, 95*). Various well-defined shapes of nanostructures will have their own application in medicine. The studies reported here will contribute to definition of requirements that may allow engineering of the shape of peptide-based nanostructures.

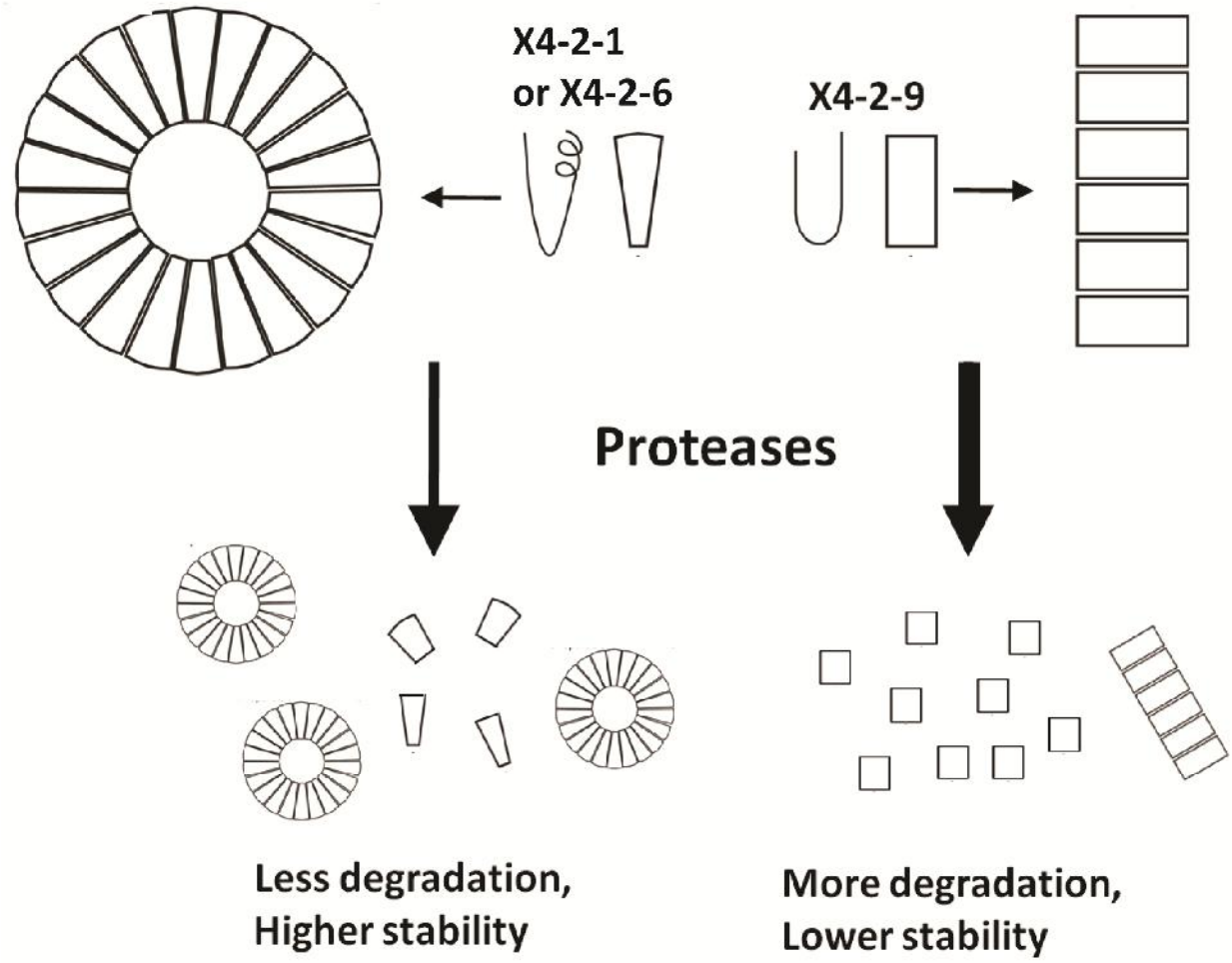

Figure 15. The model of nanoparticle assembly from the monomers of X4-2-6 or X4-2-9. The conical shape of X4-2-1 or X4-2-6 monomer leads to spherical nanoparticles whereas the cylindrical X4-2-9 monomer prefers to form fibrils. The nanospheres are protected from proteolysis more than peptide fibrils because of tighter intermolecular interactions in nanospheres.

III. BIOLOGYCAL ACTIVITY OF X4-2-6 NANOPARTICLES

3.1. Introduction

Recent reports indicate the crucial role of CXCR4 signaling in neoplastic transformation and progression. CXCR4 is the most common chemokine receptor expressed in human cancer (*96*). Expression of its ligand SDF-1 is highest in the common sites of cancer metastasis including lung, liver, bone marrow, and lymph nodes (*5-8*). There is extensive evidence that SDF-1 promotes migration and chemotaxis of neoplastic cells via the CXCR4 receptor (*96, 97*). Moreover, enhanced expression of CXCR4 correlates with poor prognosis and low survival rates in patients with breast cancer(*98, 99*), renal clear cell cancers(*100, 101*), colorectal cancer(*102-104*), osteosarcoma(*105, 106*), neuroblastoma (*107, 108*), malignant melanoma (*109*), and squamous cell head and neck carcinoma (*110, 111*). Many antagonists of CXCR4 such as AMD3100, T140 and T22 had been developed and show anti-HIV or anti-metastatic activity. Also, Anti-CXCR4 monoclonal antibodies decrease proliferation of non-Hodgkin's lymphoma cells, and metastasis of breast cancer cells (*6, 39*). Inhibition of CXCR4 by siRNA prevents metastasis of grafted breast cancer cells in a mouse model and reduces glioma and breast cancer cell invasion in *in vitro* assays (*40, 41*). Although CXCR4 is an excellent drug target, inhibition of this chemokine receptor may cause long-term immune system side effects. The use of functionalized nanoparticles capable of targeting of CXCR4 inhibitors to tumor cells could alleviate this potential problem. The X4-2-6 CXCR4 derived transmembrane peptide analog used here is a potent inhibitor of HIV replication (IC_{50}=200 nM)(*70*). In addition, X4-2-6 peptide-based nanoparticles may be further developed into anticancer pharmaceutical agents. PEG modified X4-2-6 nanoparticles kill breast cancer cells and prolong survival in a mouse model of breast tumor dissipation. *In vivo* imaging experiments utilizing nanoparticles

labeled with a near infrared dye have demonstrated that the nanoparticles spread in all organs upon intravenous and intraperitoneal injections and are cleared from the body through urinary excretion.

Previous studies showed that synthetic analogs of transmembrane helixes inhibit the function of the corresponding integral membrane protein, allowing in several instances development of potent inhibitors for important drug targets (*11, 70, 112-116*). Synthetic helixes interfere with the correct assembly of the target membrane protein, thus rendering it inactive (*11*). The synthetic peptides derived from second transmembrane domain of CXCR4 were selected and inhibition activity against CXCR4 downstream effects was examined. The second transmembrane peptide modified with C-terminal two aspartates addition inhibits Ca^{2+} influx from endoplasmic reticulum (ER) to cytoplasm (*70*). The second transmembrane peptide also fails to regulate the adenylyl cyclase resulting in up-regulation of cAMP and disrupts homodimerization of CXCR4 by leading conformational change of the receptor (*11*). However, there is no clear evidence that how the peptide inhibit CXCR4 downstream effects. In this chapter, I would like to address the inhibition mechanism of second transmembrane derived peptide X4-2-6 against CXCR4.

We study interactions between X4-2-6 nanoparticles and CXCR4 embedded into natural membranes. The CXCR4 receptor is overexperessed in mammalian cells and used in this study in the form membrane preparations. We utilize CXCR4 reductive methylation with ^{13}C-enriched formaldehyde to visualize CXCR4 conformational changes by NMR. This technique allows the use of native protein in its natural environment. In addition, due to reduced order parameters of lysine side chains we are able to observe NMR signals of large molecular weight molecular complexes. It had been previously postulated that X4-2-6 inserts into the cell membrane and

either disrupts the structure of the receptor or interferes with CXCR4 dimerization. Surprisingly, we find in the presence of X4-2-6 no significant changes in the receptor structure are observed. However, when SDF-1 chemokine is present X4-2-6 nanoparticles induce a global change in the receptor structure. It appears that the X4-2-6 amino acid sequence contains the extracellular loop between helix 2 and helix 3 of CXCR4. This extracellular loop serves as a binding site for the chemokine. This finding suggests that the chemokine may sensitize the receptor to the antagonistic action of the peptide. It is also possible that the nanoparticles also function as a decoy receptor to sequester SDF-1 away from cells expressing CXCR4. In addition, we observe conformational rearrangements in CXCR4 upon SDF-1 binding. These conformational changes involve the N-terminus of the receptor that is predicted from previous studies (*117-119*). However, in addition to this we report that there is a global change in the structure of the receptor caused by binding to SDF-1.

We also examined toxicity of X4-2-6 peptide nanoparticles against human breast cancer cells MDA-MB-231 and mouse breast cancer cells 4T1 using MTT assay. Based on MTT assay, X4-2-6 nanoparticles inhibit cell proliferation in both cancer cell lines. We also showed that the X4-2-6 peptide nanoparticles reduce secondary tumor size and prolong survival of nude mice that highly metastatic MBA-MD-231 breast cancer cells were injected.

3.2. Materials and methods

3.2.1. CD spectroscopy

The CD spectra of peptide solutions (12–50 μM) in 1 or 0.2 mm path-length quartz cuvettes were recorded at 25 °C using Aviv 202 Series CD-spectrometer (Aviv Biomedicals, Inc.)

at the wavelength interval 260–180 nm. The intensity measurements were made every 0.5 nm with the data collection interval at 5 seconds.

3.2.2. Reductive methylation of membrane preparations

Reductive methylation was performed as described previously (*120*). Human CXCR4 overexpressed in rat chem-1 cells, null membrane preparations, and SDF-1α were purchased from Millipore (Bedford, MA). Initially 4 µl of 1 M borane ammonia complex, $NH_3.BH_3$ (sigma) and 8 µl of 1 M ^{13}C-formaldehyde (Cambridge Isotope Laboratories, Inc) were added into 200 µl of 1 mg/ml of CXCR4 overexpressed membrane preparations or 200 µl of 0.5 mg/ml of null membrane preparations and the mixtures were stirred for 2 hours at 4 °C. Addition of borane ammonia complex and ^{13}C-formaldehyde was repeated and the mixtures were incubated for another 2 hours at 4 °C. After incubation, 2 µl of 1 M borane ammonia complex was added to the mixtures. The mixtures were incubated at 4°C with stirring overnight. To quench the reaction, the 1 ml of 2M Tris-HCl was added. After quenching the reaction, the both membrane preparations were ultracentrifuged for 1 hour at 110,000 g, 4 °C using Beckman Optima MAX-E. Supernatant was removed and pellet was resuspended with 200 µl of PBS (pH7.2). In order to compare chemical shifts of reductive methylated lysine signals from membrane preparations upon either SDF-1α, X4-2-6 nanoparitcles, or both SDF-1α and X4-2-6 nanoparticles, 0.5 mg/ml SDF-1α and/or X4-2-6 nanoparticles were added into methylated membrane preparations to reach final concentration of 0.84 µM of SDF-1α and 10 µM of X4-2-6 peptide nanoparticles. After addition of SDF-1α and X4-2-6 nanoparticles, the samples were dialyzed with PBS (pH 9.8) and 10% D_2O was added for further NMR expermients

3.2.3. NMR experiments

All NMR experiments were carried out on Bruker Avance 600 or 900 NMR spectrometers equipped with cryogenic probes at 298 K. The two-dimensional ^{1}H-^{13}C HSQC were acquired with 2048 data points for *t*2 and 256 for *t*1 increments. The zero-filling and sine-bell window function was applied to both direct and indirect dimensions prior to Fourier transformation. A linear prediction was applied to the data in the indirect dimension. All NMR experiments were processed and analyzed with NMRPipe software (*66*).

3.2.4. Fluorescence spectroscopy

Fluorescence measurements were performed on a PTI Quantamaster instrument. All experiments were carried out in quartz cuvettes using 1200 µl of X4-2-6 nanoparticles, SDF-1α, or mixture of nanoparticles and SDF-1α at 25 °C. The emission profile was scanned from 300 to 420 nm when the excitation was set to 280 nm. The concentration of X4-2-6 nanoparticles and SDF-1α was maintained as 1 µM and 0.083 µM, respectively, in all measurements.

3.2.5. *In vitro* toxicity assay

MDA-MB-231 cells and 4T1 cells were obtained from American Type Cell Culture Collection. Cells were grown in RPMI medium 1640 supplemented with 10% fetal bovine serum (FBS). For the assay, cells were seeded into 96-well plates in medium containing 5% FBS and 100 µl of a cell suspension containing 5,000 cells per well were used for each well. After 1 d incubation, the 5% FBS medium was aspirated and replaced with 100 µl of serum-free RPMI medium 1640 containing 1 mg bovine serum albumin (BSA) per 1 ml RPMI medium 1640. The compounds were prepared to the desired dilutions in no serum medium containing 1 mg BSA/ml. 75 µl of compounds were added to the wells followed by addition of 25 µl of human recombinant SDF-1α (Peprotech) to attain final concentrations of 10 ng SDF-1α / ml medium. Cell growth

was evaluated utilizing MTT (3-(4,5-Dimethylthiazol-2-yl)-2,5-diphenyltetrazolium bromide). The absorbance of the wells at 544 nm was determined by a FLUOstar/POLARstar Galaxy (BMG Lab Technologies GmbH) microplate reader. The activity was calculated from the data using the formula: $100 \times [(T - T0)/(C - T0)]$ for $T > T0$ and $100 \times [(T - T0)/T0]$ for $T < T0$. T0 corresponds to cell density at the time of compound addition and C is the density of untreated cells.

3.2.6. Animal studies

The 10^6 MDA-MB-231 breast cancer cells have been injected intravenously into 4-week-old (20–22 g) female athymic Ncr-nu/nu mice (Animal Production Area of the National Cancer Institute). The mice were divided into three groups, five mice in each group and the treatment was initiated the following day after injection of tumor cells. The control group received PBS solution intraperitoneally once every 3 day. Two other groups were treated once every 3 day with 200 μl of either 0.3 mg/ml (3 mg/kg dose) or 1.2 mg/ml (12 mg/kg dose) X4-2-6 solution in PBS containing 1.25% (v/v) DMSO.

3.3. Results

3.3.1. Prediction of secondary structure of 2TM peptides in the membrane-mimic condition

In the previous study, the transmembrane helix derived peptides were localized in the plasmamembrane where functional CXCR4 is positioned (*70*). We examined whether hairpin-like structure of X4-2-6 peptide is changed to alpha helix which is a native TM structure in the membrane mimic condition. The secondary structure of the X4-2-6 peptide in dodecylphosphocholine micelles was determined and compared to the secondary structure of the peptide in the aqueous solution using CD spectroscopy. The presence of distinctive negative

band at ~ 220 nm and a positive band between 190 and 220 nm on CD spectra strongly suggests that CXCR4 second transmembrane derivatives adopt predominantly beta-type conformation during self-assembly into nanoparticles in aqueous solutions. The peptide undergoes transition into mostly helical structure in membrane-mimicking dodecylphosphocholine micelles that is accompanied by appearance of a characteristic negative band at 208 nm (Figure 14). CXCR4 TM2 derivative that forms nanoparticles with a tendency to form super aggregates, X4-2-1 is also predominantly helical in the micelles (Figure 15). However, aqueous solutions of X4-2-1 have CD spectra that suggest significant degree of disordering, which probably results from random aggregation of the nanoparticles. The ^{1}H-^{13}C HSQC NMR spectra (Figure 16) further confirmed this transition. A profound downfield shift of $^{13}C\alpha$ resonances and an upfield shift of $^{1}H\alpha$ resonances indicate that the X4-2-1 peptide adopts a helical conformation in dodecylphosphocholine micelles.

3.3.2. Interaction between X4-2-6 peptide nanoparticles and reductively methylated CXCR4

To study the interactions of the peptide-based nanoparticle antagonists of CXCR4 with the receptor we reductively methylated membrane preparations from mammalian cells over expressing CXCR4 and from cells that were null for CXCR4 expression. The X4-2-6 peptide-based nanoparticles was added into a sample that reductively methylated CXCR4 overexpressed membrane preparation and ^{1}H-^{13}C NMR spectra were acquired on $^{13}CH_3$ groups of reductively methylated lysine residues. The results of these experiments are shown in Figure 17. Small chemical shift perturbations were observed in the spectrum of the membrane preparation from cells overexpressing CXCR4. This is a surprising result because based on several literature reports including our own we expected a more significant conformational change

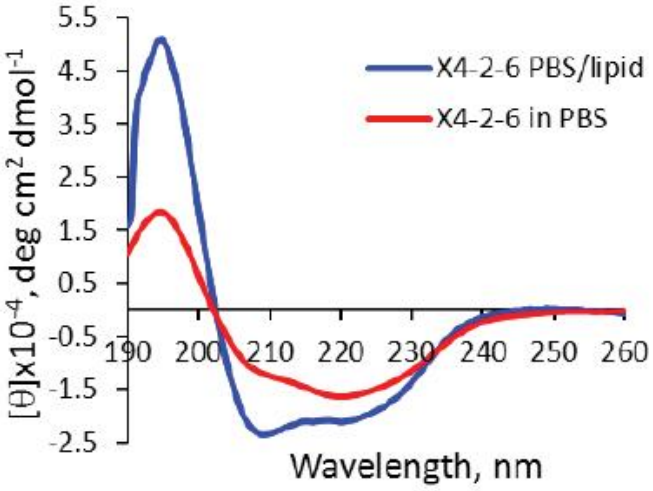

Figure 16. Comparison of CD spectra of X4-2-6 between DPC micelles and PBS solution. CD spectrum of X4-2-6 in lipid micelles demonstrate transition from predominantly beta-type conformation in aqueous solution into an α-helix upon fusion with the lipid. The experiments were done by Vadim Gaponenko.

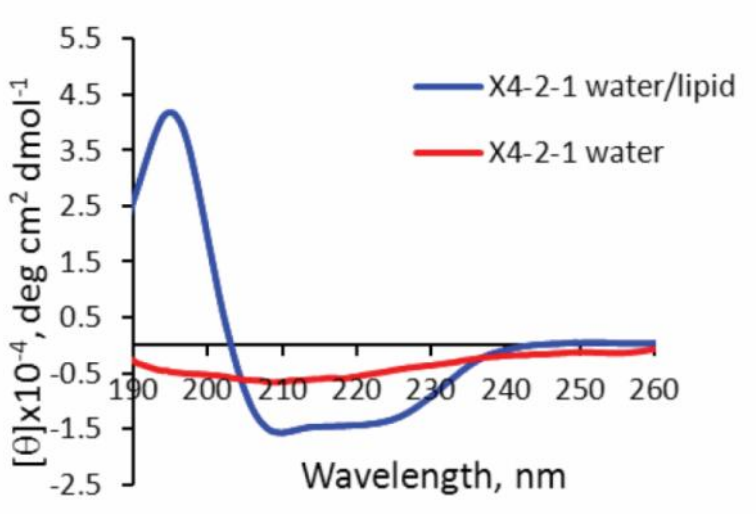

Figure 17. Comparison of CD spectra of X4-2-1 between DPC micelles and PBS solution. CD spectra of X4-2-1 micelles demonstrate transition from predominantly beta-type conformation in aqueous solution into an α-helix upon fusion with the lipid. The experiments were done by Nadya I. Tarasova.

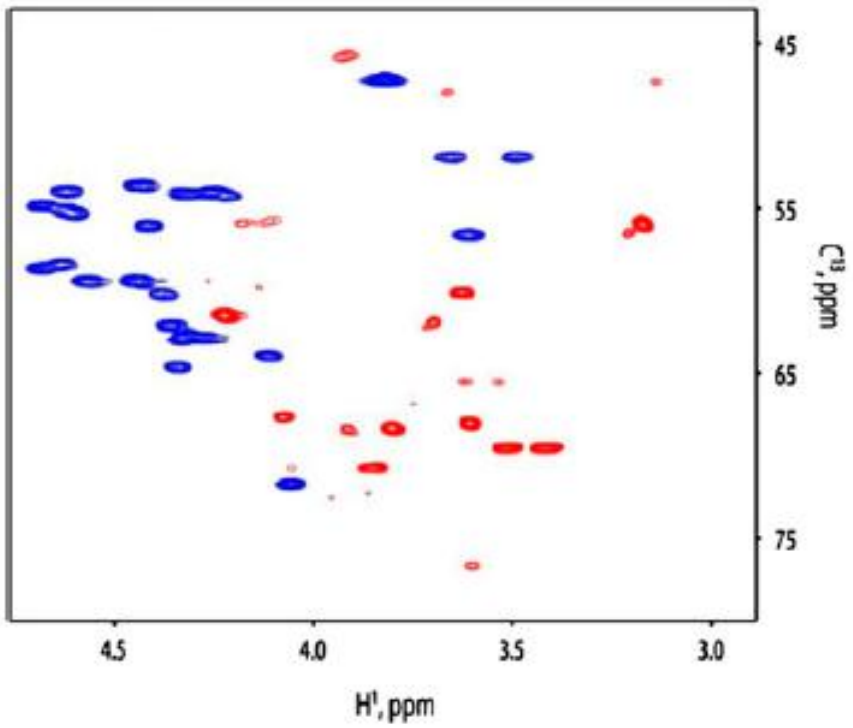

Figure 18. An overlay of Cα regions of ^{1}H-^{13}C HSQC spectra of X4-2-1 in 100% DMSO-d_6 (blue) and in dodecylphosphocholine-d_{28} micelles (red).

A profound downfiled shift of ^{13}Cα resonances and an upfield shift of ^{1}Hα resonances indicate that the X4-2-1 peptide adopts a helical conformation in dodecylphosphocholine micelles. The experiments were done by Vadim Gaponenko.

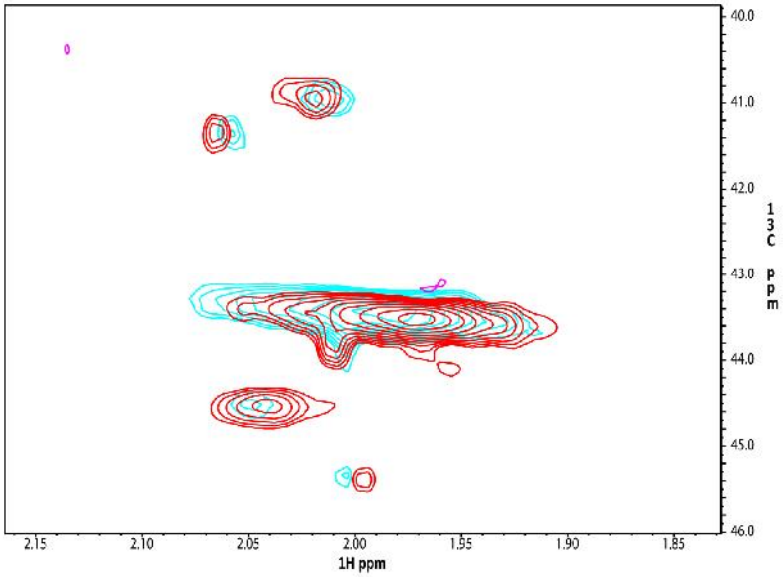

Figure 19. The overlay of ^{1}H-^{13}C HSQC spectra of reductively methylated CXCR4 overexpressed membrane preparation with X4-2-6 nanoparticles (red) and without X4-2-6 nanoparticles (cyan).

Small chemical shift perturbations were observed in the reductive methylated CXCR4 expressed membrane preparation when 200 μM of X4-2-6 nanoparticles were added. These small chemical shift perturbations do not support that X4-2-6 peptide is incorporated into 7 TM helices of CXCR4 and make the receptor inactive conformation.

in the CXCR4 chemokine receptor upon binding to the peptide antagonist. This is because it has been proposed that the peptide antagonist either disrupts the structure of the receptor after insertion into the membrane bilayer or interferes with CXCR4 dimerization.

Earlier experiments showing inhibition of CXCR4 signaling by the peptide antagonist were done in the presence of the CXCR4 cognate chemokine SDF-1. Therefore, we hypothesized that the chemokine binding event might sensitize the receptor to the action of the peptide antagonist. To test this hypothesis we added the SDF-1α to both the CXCR4 null membranes and to the membranes with overexpressed CXCR4. The results of these experiments are shown in Figure 18. As expected, no significant chemical shift perturbations were observed in the negative control containing CXCR4 null membranes. Interestingly, upon addition of SDF-1 to the membranes with overexpressed CXCR4 very large chemical shift perturbations in most of the CXCR4 methylated lysine signals were detected. This observation suggests that ligand binding either completely rearranges the structure of the membrane embedded receptor or leads to receptor dimerization.

Next, we investigated the possibility that the new conformation of the ligand-bound CXCR4 receptor is more susceptible to the action of the peptide antagonist. We treated the membranes with overexpressed CXCR4 and membranes that are null for CXCR4 with peptide antagonist nanoparticles in the presence of SDF-1α. To detect peptide binding we performed ^{1}H-^{13}C HSQC experiments. The results are shown in Figure 19. While no significant chemical shift perturbations were observed in the control sample with basal level of CXCR4 expression, addition of the antagonist to CXCR4 in the presence of SDF-1α caused a profound change in most chemical shift values. This observation indicates that SDF-1α can sensitize the receptor to the inhibitory action of the peptide antagonist.

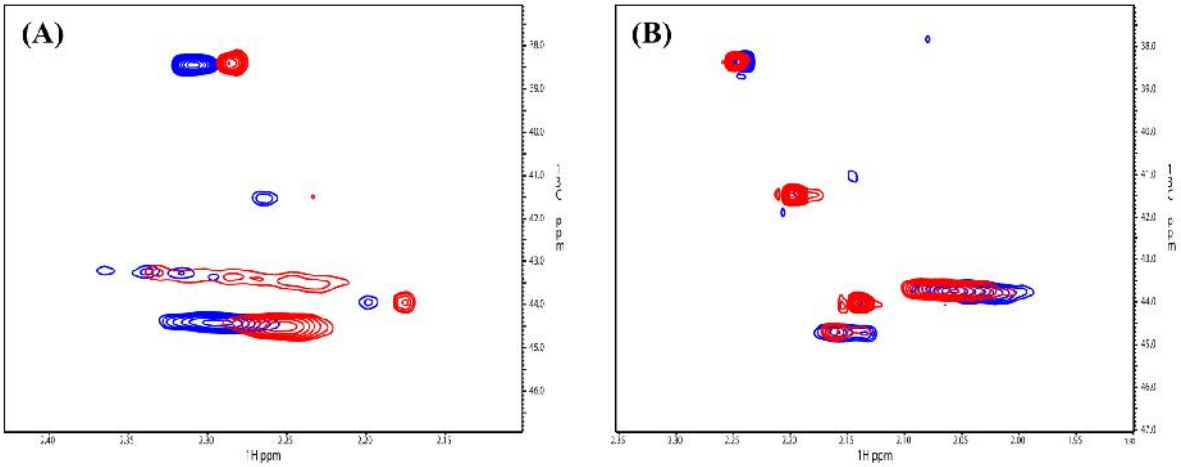

Figure 20. The partial ^{1}H-^{13}C HSQC spectra showing conformational changes of CXCR4 upon SDF-1α addition.

The overlay of ^{1}H-^{13}C HSQC spectra of (A) reductively methylated CXCR4 membrane preparation (blue) and reductively methylated CXCR4 membrane preparation with 0.5 μM of SDF-1α (red) and (B) reductively methylated null membrane preparation (blue) and reductively methylated null membrane preparation with 0.5 μM of SDF-1α (red). Significant chemical shift perturbations were observed in reductively methylated CXCR4 overexpressed membrane preparation upon SDF-1α addition.

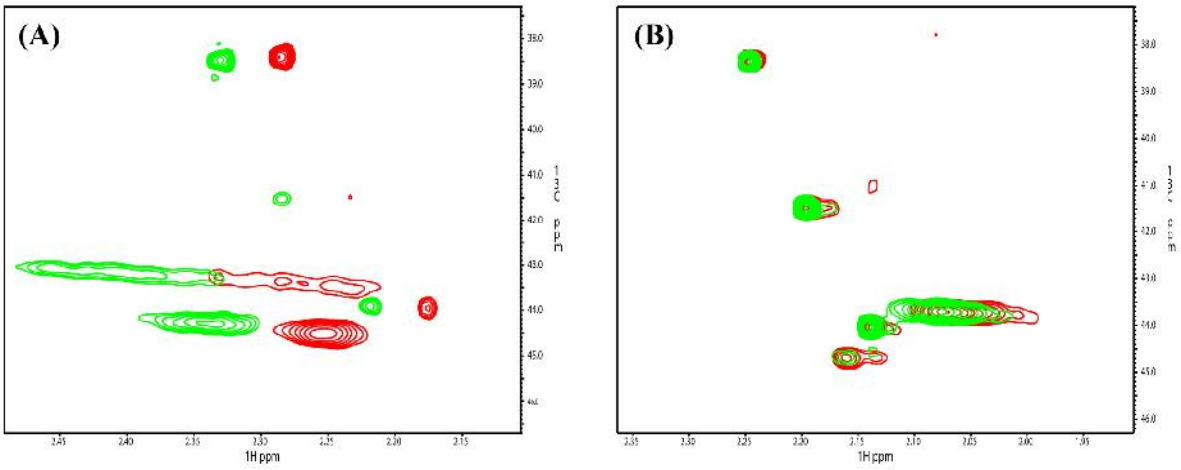

Figure 21. The partial ^{1}H-^{13}C HSQC spectra showing conformational changes of CXCR4 upon X4-2-6 peptide nanoparticle addition in the presence of SDF-1α.

The overlay of ^{1}H-^{13}C HSQC spectra of (A) reductively methylated CXCR4 membrane preparation with 0.5 μM of SDF-1α (red) and reductively methylated CXCR4 membrane preparation with 0.5 μM of SDF-1α and 22 μM of X4-2-6 peptide (green) and (B) reductively methylated null membrane preparation with 0.5 μM of SDF-1α (red) and reductively methylated null membrane preparation with 0.5 μM of SDF-1α and 22 μM of X4-2-6 peptide (green). In the presence of SDF-1α, the X4-2-6 peptide nanoparticles induce chemical shift perturbations of reductively methylated CXCR4 membrane preparation while did not affect the signals of reductively methylated null membrane preparation.

One possibility for the chemokine to enhance the antagonistic activity of the peptide is through recruitment of the peptide to the receptor. This can happen as part of the peptide includes a chemokine binding site. The peptide was originally designed to correspond to the second transmembrane helix of CXCR4. However, the peptide design was based on a prediction of transmembrane helices in CXCR4 when the x-ray structure of the receptor was not yet available. As can be seen in x-ray structure shown Figure 20 (*121*), the peptide amino acid sequence does not precisely correspond to the second transmembrane helix. Instead, it includes a significant portion of the second transmembrane helix and small part of helix 3 connected via an extracellular loop. Extracellular loops as well as the N-terminus of CXCR4 have previously been implicated in binding the chemokine (*117, 118, 122, 123*).

3.3.3. Interaction between X4-2-6 nanoparticles and SDF-1α

To test the hypothesis that the chemokine may be recruiting the peptide antagonist to the receptor we performed a fluorescence experiment where we monitored tryptophan fluorescence of the peptide upon addition of SDF-1α. The results of the experiment are shown in Figure 21. Upon addition of SDF-1α to the peptide nanoparticles we observed a 10 nm red shift in tryptophan fluorescence from 340 nm to 350 nm indicating that SDF-1α is capable of binding to the X4-2-6 peptide. The fluorescence maximum of SDF-1α alone was 305 nm suggesting that the observed red shift was not due to contribution from SDF-1α fluorescence.

3.3.4. Anti-cancer activity of X4-2-6 peptide nanoparticles using MDA-MB-231 and 4T1 cells

In order to examine anti-cancer activity of X4-2-6 peptide, human breast cancer cells, MDA-MB-231, and mouse breast cancer cells, 4T1 were selected for MTT assay. The diverse concentrations of X4-2-6 peptide nanoparticles and 10 ng/ml of SDF-1α were treated with 4T1

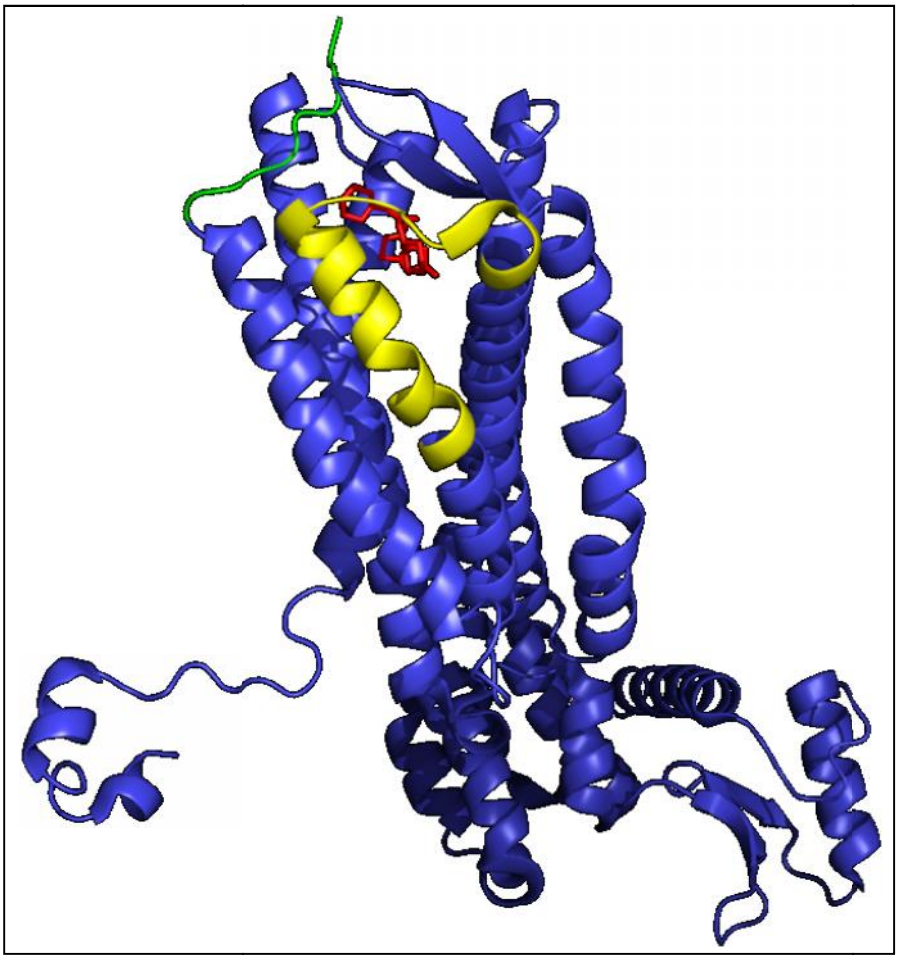

Figure 22. The crystal structure of CXCR4 (PDB: 3ODU).
Unstructured N-terminal domain is shown in green and small antagonist IT1t is shown in red. The origin of the X4-2-6 peptide is colored in yellow. The peptide region (residues 93-115) of CXCR4 contains second and third TMs and first extra cellular loop.

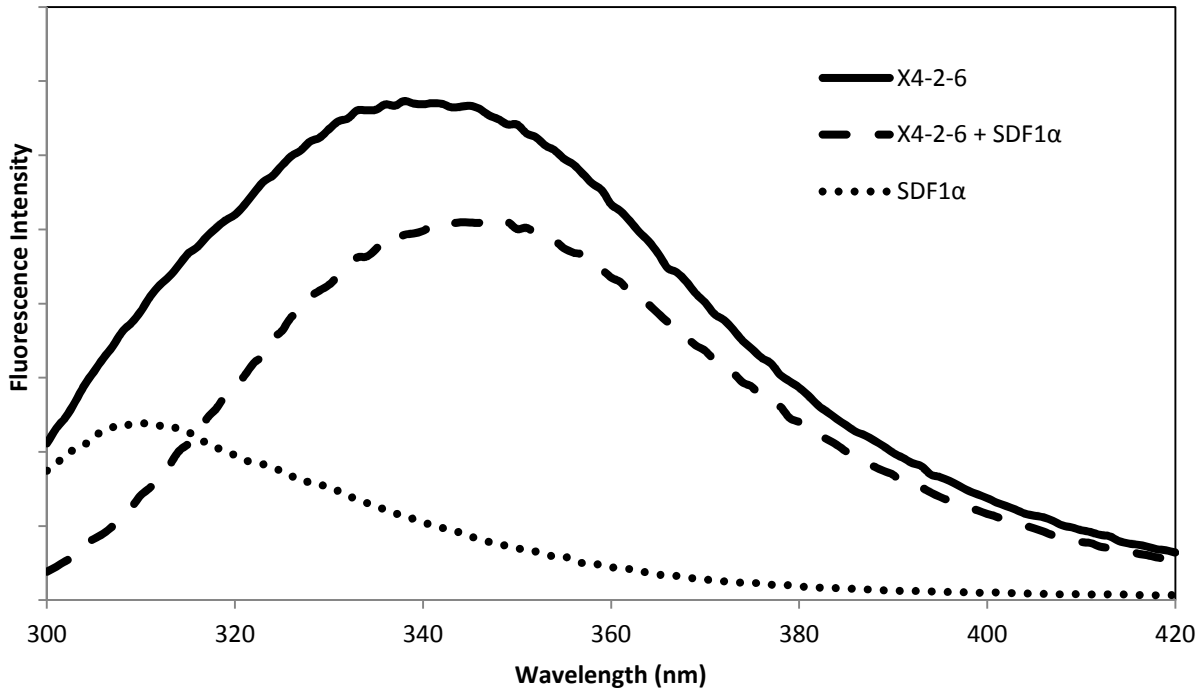

Figure 23. Fluorescence intensity of emission scan of X4-2-6, SDF-1α, and the mixture of X4-2-6 and SDF-1α.

All samples were excited at 280 nm and scanned emission from 300 nm to 420 nm. The red shift was observed when SDF-1α was added to X4-2-6 solution. The concentration of X4-2-6 and SDF-1α was maintained at 1 μM and 83 nM, respectively.

and MDA-MB-231 cells. Nanoparticles formed by X4-2-6 inhibited growth and killed human and mouse breast cancer cells grown in the presence of SDF-1α in serum-free medium (Figure 22).

3.3.5. Anti-cancer activity of X4-2-6 peptide nanoparticles using a mouse model of breast cancer dissipation

To explore the therapeutic potential of the CXCR4 TM peptide nanoparticles modified with PEG (X4-2-6 peptide-based nanoparticles) were tested in a mouse model of breast cancer dissipation. CXCR4 is known to play a critical role in tumor metastasis in the lung and bone, where expression of CXCR4 agonist, SDF-1α is particularly high. Nude mice were injected intravenously with highly metastatic MDA-MB-231 breast cancer cells (1 million cells per mouse). The mice were divided into three groups, five mice in each group. The control group received PBS solution intraperitoneal once in three days. The remaining two groups were treated once in every three days with X4-2-6 peptide-based nanoparticles at doses of 3 mg/kg and 12 mg/kg, respectively. Control animals started dying or had to be sacrificed in about two month after the start of the experiment. Necropsy revealed numerous tumors mostly in the lung. Nanoparticles slowed the growth of the tumors and significantly prolonged the life of animals (Figure 23).

3.4. Discussion

Here we use reductive methylation of lysine residues for NMR analysis of binding of peptide nanoparticle antagonists to CXCR4 chemokine receptor overexpressed in mammalian membrane preparations. The unique advantage of this approach is that the receptor adopts its native conformation because it is produced in the mammalian cells and it is correctly embedded

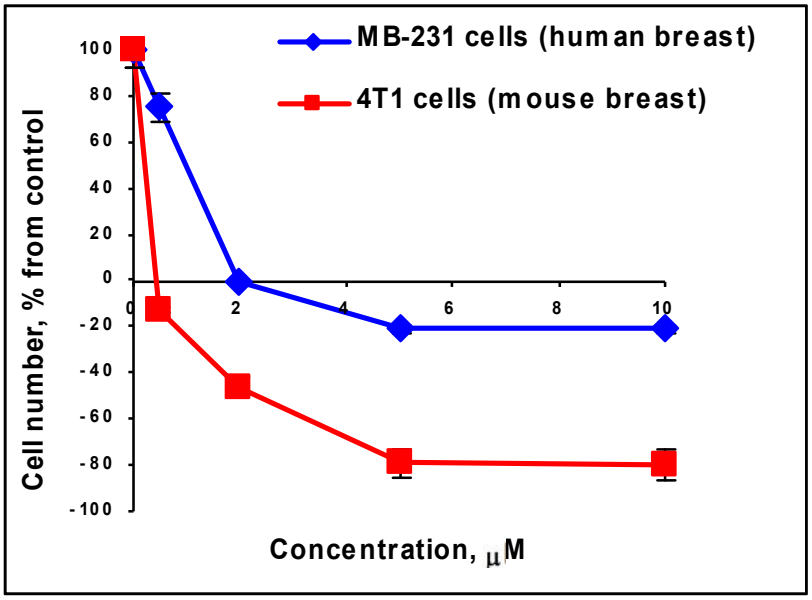

Figure 24. The plot of cell viability as a function of various X4-2-6 peptide concentration using MTT assay.

Nanoparticles formed by X4-2-6 inhibited growth and killed human (blue) and mouse breast cancer cells (red) grown in the presence of 10 ng/ml of SDF-1α in serum free medium. The experiments were done by Nadya I. Tarasova.

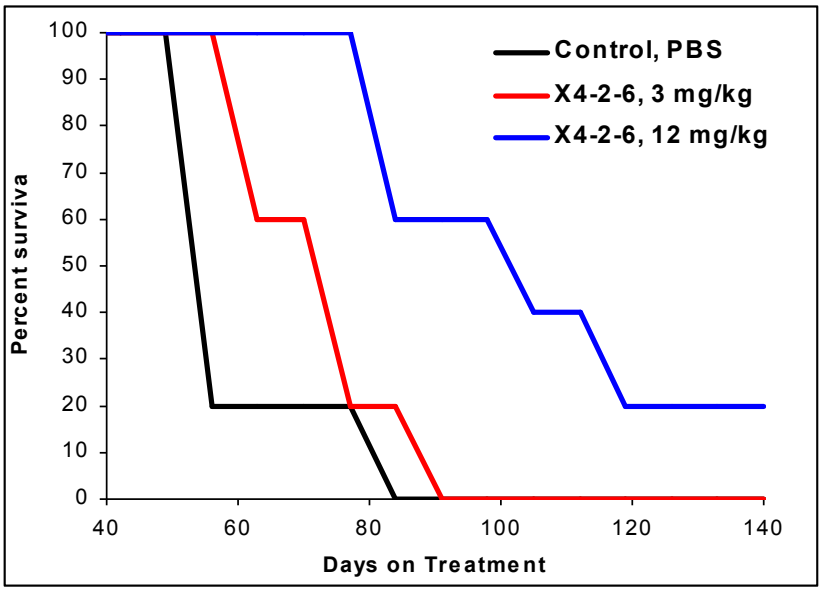

Figure 25. The plot of survival rate of metastatic breast cancer mouse model received PBS (black), 3 mg/kg of X4-2-6 solution (red), and 12 mg/kg of X4-2-6 (blue).
Nude mice were injected with MDA-MB-231 breast cancer cells intravenously. Intraperitoneal treatment with X4-2-6 was started the day following the injection of cancer cells and was given every 3 d thereafter. X4-2-6 prolonged survival in a group of mice that X4-2-6 solution was injected in the concentration dependent manner. The experiments were done by Nadya I. Tarasova.

into the native plasma membrane. By doing this analysis we uncovered several surprising features about the interaction of the peptide antagonist and CXCR4. First, the peptide alone does not significantly affect reductively methylated lysines in the receptor (Figure 17). This is in marked contradiction with the previous view that the antagonist either disrupts the receptor structure or interferes with its dimerization. If either of these propositions were correct we would have expected significant chemical shift perturbations in the ^{13}C methyl groups on CXCR4 lysines. We previously demonstrated that reductive methylation can be instrumental in detection of conformational changes in protein molecules by NMR (*124, 125*).

The second discovery was that the CXCR4 antagonist nanoparticles were able to induce a significant change in the conformation of the receptor in the presence of SDF-1α (Figure 18). This observation implies that the nanoparticles can specifically target CXCR4 that is activated by its ligand presenting a unique opportunity to only interfere with receptor signaling at the site of cytokine action. This phenomenon is possible because the peptide antagonist includes the receptor extracellular loop between helices 2 and 3 (Figure 20). It is known that SDF-1α interacts with its cognate receptor through the N-terminal region as well as the extracellular loops. It is possible that the first extracellular loop of CXCR4 participates in chemokine binding. We tested this possibility by performing a fluorescence assay. Our results show that the peptide nanoparticles are capable of interaction with SDF-1α even in the absence of the receptor. This observation suggests another mode of therapeutic action of X4-2-6 nanoparticles. In addition to disrupting CXCR4 structure in the membrane, the nanoparticles may also sequester the chemokine by acting as a decoy receptor. Therefore, we have discovered another possible mechanism that can be used by X4-2-6 nanoparticles. Although targeting activated receptors is not a completely novel strategy to increase antagonist efficiency, a

combination of at least two different mechanisms of chemokine receptor targeting is a new concept.

We also showed anti-cancer activity of X4-2-6 nanoparticles by MTT assay. The proliferation of human and mouse breast cancer cell lines, MBA-MD-231 and 4T1 cells, was significantly reduced when X4-2-6 nanoparticles were added. Although we could not identify the detailed mechanism for decreasing of cancer cell proliferation, it is possible that inactive CXCR4 reduces Akt activity. Liang *et al* showed that CXCR4/SDF-1 can induce Akt phosphorylation resulting in upregulation of vascular endothelial growth factor (VEGF) which is a marker for angiogenesis of cancer and inhibition of CXCR4 with its antagonist suppressed tumor angiogenesis and growth *in vivo* (*126*).

X4-2-6 nanoparticles also have a potential to be used as therapeutics for the cancer treatment. Nanoparticles slowed the growth of the tumors and reduced metastasis of the tumors in vivo mouse model. The spherical nanoparticles made of peptide offer advantages having both current nanoparticle-based drug delivery systems and peptide drugs. X4-2-6 peptide provide specific interaction with CXCR4 through SDF-1α binding and this specific interaction will diminish nonspecific interaction leading to low toxicity. Since X4-2-6 peptides are self-assembled into nanoparticles, functional peptide can be protected from proteases and can be localized into tumor tissue.

IV. CONCLUSION

CXCR4 is a chemokine receptor that induces cell migration upon its ligand SDF-1 binding. Recent studies show that CXCR4 is highly expressed on many kinds of cancer including breast cancer, prostate cancer, and lung cancer. Moreover, tumors that express high level of CXCR4 induce metastasis and angiogenesis so that they associate with poor prognosis (*30, 109*).

A peptide antagonist X4-2-6 was developed using the region from Leu^{93} to Asn^{115} of CXCR4. Two of negative charged aspartates were added to C-terminal of the analog to mimic orientation when the X4-2-6 peptide is inserted plasmamembrane. X4-2-6 also has hydrophilic 27 units of PEG. PEG has several advantages and few negative aspects as a therapeutic. PEG improves circulation time due to evasion of renal clearance and is resistant to proteolysis. PEGylated nanoparticles overcome low solubility of encapsulated drugs and reduce toxicity because of improving passive targeting. It also has been reported that PEG reduces immune response to inhibit interaction with opsonin which is a molecule targeting antigen (*127*). The PEG will contribute the antagonist effects of X4-2-6 by improving stability of nanoparticles structure, proteolytic stability, and half-life time of the peptide (*128, 129*). As a result, mice having metastatic breast tumor survived longer when they received the X4-2-6 peptide antagonist of CXCR4. The X4-2-6 peptide inhibited metastasis of breast tumor and decreased tumor growth as well in a mouse model of breast tumor. The inhibition of metastasis is well known phenomenon when CXCR4/SDF-1 activation is inhibited by antagonists, siRNA for down-regulation CXCR4 expression, or an antibody against CXCR4. The X4-2-6 peptide also decreases cell proliferation of mouse and human breast cancer cells *in vitro*. The one of the possible mechanisms of cell growth inhibition is that CXCR4 antagonists reduce activity of Akt

leading to down-regulation of VEGF, which is an important signaling molecule for tumor angiogenesis.

Our hypothesis that the TM analog may disrupt the active conformation of the corresponding receptor is verified by using X4-2-6 peptide derived from CXCR4 chemokine receptor. The TM derived peptide was inserted into plasma membrane due to highly hydrophobic nature. The structure of the peptide was changed to an α-helix in lipid condition confirmed by CD and NMR. The α-helical peptide may interact with other TM helices of CXCR4 and these interactions can cause disruption of CXCR4 structure and result in inactivation. One of the future directions of this research is to use acquired knowledge of peptide assembly mechanisms to design antagonists of other membrane proteins such as G-protein coupled receptor (GPCR). We have several TM analog peptides of GPCRs, for which further experiments are needed. Among them, a 5TM analog of ATP-binding cassette (ABC) transporter p-glycoprotein was able to inhibit the function of the corresponding membrane protein (*115*). We will characterize the inhibition mechanism of 5TM peptide for p-glycoprotein in the future.

We showed that X4-2-6 induces significant CXCR4 conformational changes only in the presence of SDF-1α using the reductive methylation technique. The global conformational changes of CXCR4 make it an inactive form resulting in inhibition of Ca^{2+} flux, increasing cAMP production, and disruption of receptor homodimerization. We also showed that the X4-2-6 peptide directly interacts with SDF-1α using fluorescence spectroscopy. It is possible that the first extracellular loop region of the peptide is involved in binding to SDF-1α. When the SDF-1α interacts with CXCR4, X4-2-6 peptide bound SDF-1α is inserted into CXCR4 TM helices and induces an inactive conformation of CXCR4. This mechanism suggests that X4-2-6 can inhibit

only SDF-1 induced CXCR4. In other words, X4-2-6 is able to inhibit down-stream signaling for metastatic CXCR4.

2TM analogs of CXCR4 were able to form diverse nanoparticles including spherical nanoparticles and fibrils. The major driving force for self-assembly in the aqueous solution is the hydrophobic interaction because the peptides consist of hydrophobic residues. In order to understand mechanism of assembly, I determined monomer structures of X4-2-1 and X4-2-9 that were assembled into spherical nanoparticles and fibrils, respectively. We could assume that the monomer structure of X4-2-1 is almost identical to structure of X4-2-6 because ^{1}H-^{13}C HSQC spectrum of X4-2-1 is almost same as ^{1}H-^{13}C HSQC spectrum of X4-2-6 except for the N- and C-termini. Based on the structure comparison, we can conclude that conical shape of peptide monomer forms spherical nanoparticles while cylindrical monomers prefer to assemble into fibrils (Figure 15). These mechanisms were observed from many literature reports describing self-assembled particles made of short peptides that do not have secondary or tertiary structure or dendrimers to provide very rigid structure by covalent bonds. However, it has not reported that relatively long peptides that have three dimensional structures followed this mechanism. I propose that in the future this self-assembly mechanism be tested for universal application to assembly of peptides. The next step will be determination of 5TM peptide of p-glycoprotein monomer structure that is also self-assembled into spherical nanoparticles.

Nanoparticle formation is important for the targeting tumor as we discussed previously. Nano-sized molecule can be localized in tumor tissue passively because of EPR effects. The passive targeting of nanoparticles reduces toxicity due to diminishing undesired localization. However, active targeting of nanoparticles may be needed to reduce unwanted targeting to organs that have leaky endothelial cells such as liver and spleen (*50, 130*). Active targeting can

be achieved by attachment of an epitope or antibody to the surface of nanoparticles. In order to attain active targeting of CXCR4 antagonist to the tumor tissue, we will modify C-terminal of X4-2-6 peptide with a bombesin peptide analog. The bombesin peptide is known to interact with bombesin receptors such as gastrin-releasing peptide (GRP) receptor that highly expressed on several cancer types including prostate cancer and breast cancer (*131-134*). Double targeting may decrease toxicity significantly and increase the antagonist effects.

CHAPTER 2.

THE USE OF REDUCTIVE METHYLATION TECHNIQUE TO STUDY PROTEIN-PROTEIN INTERACTIONS BY SOLUTION NMR

I. INTRODUCTION

While solution state NMR is very well suited for analysis of protein-protein interactions occurring with a wide range of affinities, it suffers from one significant weakness, known as the molecular weight limitation. This limitation stems from the efficient nuclear relaxation processes in macromolecules larger than 30 kDa (*135*). These relaxation processes cause rapid decay of NMR signal. Although the use of transverse relaxation optimized spectroscopy (TROSY) approaches has made solution state NMR of large proteins and protein-protein complexes more feasible, it is still limited by the ability to produce isotope enriched proteins (*136*). However, there is a significant number of proteins for which no convenient system for stable isotope incorporation exists. We recently utilized reductive methylation methodology to demonstrate that it is possible to introduce ^{13}C-enriched methyl groups into lysine residues in otherwise unlabeled proteins with the purpose of studying protein-ligand and protein-protein interactions by NMR (*124*).

Reductive methylation is commonly used to improve crystallization of proteins (*137*). Studies show that success of protein crystallization improves significantly through reductive methylation of solvent exposed lysines due to a reduction in surface entropy. Reductive methylation does not alter significantly protein structure and native protein-protein interactions (*138-141*). Despite clear advantages offered by reductive methylation, this technique remains underutilized in solution NMR. Here we show that reductive methylation allows characterization of high molecular weight protein-protein complexes that is not achievable using traditional NMR approaches.

For reductive methylation of NMR protein samples, ^{13}C-enriched carbonyl compound (e.g. ^{13}C-formaldehyde) and reducing agents are required. The primary amine of lysine in polypeptide molecules acting as a nucleophile attacks the carbonyl group of formaldehyde. This reaction results in formation of an intermediate imine through the carbonyl-condensation process. The intermediate imine subsequently reacts with a proton donor to give rise to the higher order amine (Figure 24). The solvent exposed lysine residues are frequently dimethylated when a sufficient amount of formaldehyde is present.

The reductive methylation technique offers several advantages. First, proteins purified from their native hosts can be directly used for enrichment with stable isotopes. In this way, the protein molecules are likely to retain their correct fold and post-translational modifications. Second, since only a small amount of ^{13}C-labeled formaldehyde is used in the reaction the reductive methylation procedure is significantly more economical than the traditional isotope enrichment protocols. Finally, the use of ^{13}C-labeled methyl groups in lysines offers an opportunity to observe NMR signals with favorable relaxation properties in large molecular weight proteins due to reduced order parameters for lysine side-chains (*125*). In this report we not only demonstrate that observation of NMR signals in high molecular weight non-isotope enriched proteins is possible but also that investigation of conformational changes due to binding in protein-protein complexes is amenable to solution state NMR through reductive methylation.

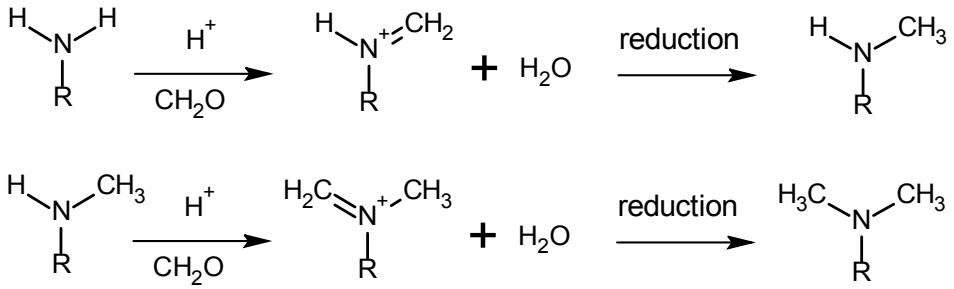

Figure 26. Schematic of reductive methylation reaction.
In the presence of formaldehyde and a reducing agent a methyl group is added to an ε-amino group of a lysine residue or the N-terminal α-amino group through the formation of a intermediate imine (A). In the presence of sufficient reagents the reaction proceeds rapidly to give rise to the di-methylated product (B). The di-methylated lysines still retain their net positive charge.

II. ACTIN, TROPOMYOSIN, AND TROPOMYOSIN COMPLEX

2.1. Introduction

Muscle contraction is caused by cyclic interaction between myosin and actin filaments. In cardiac muscle, regulation of contraction is controlled by the troponin complex and tropomyosin which bind to the actin filament (*142-144*). The actin filaments consist of polymerized actin (F-actin) molecules which contain myosin binding sites. At rest, the myosin binding site is concealed by tropomyosin forming a coiled-coil dimer that lies in the two grooves of actin. Seven actin molecules interact with one tropomyosin dimer. Each tropomyosin dimer also binds one troponin complex composed of three subunits: troponin C, troponin I, and troponin T. The N-terminal domain of troponin C has a calcium binding pocket. The troponin complex, together with tropomyosin, regulates muscle contraction in a Ca^{2+}-dependent manner. This is accomplished by altering accessibility of actin binding sites to myosin. Being a Ca^{2+} sensor, troponin functions as an on/off switch for muscle contraction. Muscle contraction occurs when Ca^{2+} binds to the regulatory site in troponin. Conversely, the muscle relaxes when Ca^{2+} dissociates. When Ca^{2+} concentration is high, Ca^{2+} binding to troponin C induces a structural change in the troponin complex that causes relocation of tropomyosin away from the actin groove. Due to tropomyosin relocation, the myosin binding site on actin is exposed and cross-bridge formation is initiated between actin and myosin. Troponin I is known to inhibit myosin cross-bridge formation by inducing relocation of tropomyosin. Troponin T associates with troponin C and I to form the complete troponin complex. Troponin T also binds to tropomyosin and actin to inhibit myosin binding to thin filaments.

Alpha-helical coiled-coil tropomyosin assembles into filaments in the end-to-end configuration and interacts with actin polymers. When bound to polymerized actin, the tropomyosin filament spans seven consecutive actin monomers forming a 369 kDa complex. One troponin binds to each tropomyosin coiled-coil dimer such that the molecular ratio for actin, tropomyosin, and troponin is 7:2:1. There are two kinds of interaction between the troponin complex and actin-tropomyosin. One is Ca^{2+}-independent binding through troponin T, anchoring the troponin complex to actin-tropomyosin. The other is Ca^{2+}-dependent regulatory interactions through inhibitory C-terminal half of troponin I, turning muscle contraction "on" and "off". The cytoplasmic Ca^{2+} concentration is essential for muscle contraction. However, allosteric regulation of the troponin complex is also known to be an important contributor. Solution NMR can detect conformational changes in protein molecules and thus is a good tool to study the allosteric regulation. We utilize the reductive methylation technique because the thin fiber is a large protein-protein complex containing molecules that are difficult to produce as recombinant proteins for enrichment with stable isotopes.

2.2 Materials and methods

Globular actin was dialyzed into 10 mM phosphate buffered saline, pH 7.4, 0.1 mM $MgCl_2$, 1 mM dithiothreitol, 0.1 mM ATP, and 0.01 % NaN_3, to make actin filaments. Initially 20 mM borane ammonia complex and 40 mM ^{13}C-formaldehyde (20% w/w in H_2O) were added into 0.7 ml of 60 μM F-actin and the mixture was stirred for 2 hours at 4 °C. Addition of borane ammonia complex and ^{13}C-formaldehyde was repeated and mixture was incubated for another 2 hours at 4°C. After incubation, 10 mM borane ammonia complex was added to the mixture. The mixture was incubated at 4 °C with stirring overnight. To quench the reaction, the 50 μl of 2M Tris-HCl was added. To study the change in actin structures upon binding of tropomyosin,

tropomyosin is added into ^{13}C methylated F-actin to make 7.5 μM of final tropomyosin concentration whereas the concentration of F-actin is 37 μM. The molar ratio of actin and tropomyosin was 5 to 1. The samples were dialyzed against 10 mM phosphate buffered saline, pH 7.4, with 1 mM $MgCl_2$, 0.1 mM ATP, 0.01 % NaN_3 and 10% D_2O was added for further NMR experiments. All NMR experminents were carried out on Bruker Avance 600 or 900 NMR spectrometers equipped with cryogenic probes. The 2D ^{1}H-^{13}C HSQC experiments were processed with NMRPipe software (*66*)

2.3 Results

To assess conformational changes occurring in polymerized actin upon binding tropomyosin we performed a reductive methylation reaction on actin and carried out ^{1}H-^{13}C HSQC experiments on actin alone and on actin in the presence of tropomyosin (Figure 25). In the spectrum of polymerized actin seven out of nineteen expected signals were observable. Significant chemical shift changes in four out of seven signals in actin were detected upon tropomyosin binding. Lysines are evenly distributed in the actin structure with no accumulation in any one particular area (Figure 26). Therefore, the data shown here indicates that binding of tropomyosin causes a global conformational change in the structure of polymerized actin even though we are not able to assign the seven signals. This observation is contrary to many computational models that propose that tropomyosin binding sites in actin are small and global changes do not occur in the actin-tropomyosin complex.

Next, we wish to address whether the troponin complex is able to control muscle contraction in a Ca^{2+}-independent mode. In order to test allosteric regulation of troponin

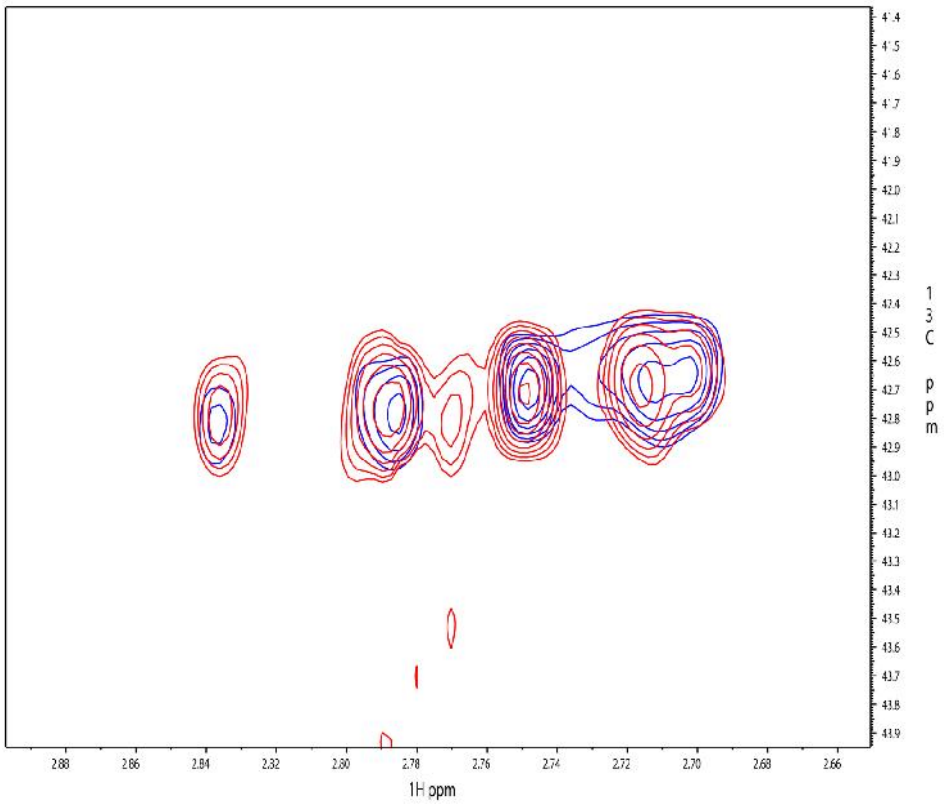

Figure 27. The overlay of partial ^{1}H-^{13}C HSQC spectra of reductively methylated actin (blue) and reductively methylated actin with tropomyosin (red).

The 37 μM of actin and the 37 μM of actin with 7.5 μM of tropomyosin were dissolved in the PBS buffer, pH 7.4 containing 0.1 mM ATP, 1 mM $MgCl_2$, 0.01 % NaN_3, 1 mM DTT.

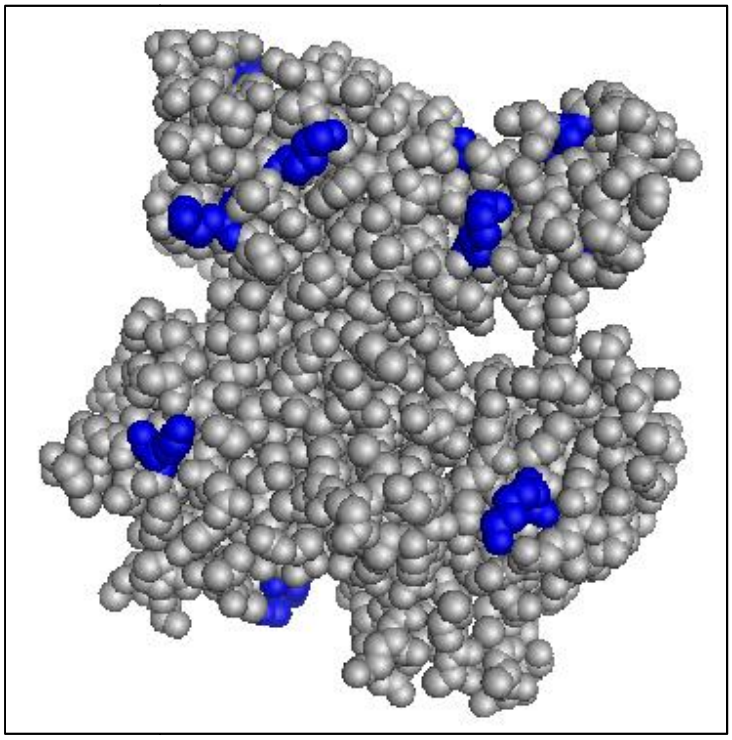

Figure 28. Overall structure of globular actin (PDB: 1ATN).
18 Lysine residues colored in blue are distributed evenly in the G-actin structure.

complex, the inhibitory domain of human cardiac Troponin I, $G^{1}KWKRPTLRRVRISAD^{16}$, was synthesized and was added into either methylated actin filaments or complex of methylated f-actin and tropomyosin in the abcense of Ca^{2+}. We observed that three signals of reductively methylated actin are shifted upon addition of inhibitory peptide (Figure 27A) .The inhibitory peptide also caused chemical shift perturbation of methylated actin filaments in the presence of tropomyosin (Figure 27B). The binding of inhibitory peptide, however, induce actin conformational changes differently depending on presence of tropomyosin.

2.4 Discussion

Using cardiac troponin C as a model system, for which structural information is available, we confirmed that the proposed methodology allows detection of conformational rearrangements in cardiac troponin C upon Ca^{2+} binding. This was done in the context of the full-length troponin complex. Similar experiments would have been very difficult to perform using conventional NMR approaches due to the high molecular weight limitation. We show that reductive methylation can be used to discover novel conformational changes in a 369 kDa actin-tropomyosin complex. For the first time we show that actin undergoes a global conformational change upon tropomyosin binding. We also observed different chemical shifts perturbations of reductively methylated actin upon addition of the inhibitory peptide in the presence or absence of tropomyosin. Also these interactions between inhibitory peptide and actin or actin-tropomyosin complex were observed in the absence of Ca^{2+}. It suggests that inhibitory peptide of troponin I may work tropomyosin and Ca^{2+} independently. This observation would support the inhibition mechanism of troponin I.

This appears to be the only way such molecular events can be observed. The available computational models were unable to predict this phenomenon. Electron microscopy images of the cardiac thin fiber are too low resolution to detect a conformational change in actin. Crystallization of polymerized actin is not feasible due to heterogeneity of actin fibers. In addition, there is no good procedure for production of recombinant actin that would allow traditional approaches for stable isotope enrichment for NMR. The functional significance of actin conformational rearrangements upon binding of tropomyosin is still under investigation. However, the discovery that these conformational changes occur in actin is a significant step forward.

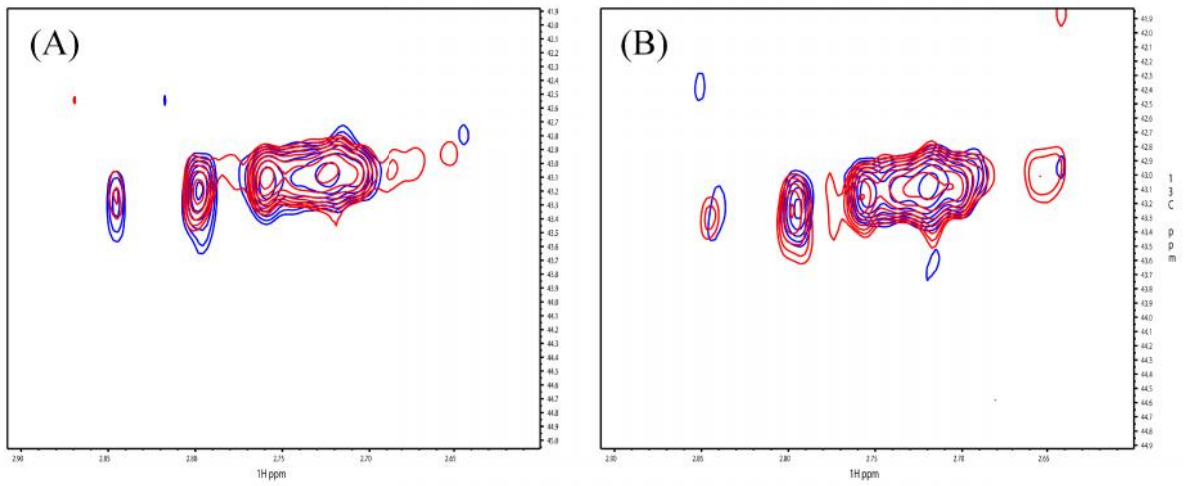

Figure 29. The overlay of ^{1}H-^{13}C HSQC spectra showing that inhibitory peptide binds to actin filaments different ways depending on the presence of tropomyosin.

The overlay of ^{1}H-^{13}C HSQC spectra of (A) reductively methylated actin filaments (blue) and methylated actin filaments with inhibitory peptide (red) and (B) reductively methylated actin filaments with tropomyosin (blue) and reductively methylated actin filaments with tropomyosin and inhibitory peptide (red).

II. CONCLUSION

In conclusion, we have described an important novel application of the reductive methylation methodology to observation of conformational changes in high molecular weight protein-protein complexes by NMR. In the previous Chapter, we showed that surface exposed lysine residues of CXCR4 inserted in the plasma membrane was successfully labelled with ^{13}C using reductive methylation and the reductively methylation signals of CXCR4 were sensitive enough to detect conformational changes of the receptor upon bound to the peptide antagonist or chemokine. The reductive methylation technique accompanied with solution NMR will be applied to study the protein-protein interactions undoubtedly. It has been known that membrane proteins, including transmembrane proteins and integral membrane proteins are important signal transducer. Moreover, membrane receptors have been drug targets for the treatment of many diseases. However, there are difficulties in studying a membrane protein structure due to aggregation and unnatural structures in available regular buffers or membrane mimic conditions. We demonstrated the crude membrane preparation with high level of CXCR4 expression can be applied for solution NMR spectroscopy using reductive methylation. We also showed that reductive methylation can be used to discover conformational changes in a 371 kDa actin-tropomyosin-inhibitory peptide complex in the Chapter 2. This reveals that conventional NMR overcomes its disadvantages such as molecular weight limitation and high expenses for ^{13}C and ^{15}N labelling.

REFERENCES

1. Miao, Z., Luker, K. E., Summers, B. C., Berahovich, R., Bhojani, M. S., Rehemtulla, A., Kleer, C. G., Essner, J. J., Nasevicius, A., Luker, G. D., Howard, M. C., and Schall, T. J. (2007) CXCR7 (RDC1) promotes breast and lung tumor growth in vivo and is expressed on tumor-associated vasculature, *Proceedings of the National Academy of Sciences of the United States of America 104*, 15735-15740.
2. Murdoch, C. (2000) CXCR4: chemokine receptor extraordinaire, *Immunological reviews 177*, 175-184.
3. Nagasawa, T., Tachibana, K., and Kishimoto, T. (1998) A novel CXC chemokine PBSF/SDF-1 and its receptor CXCR4: their functions in development, hematopoiesis and HIV infection, *Seminars in immunology 10*, 179-185.
4. De La Luz Sierra, M., Yang, F., Narazaki, M., Salvucci, O., Davis, D., Yarchoan, R., Zhang, H. H., Fales, H., and Tosato, G. (2004) Differential processing of stromal-derived factor-1alpha and stromal-derived factor-1beta explains functional diversity, *Blood 103*, 2452-2459.
5. Imai, K., Kobayashi, M., Wang, J., Shinobu, N., Yoshida, H., Hamada, J., Shindo, M., Higashino, F., Tanaka, J., Asaka, M., and Hosokawa, M. (1999) Selective secretion of chemoattractants for haemopoietic progenitor cells by bone marrow endothelial cells: a possible role in homing of haemopoietic progenitor cells to bone marrow, *British journal of haematology 106*, 905-911.
6. Muller, A., Homey, B., Soto, H., Ge, N., Catron, D., Buchanan, M. E., McClanahan, T., Murphy, E., Yuan, W., Wagner, S. N., Barrera, J. L., Mohar, A., Verastegui, E., and Zlotnik, A. (2001) Involvement of chemokine receptors in breast cancer metastasis, *Nature 410*, 50-56.
7. Ponomaryov, T., Peled, A., Petit, I., Taichman, R. S., Habler, L., Sandbank, J., Arenzana-Seisdedos, F., Magerus, A., Caruz, A., Fujii, N., Nagler, A., Lahav, M., Szyper-Kravitz, M., Zipori, D., and Lapidot, T. (2000) Induction of the chemokine stromal-derived factor-1 following DNA damage improves human stem cell function, *The Journal of clinical investigation 106*, 1331-1339.
8. Zhou, Y. B., Gerchman, S. E., Ramakrishnan, V., Travers, A., and Muyldermans, S. (1998) Position and orientation of the globular domain of linker histone H5 on the nucleosome, *Nature 395*, 402-405.
9. Barbero, S., Bonavia, R., Bajetto, A., Porcile, C., Pirani, P., Ravetti, J. L., Zona, G. L., Spaziante, R., Florio, T., and Schettini, G. (2003) Stromal cell-derived factor 1alpha stimulates human glioblastoma cell growth through the activation of both extracellular signal-regulated kinases 1/2 and Akt, *Cancer research 63*, 1969-1974.
10. Babcock, G. J., Farzan, M., and Sodroski, J. (2003) Ligand-independent dimerization of CXCR4, a principal HIV-1 coreceptor, *The Journal of biological chemistry 278*, 3378-3385.
11. Percherancier, Y., Berchiche, Y. A., Slight, I., Volkmer-Engert, R., Tamamura, H., Fujii, N., Bouvier, M., and Heveker, N. (2005) Bioluminescence resonance energy transfer reveals ligand-induced conformational changes in CXCR4 homo- and heterodimers, *The Journal of biological chemistry 280*, 9895-9903.

12. Wang, J., He, L., Combs, C. A., Roderiquez, G., and Norcross, M. A. (2006) Dimerization of CXCR4 in living malignant cells: control of cell migration by a synthetic peptide that reduces homologous CXCR4 interactions, *Molecular cancer therapeutics 5*, 2474-2483.
13. Kalatskaya, I., Berchiche, Y. A., Gravel, S., Limberg, B. J., Rosenbaum, J. S., and Heveker, N. (2009) AMD3100 is a CXCR7 ligand with allosteric agonist properties, *Molecular pharmacology 75*, 1240-1247.
14. Sohy, D., Yano, H., de Nadai, P., Urizar, E., Guillabert, A., Javitch, J. A., Parmentier, M., and Springael, J. Y. (2009) Hetero-oligomerization of CCR2, CCR5, and CXCR4 and the protean effects of "selective" antagonists, *The Journal of biological chemistry 284*, 31270-31279.
15. Vila-Coro, A. J., Rodriguez-Frade, J. M., Martin De Ana, A., Moreno-Ortiz, M. C., Martinez, A. C., and Mellado, M. (1999) The chemokine SDF-1alpha triggers CXCR4 receptor dimerization and activates the JAK/STAT pathway, *Faseb J 13*, 1699-1710.
16. Feng, Y., Broder, C. C., Kennedy, P. E., and Berger, E. A. (1996) HIV-1 entry cofactor: functional cDNA cloning of a seven-transmembrane, G protein-coupled receptor, *Science 272*, 872-877.
17. Steen, A., Schwartz, T. W., and Rosenkilde, M. M. (2009) Targeting CXCR4 in HIV cell-entry inhibition, *Mini reviews in medicinal chemistry 9*, 1605-1621.
18. Kuritzkes, D. R. (2009) HIV-1 entry inhibitors: an overview, *Current opinion in HIV and AIDS 4*, 82-87.
19. Donzella, G. A., Schols, D., Lin, S. W., Este, J. A., Nagashima, K. A., Maddon, P. J., Allaway, G. P., Sakmar, T. P., Henson, G., De Clercq, E., and Moore, J. P. (1998) AMD3100, a small molecule inhibitor of HIV-1 entry via the CXCR4 co-receptor, *Nature medicine 4*, 72-77.
20. Bachelder, R. E., Wendt, M. A., and Mercurio, A. M. (2002) Vascular endothelial growth factor promotes breast carcinoma invasion in an autocrine manner by regulating the chemokine receptor CXCR4, *Cancer research 62*, 7203-7206.
21. Bogenrieder, T., and Herlyn, M. (2003) Axis of evil: molecular mechanisms of cancer metastasis, *Oncogene 22*, 6524-6536.
22. Geminder, H., Sagi-Assif, O., Goldberg, L., Meshel, T., Rechavi, G., Witz, I. P., and Ben-Baruch, A. (2001) A possible role for CXCR4 and its ligand, the CXC chemokine stromal cell-derived factor-1, in the development of bone marrow metastases in neuroblastoma, *J Immunol 167*, 4747-4757.
23. Naora, H., and Montell, D. J. (2005) Ovarian cancer metastasis: integrating insights from disparate model organisms, *Nat Rev Cancer 5*, 355-366.
24. Zeelenberg, I. S., Ruuls-Van Stalle, L., and Roos, E. (2003) The chemokine receptor CXCR4 is required for outgrowth of colon carcinoma micrometastases, *Cancer research 63*, 3833-3839.
25. Erler, J. T., Bennewith, K. L., Nicolau, M., Dornhofer, N., Kong, C., Le, Q. T., Chi, J. T., Jeffrey, S. S., and Giaccia, A. J. (2006) Lysyl oxidase is essential for hypoxia-induced metastasis, *Nature 440*, 1222-1226.
26. Liu, Y. L., Yu, J. M., Song, X. R., Wang, X. W., Xing, L. G., and Gao, B. B. (2006) Regulation of the chemokine receptor CXCR4 and metastasis by hypoxia-inducible factor in non small cell lung cancer cell lines, *Cancer biology & therapy 5*, 1320-1326.

27. Schioppa, T., Uranchimeg, B., Saccani, A., Biswas, S. K., Doni, A., Rapisarda, A., Bernasconi, S., Saccani, S., Nebuloni, M., Vago, L., Mantovani, A., Melillo, G., and Sica, A. (2003) Regulation of the chemokine receptor CXCR4 by hypoxia, *The Journal of experimental medicine 198*, 1391-1402.
28. Xu, Q., Yuan, X., Xu, M., McLafferty, F., Hu, J., Lee, B. S., Liu, G., Zeng, Z., Black, K. L., and Yu, J. S. (2009) Chemokine CXC receptor 4--mediated glioma tumor tracking by bone marrow--derived neural progenitor/stem cells, *Molecular cancer therapeutics 8*, 2746-2753.
29. Sauve, K., Lepage, J., Sanchez, M., Heveker, N., and Tremblay, A. (2009) Positive feedback activation of estrogen receptors by the CXCL12-CXCR4 pathway, *Cancer research 69*, 5793-5800.
30. De Falco, V., Guarino, V., Avilla, E., Castellone, M. D., Salerno, P., Salvatore, G., Faviana, P., Basolo, F., Santoro, M., and Melillo, R. M. (2007) Biological role and potential therapeutic targeting of the chemokine receptor CXCR4 in undifferentiated thyroid cancer, *Cancer research 67*, 11821-11829.
31. Ohira, S., Sasaki, M., Harada, K., Sato, Y., Zen, Y., Isse, K., Kozaka, K., Ishikawa, A., Oda, K., Nimura, Y., and Nakanuma, Y. (2006) Possible regulation of migration of intrahepatic cholangiocarcinoma cells by interaction of CXCR4 expressed in carcinoma cells with tumor necrosis factor-alpha and stromal-derived factor-1 released in stroma, *The American journal of pathology 168*, 1155-1168.
32. Ottaiano, A., Franco, R., Aiello Talamanca, A., Liguori, G., Tatangelo, F., Delrio, P., Nasti, G., Barletta, E., Facchini, G., Daniele, B., Di Blasi, A., Napolitano, M., Ierano, C., Calemma, R., Leonardi, E., Albino, V., De Angelis, V., Falanga, M., Boccia, V., Capuozzo, M., Parisi, V., Botti, G., Castello, G., Vincenzo Iaffaioli, R., and Scala, S. (2006) Overexpression of both CXC chemokine receptor 4 and vascular endothelial growth factor proteins predicts early distant relapse in stage II-III colorectal cancer patients, *Clin Cancer Res 12*, 2795-2803.
33. Smith, M. C., Luker, K. E., Garbow, J. R., Prior, J. L., Jackson, E., Piwnica-Worms, D., and Luker, G. D. (2004) CXCR4 regulates growth of both primary and metastatic breast cancer, *Cancer research 64*, 8604-8612.
34. Tamamura, H., Fujisawa, M., Hiramatsu, K., Mizumoto, M., Nakashima, H., Yamamoto, N., Otaka, A., and Fujii, N. (2004) Identification of a CXCR4 antagonist, a T140 analog, as an anti-rheumatoid arthritis agent, *FEBS letters 569*, 99-104.
35. Arakaki, R., Tamamura, H., Premanathan, M., Kanbara, K., Ramanan, S., Mochizuki, K., Baba, M., Fujii, N., and Nakashima, H. (1999) T134, a small-molecule CXCR4 inhibitor, has no cross-drug resistance with AMD3100, a CXCR4 antagonist with a different structure, *Journal of virology 73*, 1719-1723.
36. Doranz, B. J., Filion, L. G., Diaz-Mitoma, F., Sitar, D. S., Sahai, J., Baribaud, F., Orsini, M. J., Benovic, J. L., Cameron, W., and Doms, R. W. (2001) Safe use of the CXCR4 inhibitor ALX40-4C in humans, *AIDS research and human retroviruses 17*, 475-486.
37. Doranz, B. J., Grovit-Ferbas, K., Sharron, M. P., Mao, S. H., Goetz, M. B., Daar, E. S., Doms, R. W., and O'Brien, W. A. (1997) A small-molecule inhibitor directed against the chemokine receptor CXCR4 prevents its use as an HIV-1 coreceptor, *The Journal of experimental medicine 186*, 1395-1400.
38. Murakami, T., Zhang, T. Y., Koyanagi, Y., Tanaka, Y., Kim, J., Suzuki, Y., Minoguchi, S., Tamamura, H., Waki, M., Matsumoto, A., Fujii, N., Shida, H., Hoxie, J. A., Peiper, S.

C., and Yamamoto, N. (1999) Inhibitory mechanism of the CXCR4 antagonist T22 against human immunodeficiency virus type 1 infection, *Journal of virology 73*, 7489-7496.

39. Bertolini, F., Dell'Agnola, C., Mancuso, P., Rabascio, C., Burlini, A., Monestiroli, S., Gobbi, A., Pruneri, G., and Martinelli, G. (2002) CXCR4 neutralization, a novel therapeutic approach for non-Hodgkin's lymphoma, *Cancer research 62*, 3106-3112.
40. Chen, Y., Stamatoyannopoulos, G., and Song, C. Z. (2003) Down-regulation of CXCR4 by inducible small interfering RNA inhibits breast cancer cell invasion in vitro, *Cancer research 63*, 4801-4804.
41. Zhang, J., Sarkar, S., and Yong, V. W. (2005) The chemokine stromal cell derived factor-1 (CXCL12) promotes glioma invasiveness through MT2-matrix metalloproteinase, *Carcinogenesis 26*, 2069-2077.
42. Heath, J. R., and Davis, M. E. (2008) Nanotechnology and cancer, *Annual review of medicine 59*, 251-265.
43. Shehata, M., Mukherjee, A., Sharma, R., and Chan, S. (2007) Liposomal doxorubicin in breast cancer, *Women's health (London, England) 3*, 557-569.
44. Patil, R. R., Guhagarkar, S. A., and Devarajan, P. V. (2008) Engineered nanocarriers of doxorubicin: a current update, *Critical reviews in therapeutic drug carrier systems 25*, 1-61.
45. Kratz, F. (2008) Albumin as a drug carrier: design of prodrugs, drug conjugates and nanoparticles, *J Control Release 132*, 171-183.
46. Abraham, S. A., Waterhouse, D. N., Mayer, L. D., Cullis, P. R., Madden, T. D., and Bally, M. B. (2005) The liposomal formulation of doxorubicin, *Methods in enzymology 391*, 71-97.
47. Wu, J., Akaike, T., Hayashida, K., Okamoto, T., Okuyama, A., and Maeda, H. (2001) Enhanced vascular permeability in solid tumor involving peroxynitrite and matrix metalloproteinases, *Jpn J Cancer Res 92*, 439-451.
48. Cirstoiu-Hapca, A., Bossy-Nobs, L., Buchegger, F., Gurny, R., and Delie, F. (2007) Differential tumor cell targeting of anti-HER2 (Herceptin) and anti-CD20 (Mabthera) coupled nanoparticles, *International journal of pharmaceutics 331*, 190-196.
49. Agarwal, A., Saraf, S., Asthana, A., Gupta, U., Gajbhiye, V., and Jain, N. K. (2008) Ligand based dendritic systems for tumor targeting, *International journal of pharmaceutics 350*, 3-13.
50. Simon, B. H., Ando, H. Y., and Gupta, P. K. (1995) Circulation time and body distribution of 14C-labeled amino-modified polystyrene nanoparticles in mice, *Journal of pharmaceutical sciences 84*, 1249-1253.
51. Nornoo, A. O., and Chow, D. S. (2008) Cremophor-free intravenous microemulsions for paclitaxel II. Stability, in vitro release and pharmacokinetics, *International journal of pharmaceutics 349*, 117-123.
52. Hamilton, A., Biganzoli, L., Coleman, R., Mauriac, L., Hennebert, P., Awada, A., Nooij, M., Beex, L., Piccart, M., Van Hoorebeeck, I., Bruning, P., and de Valeriola, D. (2002) EORTC 10968: a phase I clinical and pharmacokinetic study of polyethylene glycol liposomal doxorubicin (Caelyx, Doxil) at a 6-week interval in patients with metastatic breast cancer. European Organization for Research and Treatment of Cancer, *Ann Oncol 13*, 910-918.

53. Haubner, R., Wester, H. J., Burkhart, F., Senekowitsch-Schmidtke, R., Weber, W., Goodman, S. L., Kessler, H., and Schwaiger, M. (2001) Glycosylated RGD-containing peptides: tracer for tumor targeting and angiogenesis imaging with improved biokinetics, *J Nucl Med 42*, 326-336.
54. Kim, T. H., Lee, H., and Park, T. G. (2002) Pegylated recombinant human epidermal growth factor (rhEGF) for sustained release from biodegradable PLGA microspheres, *Biomaterials 23*, 2311-2317.
55. Wang, Z. X., Berson, J. F., Zhang, T. Y., Cen, Y. H., Sun, Y., Sharron, M., Lu, Z. H., and Peiper, S. C. (1998) CXCR4 sequences involved in coreceptor determination of human immunodeficiency virus type-1 tropism. Unmasking of activity with M-tropic Env glycoproteins, *The Journal of biological chemistry 273*, 15007-15015.
56. Raman, S., Machaidze, G., Lustig, A., Aebi, U., and Burkhard, P. (2006) Structure-based design of peptides that self-assemble into regular polyhedral nanoparticles, *Nanomedicine 2*, 95-102.
57. Qiu, J., Wei, X. H., Geng, F., Liu, R., Zhang, J. W., and Xu, Y. H. (2005) Multivesicular liposome formulations for the sustained delivery of interferon alpha-2b, *Acta pharmacologica Sinica 26*, 1395-1401.
58. Reches, M., and Gazit, E. (2006) Molecular self-assembly of peptide nanostructures: mechanism of association and potential uses, *Curr Nanosci 2*, 105-111.
59. Reches, M., and Gazit, E. (2006) Designed aromatic homo-dipeptides: formation of ordered nanostructures and potential nanotechnological applications, *Physical biology 3*, S10-19.
60. Singh, S. Nanomedicine-nanoscale drugs and delivery systems, *Journal of nanoscience and nanotechnology 10*, 7906-7918.
61. Nie, S., Xing, Y., Kim, G. J., and Simons, J. W. (2007) Nanotechnology applications in cancer, *Annual review of biomedical engineering 9*, 257-288.
62. Tarasov, S. G., Gaponenko, V., Howard, O. M. Z., Chen, Y., Oppenheim, J. J., Dyba, M. A., Subramaniam, S., Lee, Y., Michejda, C. J., and Tarasova, N. I. (2011) Structural plasticity of a transmembrane peptide allows selfassembly into biologically active nanoparticles, *Proceedings of the National Academy of Sciences of the United States of America 108*, 9798-9803.
63. Brasseur, R., De Meutter, J., Goormaghtigh, E., and Ruysschaert, J. M. (1983) Mode of organization of galactolipids: a conformational analysis, *Biochemical and biophysical research communications 115*, 666-672.
64. Nieto-Draghi, C., Bonet Ávalos, J., and Rousseau, B. (2003) Transport properties of dimethyl sulfoxide aqueous solutions *J. Chem. Phys 119*, 4782-4789.
65. Viggiano, G., Ragozzino, E., D'Ambrosio, L., and Santamaria, R. (1973) Water-DMSO and water-DMSO-urea systems, *Bollettino chimico farmaceutico 112*, 746-752.
66. Delaglio, F., Grzesiek, S., Vuister, G. W., Zhu, G., Pfeifer, J., and Bax, A. (1995) NMRPipe: a multidimensional spectral processing system based on UNIX pipes, *Journal of biomolecular NMR 6*, 277-293.
67. Cornilescu, G., Delaglio, F., and Bax, A. (1999) Protein backbone angle restraints from searching a database for chemical shift and sequence homology, *Journal of biomolecular NMR 13*, 289-302.
68. Brunger, A. T., Adams, P. D., Clore, G. M., DeLano, W. L., Gros, P., Grosse-Kunstleve, R. W., Jiang, J. S., Kuszewski, J., Nilges, M., Pannu, N. S., Read, R. J., Rice, L. M.,

Simonson, T., and Warren, G. L. (1998) Crystallography & NMR system: A new software suite for macromolecular structure determination, *Acta crystallographica 54*, 905-921.

69. Koradi, R., Billeter, M., and Wuthrich, K. (1996) MOLMOL: a program for display and analysis of macromolecular structures, *Journal of molecular graphics 14*, 51-55, 29-32.
70. Tarasova, N. I., Rice, W. G., and Michejda, C. J. (1999) Inhibition of G-protein-coupled receptor function by disruption of transmembrane domain interactions, *The Journal of biological chemistry 274*, 34911-34915.
71. Toyama, B. H., Kelly, M. J., Gross, J. D., and Weissman, J. S. (2007) The structural basis of yeast prion strain variants, *Nature 449*, 233-237.
72. Wolfe, L. S., Calabrese, M. F., Nath, A., Blaho, D. V., Miranker, A. D., and Xiong, Y. Protein-induced photophysical changes to the amyloid indicator dye thioflavin T, *Proceedings of the National Academy of Sciences of the United States of America 107*, 16863-16868.
73. LeVine, H., 3rd. (1993) Thioflavine T interaction with synthetic Alzheimer's disease beta-amyloid peptides: detection of amyloid aggregation in solution, *Protein Sci 2*, 404-410.
74. Ferreira, S. A., Coutinho, P. J., and Gama, F. M. Self-assembled nanogel made of mannan: synthesis and characterization, *Langmuir 26*, 11413-11420.
75. Park, K., Kim, K., Kwon, I. C., Kim, S. K., Lee, S., Lee, D. Y., and Byun, Y. (2004) Preparation and characterization of self-assembled nanoparticles of heparin-deoxycholic acid conjugates, *Langmuir 20*, 11726-11731.
76. Wilhelm, M., Zhao, C. L., Wang, Y., Xu, R., Winnik, M. A., Mura, J. L., Riess, G., and Croucher, M. D. (1991) Poly(styrene-ethylene oxide) block copolymer micelle formation in water: a fluorescence probe study, *Macromolecules 24*, 1033-1049.
77. Liu, L., Guo, K., Lu, J., Venkatraman, S. S., Luo, D., Ng, K. C., Ling, E. A., Moochhala, S., and Yang, Y. Y. (2008) Biologically active core/shell nanoparticles self-assembled from cholesterol-terminated PEG-TAT for drug delivery across the blood-brain barrier, *Biomaterials 29*, 1509-1517.
78. Choi, H., Ahn, J. Y., Sim, S. J., and Lee, J. (2005) Glutamate decarboxylase-derived IDDM autoantigens displayed on self-assembled protein nanoparticles, *Biochemical and biophysical research communications 327*, 604-608.
79. Dreher, M. R., Simnick, A. J., Fischer, K., Smith, R. J., Patel, A., Schmidt, M., and Chilkoti, A. (2008) Temperature triggered self-assembly of polypeptides into multivalent spherical micelles, *Journal of the American Chemical Society 130*, 687-694.
80. Hamley, I. W. (2007) Peptide fibrillization, *Angewandte Chemie (International ed 46*, 8128-8147.
81. Sandberg, A., Luheshi, L. M., Sollvander, S., Pereira de Barros, T., Macao, B., Knowles, T. P., Biverstal, H., Lendel, C., Ekholm-Petterson, F., Dubnovitsky, A., Lannfelt, L., Dobson, C. M., and Hard, T. Stabilization of neurotoxic Alzheimer amyloid-beta oligomers by protein engineering, *Proceedings of the National Academy of Sciences of the United States of America 107*, 15595-15600.
82. Reches, M., and Gazit, E. (2003) Casting metal nanowires within discrete self-assembled peptide nanotubes, *Science (New York, N.Y 300*, 625-627.

83. Adler-Abramovich, L., Aronov, D., Beker, P., Yevnin, M., Stempler, S., Buzhansky, L., Rosenman, G., and Gazit, E. (2009) Self-assembled arrays of peptide nanotubes by vapour deposition, *Nature nanotechnology 4*, 849-854.
84. Kwon, S., Jeon, A., Yoo, S. H., Chung, I. S., and Lee, H. S. Unprecedented molecular architectures by the controlled self-assembly of a beta-peptide foldamer, *Angewandte Chemie (International ed 49*, 8232-8236.
85. Branco, M. C., and Schneider, J. P. (2009) Self-assembling materials for therapeutic delivery, *Acta biomaterialia 5*, 817-831.
86. Liu, L., Busuttil, K., Zhang, S., Yang, Y., Wang, C., Besenbacher, F., and Dong, M. The role of self-assembling polypeptides in building nanomaterials, *Phys Chem Chem Phys 13*, 17435-17444.
87. Zhao, X., Pan, F., Xu, H., Yaseen, M., Shan, H., Hauser, C. A., Zhang, S., and Lu, J. R. Molecular self-assembly and applications of designer peptide amphiphiles, *Chemical Society reviews 39*, 3480-3498.
88. van Hell, A. J., Costa, C. I., Flesch, F. M., Sutter, M., Jiskoot, W., Crommelin, D. J., Hennink, W. E., and Mastrobattista, E. (2007) Self-assembly of recombinant amphiphilic oligopeptides into vesicles, *Biomacromolecules 8*, 2753-2761.
89. Castelletto, V., and Hamley, I. W. (2009) Self assembly of a model amphiphilic phenylalanine peptide/polyethylene glycol block copolymer in aqueous solution, *Biophysical chemistry 141*, 169-174.
90. Dong, Y., and Feng, S. S. (2004) Methoxy poly(ethylene glycol)-poly(lactide) (MPEG-PLA) nanoparticles for controlled delivery of anticancer drugs, *Biomaterials 25*, 2843-2849.
91. Xiao, R. Z., Zeng, Z. W., Zhou, G. L., Wang, J. J., Li, F. Z., and Wang, A. M. Recent advances in PEG-PLA block copolymer nanoparticles, *International journal of nanomedicine 5*, 1057-1065.
92. Reed, C. R., Han, L., Andrady, A., Caballero, M., Jack, M. C., Collins, J. B., Saba, S. C., Loboa, E. G., Cairns, B. A., and van Aalst, J. A. (2009) Composite tissue engineering on polycaprolactone nanofiber scaffolds, *Annals of plastic surgery 62*, 505-512.
93. Bhattacharyya, S., Kumbar, S. G., Khan, Y. M., Nair, L. S., Singh, A., Krogman, N. R., Brown, P. W., Allcock, H. R., and Laurencin, C. T. (2009) Biodegradable polyphosphazene-nanohydroxyapatite composite nanofibers: scaffolds for bone tissue engineering, *Journal of biomedical nanotechnology 5*, 69-75.
94. Kuperstein, I., Broersen, K., Benilova, I., Rozenski, J., Jonckheere, W., Debulpaep, M., Vandersteen, A., Segers-Nolten, I., Van Der Werf, K., Subramaniam, V., Braeken, D., Callewaert, G., Bartic, C., D'Hooge, R., Martins, I. C., Rousseau, F., Schymkowitz, J., and De Strooper, B. Neurotoxicity of Alzheimer's disease Abeta peptides is induced by small changes in the Abeta42 to Abeta40 ratio, *The EMBO journal 29*, 3408-3420.
95. Finder, V. H., Vodopivec, I., Nitsch, R. M., and Glockshuber, R. The recombinant amyloid-beta peptide Abeta1-42 aggregates faster and is more neurotoxic than synthetic Abeta1-42, *Journal of molecular biology 396*, 9-18.
96. Balkwill, F. (2004) The significance of cancer cell expression of the chemokine receptor CXCR4, *Seminars in cancer biology 14*, 171-179.
97. Libura, J., Drukala, J., Majka, M., Tomescu, O., Navenot, J. M., Kucia, M., Marquez, L., Peiper, S. C., Barr, F. G., Janowska-Wieczorek, A., and Ratajczak, M. Z. (2002) CXCR4-

SDF-1 signaling is active in rhabdomyosarcoma cells and regulates locomotion, chemotaxis, and adhesion, *Blood 100*, 2597-2606.

98. Holm, N. T., Abreo, F., Johnson, L. W., Li, B. D., and Chu, Q. D. (2009) Elevated chemokine receptor CXCR4 expression in primary tumors following neoadjuvant chemotherapy predicts poor outcomes for patients with locally advanced breast cancer (LABC), *Breast cancer research and treatment 113*, 293-299.
99. Li, Y. M., Pan, Y., Wei, Y., Cheng, X., Zhou, B. P., Tan, M., Zhou, X., Xia, W., Hortobagyi, G. N., Yu, D., and Hung, M. C. (2004) Upregulation of CXCR4 is essential for HER2-mediated tumor metastasis, *Cancer cell 6*, 459-469.
100. Zagzag, D., Krishnamachary, B., Yee, H., Okuyama, H., Chiriboga, L., Ali, M. A., Melamed, J., and Semenza, G. L. (2005) Stromal cell-derived factor-1alpha and CXCR4 expression in hemangioblastoma and clear cell-renal cell carcinoma: von Hippel-Lindau loss-of-function induces expression of a ligand and its receptor, *Cancer research 65*, 6178-6188.
101. Struckmann, K., Mertz, K., Staller, P., Krek, W., Schraml, P., and Moch, H. (2005) [mRNA expression analysis of metastatic markers in clear-cell renal cell carcinoma], *Verhandlungen der Deutschen Gesellschaft fur Pathologie 89*, 178-183.
102. Schimanski, C. C., Schwald, S., Simiantonaki, N., Jayasinghe, C., Gonner, U., Wilsberg, V., Junginger, T., Berger, M. R., Galle, P. R., and Moehler, M. (2005) Effect of chemokine receptors CXCR4 and CCR7 on the metastatic behavior of human colorectal cancer, *Clin Cancer Res 11*, 1743-1750.
103. Saigusa, S., Toiyama, Y., Tanaka, K., Yokoe, T., Okugawa, Y., Kawamoto, A., Yasuda, H., Inoue, Y., Miki, C., and Kusunoki, M. Stromal CXCR4 and CXCL12 expression is associated with distant recurrence and poor prognosis in rectal cancer after chemoradiotherapy, *Annals of surgical oncology 17*, 2051-2058.
104. Kim, J., Takeuchi, H., Lam, S. T., Turner, R. R., Wang, H. J., Kuo, C., Foshag, L., Bilchik, A. J., and Hoon, D. S. (2005) Chemokine receptor CXCR4 expression in colorectal cancer patients increases the risk for recurrence and for poor survival, *J Clin Oncol 23*, 2744-2753.
105. Laverdiere, C., Hoang, B. H., Yang, R., Sowers, R., Qin, J., Meyers, P. A., Huvos, A. G., Healey, J. H., and Gorlick, R. (2005) Messenger RNA expression levels of CXCR4 correlate with metastatic behavior and outcome in patients with osteosarcoma, *Clin Cancer Res 11*, 2561-2567.
106. Bennani-Baiti, I. M., Cooper, A., Lawlor, E. R., Kauer, M., Ban, J., Aryee, D. N., and Kovar, H. Intercohort gene expression co-analysis reveals chemokine receptors as prognostic indicators in Ewing's sarcoma, *Clin Cancer Res 16*, 3769-3778.
107. Vasudevan, S. A., Nuchtern, J. G., and Shohet, J. M. (2005) Gene profiling of high risk neuroblastoma, *World journal of surgery 29*, 317-324.
108. Russell, H. V., Hicks, J., Okcu, M. F., and Nuchtern, J. G. (2004) CXCR4 expression in neuroblastoma primary tumors is associated with clinical presentation of bone and bone marrow metastases, *Journal of pediatric surgery 39*, 1506-1511.
109. Scala, S., Ottaiano, A., Ascierto, P. A., Cavalli, M., Simeone, E., Giuliano, P., Napolitano, M., Franco, R., Botti, G., and Castello, G. (2005) Expression of CXCR4 predicts poor prognosis in patients with malignant melanoma, *Clin Cancer Res 11*, 1835-1841.
110. Muller, A., Sonkoly, E., Eulert, C., Gerber, P. A., Kubitza, R., Schirlau, K., Franken-Kunkel, P., Poremba, C., Snyderman, C., Klotz, L. O., Ruzicka, T., Bier, H., Zlotnik, A.,

Whiteside, T. L., Homey, B., and Hoffmann, T. K. (2006) Chemokine receptors in head and neck cancer: association with metastatic spread and regulation during chemotherapy, *International journal of cancer 118*, 2147-2157.

111. Kaifi, J. T., Yekebas, E. F., Schurr, P., Obonyo, D., Wachowiak, R., Busch, P., Heinecke, A., Pantel, K., and Izbicki, J. R. (2005) Tumor-cell homing to lymph nodes and bone marrow and CXCR4 expression in esophageal cancer, *Journal of the National Cancer Institute 97*, 1840-1847.
112. George, S. R., Lee, S. P., Varghese, G., Zeman, P. R., Seeman, P., Ng, G. Y., and O'Dowd, B. F. (1998) A transmembrane domain-derived peptide inhibits D1 dopamine receptor function without affecting receptor oligomerization, *The Journal of biological chemistry 273*, 30244-30248.
113. Hebert, T. E., Moffett, S., Morello, J. P., Loisel, T. P., Bichet, D. G., Barret, C., and Bouvier, M. (1996) A peptide derived from a beta2-adrenergic receptor transmembrane domain inhibits both receptor dimerization and activation, *The Journal of biological chemistry 271*, 16384-16392.
114. Partridge, A. W., Melnyk, R. A., Yang, D., Bowie, J. U., and Deber, C. M. (2003) A transmembrane segment mimic derived from Escherichia coli diacylglycerol kinase inhibits protein activity, *The Journal of biological chemistry 278*, 22056-22060.
115. Tarasova, N. I., Seth, R., Tarasov, S. G., Kosakowska-Cholody, T., Hrycyna, C. A., Gottesman, M. M., and Michejda, C. J. (2005) Transmembrane inhibitors of P-glycoprotein, an ABC transporter, *Journal of medicinal chemistry 48*, 3768-3775.
116. Yin, H., Slusky, J. S., Berger, B. W., Walters, R. S., Vilaire, G., Litvinov, R. I., Lear, J. D., Caputo, G. A., Bennett, J. S., and DeGrado, W. F. (2007) Computational design of peptides that target transmembrane helices, *Science (New York, N.Y 315*, 1817-1822.
117. Loetscher, P., Gong, J. H., Dewald, B., Baggiolini, M., and Clark-Lewis, I. (1998) N-terminal peptides of stromal cell-derived factor-1 with CXC chemokine receptor 4 agonist and antagonist activities, *The Journal of biological chemistry 273*, 22279-22283.
118. Crump, M. P., Gong, J. H., Loetscher, P., Rajarathnam, K., Amara, A., Arenzana-Seisdedos, F., Virelizier, J. L., Baggiolini, M., Sykes, B. D., and Clark-Lewis, I. (1997) Solution structure and basis for functional activity of stromal cell-derived factor-1; dissociation of CXCR4 activation from binding and inhibition of HIV-1, *The EMBO journal 16*, 6996-7007.
119. Baryshnikova, O. K., Rainey, J. K., and Sykes, B. D. (2005) Nuclear magnetic resonance studies of CXC chemokine receptor 4 allosteric peptide agonists in solution, *J Pept Res 66 Suppl 1*, 12-21.
120. Means, G. E., and Feeney, R. E. (1968) Reductive alkylation of amino groups in proteins, *Biochemistry 7*, 2192-2201.
121. Wu, B., Chien, E. Y., Mol, C. D., Fenalti, G., Liu, W., Katritch, V., Abagyan, R., Brooun, A., Wells, P., Bi, F. C., Hamel, D. J., Kuhn, P., Handel, T. M., Cherezov, V., and Stevens, R. C. Structures of the CXCR4 chemokine GPCR with small-molecule and cyclic peptide antagonists, *Science (New York, N.Y 330*, 1066-1071.
122. Brelot, A., Heveker, N., Pleskoff, O., Sol, N., and Alizon, M. (1997) Role of the first and third extracellular domains of CXCR-4 in human immunodeficiency virus coreceptor activity, *Journal of virology 71*, 4744-4751.

123. Brelot, A., Heveker, N., Montes, M., and Alizon, M. (2000) Identification of residues of CXCR4 critical for human immunodeficiency virus coreceptor and chemokine receptor activities, *The Journal of biological chemistry 275*, 23736-23744.
124. Abraham, S. J., Hoheisel, S., and Gaponenko, V. (2008) Detection of protein-ligand interactions by NMR using reductive methylation of lysine residues, *Journal of biomolecular NMR 42*, 143-148.
125. Abraham, S. J., Kobayashi, T., Solaro, R. J., and Gaponenko, V. (2009) Differences in lysine pKa values may be used to improve NMR signal dispersion in reductively methylated proteins, *Journal of biomolecular NMR 43*, 239-246.
126. Liang, Z., Brooks, J., Willard, M., Liang, K., Yoon, Y., Kang, S., and Shim, H. (2007) CXCR4/CXCL12 axis promotes VEGF-mediated tumor angiogenesis through Akt signaling pathway, *Biochemical and biophysical research communications 359*, 716-722.
127. Owens, D. E., 3rd, and Peppas, N. A. (2006) Opsonization, biodistribution, and pharmacokinetics of polymeric nanoparticles, *International journal of pharmaceutics 307*, 93-102.
128. Nishiyama, N., and Kataoka, K. (2006) Current state, achievements, and future prospects of polymeric micelles as nanocarriers for drug and gene delivery, *Pharmacology & therapeutics 112*, 630-648.
129. Uchegbu, I. F. (2006) Pharmaceutical nanotechnology: polymeric vesicles for drug and gene delivery, *Expert opinion on drug delivery 3*, 629-640.
130. Semete, B., Booysen, L., Lemmer, Y., Kalombo, L., Katata, L., Verschoor, J., and Swai, H. S. In vivo evaluation of the biodistribution and safety of PLGA nanoparticles as drug delivery systems, *Nanomedicine 6*, 662-671.
131. Chao, C., Ives, K., Hellmich, H. L., Townsend, C. M., Jr., and Hellmich, M. R. (2009) Gastrin-releasing peptide receptor in breast cancer mediates cellular migration and interleukin-8 expression, *The Journal of surgical research 156*, 26-31.
132. Maina, T., Nock, B., and Mather, S. (2006) Targeting prostate cancer with radiolabelled bombesins, *Cancer Imaging 6*, 153-157.
133. Reubi, C., Gugger, M., and Waser, B. (2002) Co-expressed peptide receptors in breast cancer as a molecular basis for in vivo multireceptor tumour targeting, *European journal of nuclear medicine and molecular imaging 29*, 855-862.
134. Bold, R. J., Lowry, P. S., Ishizuka, J., Battey, J. F., Townsend, C. M., Jr., and Thompson, J. C. (1994) Bombesin stimulates the in vitro growth of a human gastric cancer cell line, *Journal of cellular physiology 161*, 519-525.
135. Wider, G., and Wuthrich, K. (1999) NMR spectroscopy of large molecules and multimolecular assemblies in solution, *Current opinion in structural biology 9*, 594-601.
136. Pervushin, K., Riek, R., Wider, G., and Wuthrich, K. (1997) Attenuated T2 relaxation by mutual cancellation of dipole-dipole coupling and chemical shift anisotropy indicates an avenue to NMR structures of very large biological macromolecules in solution, *Proceedings of the National Academy of Sciences of the United States of America 94*, 12366-12371.
137. Schubot, F. D., and Waugh, D. S. (2004) A pivotal role for reductive methylation in the de novo crystallization of a ternary complex composed of Yersinia pestis virulence factors YopN, SycN and YscB, *Acta crystallographica 60*, 1981-1986.

138. Gerken, T. A., Jentoft, J. E., Jentoft, N., and Dearborn, D. G. (1982) Intramolecular interactions of amino groups in 13C reductively methylated hen egg-white lysozyme, *The Journal of biological chemistry 257*, 2894-2900.
139. Kurinov, I. V., Mao, C., Irvin, J. D., and Uckun, F. M. (2000) X-ray crystallographic analysis of pokeweed antiviral protein-II after reductive methylation of lysine residues, *Biochemical and biophysical research communications 275*, 549-552.
140. Rayment, I. (1997) Reductive alkylation of lysine residues to alter crystallization properties of proteins, *Methods in enzymology 276*, 171-179.
141. Walter, T. S., Meier, C., Assenberg, R., Au, K. F., Ren, J., Verma, A., Nettleship, J. E., Owens, R. J., Stuart, D. I., and Grimes, J. M. (2006) Lysine methylation as a routine rescue strategy for protein crystallization, *Structure 14*, 1617-1622.
142. Galinska-Rakoczy, A., Engel, P., Xu, C., Jung, H., Craig, R., Tobacman, L. S., and Lehman, W. (2008) Structural basis for the regulation of muscle contraction by troponin and tropomyosin, *Journal of molecular biology 379*, 929-935.
143. Kobayashi, T., Jin, L., and de Tombe, P. P. (2008) Cardiac thin filament regulation, *Pflugers Arch 457*, 37-46.
144. Kobayashi, T., and Solaro, R. J. (2005) Calcium, thin filaments, and the integrative biology of cardiac contractility, *Annual review of physiology 67*, 39-67.

APPENDIX

TABLE IV
NOES FOR STRUCTURE CALCULATION OF X4-2-1 MONOMER

assign	(residue 1 and name HA) (residue 2 and name HG)	5.0 3.2 0
assign	(residue 2 and name HN) (residue 21 and name HA#)	6.0 4.2 0
assign	(residue 2 and name HB#) (residue 3 and name HN)	5.0 3.2 0
assign	(residue 2 and name HB#) (residue 3 and name HA)	5.0 3.2 0
assign	(residue 2 and name HB#) (residue 3 and name HB#)	6.0 4.2 0
assign	(residue 2 and name HB#) (residue 3 and name HD#)	7.0 5.2 0
assign	(residue 2 and name HG#) (residue 3 and name HD#)	7.0 5.2 0
assign	(residue 2 and name HD*) (residue 19 and name HE#)	7.0 5.2 0
assign	(residue 3 and name HA) (residue 3 and name HB*)	3.5 1.7 0
assign	(residue 3 and name HA) (residue 4 and name HA)	5.0 3.2 0
assign	(residue 3 and name HA) (residue 4 and name HB)	6.0 4.2 0
assign	(residue 3 and name HA) (residue 16 and name HB#)	7.0 5.2 0
assign	(residue 3 and name HA) (residue 21 and name HA#)	6.0 4.2 0
assign	(residue 3 and name HB#) (residue 4 and name HB)	6.0 4.2 0
assign	(residue 3 and name HB#) (residue 5 and name HG2#)	7.0 5.2 0
assign	(residue 3 and name HB#) (residue 21 and name HA#)	7.0 5.2 0
assign	(residue 3 and name HD#) (residue 5 and name HG2#)	6.0 4.2 0
assign	(residue 3 and name HE#) (residue 5 and name HG2#)	7.0 5.2 0
assign	(residue 4 and name HN) (residue 4 and name HB)	5.0 3.2 0
assign	(residue 4 and name HA) (residue 15 and name HB)	6.0 4.2 0
assign	(residue 4 and name HA) (residue 17 and name HB#)	3.5 1.7 0
assign	(residue 4 and name HA) (residue 14 and name HB#)	6.0 4.2 0
assign	(residue 4 and name HB) (residue 5 and name HN)	6.0 4.2 0
assign	(residue 4 and name HB) (residue 6 and name HG2#)	7.0 5.2 0
assign	(residue 4 and name HB) (residue 15 and name HA)	6.0 4.2 0
assign	(residue 5 and name HB) (residue 6 and name HB)	6.0 4.2 0
assign	(residue 5 and name HB) (residue 6 and name HN)	6.0 4.2 0
assign	(residue 5 and name HG2#) (residue 6 and name HB)	6.0 4.2 0
assign	(residue 5 and name HG1#) (residue 6 and name HN)	6.0 4.2 0
assign	(residue 5 and name HD#) (residue 6 and name HN)	6.0 4.2 0
assign	(residue 6 and name HA) (residue 6 and name HB)	2.5 0.7 0
assign	(residue 6 and name HA) (residue 7 and name HA)	6.0 4.2 0
assign	(residue 6 and name HB) (residue 7 and name HA)	6.0 4.2 0
assign	(residue 6 and name HB) (residue 7 and name HG)	6.0 4.2 0
assign	(residue 6 and name HB) (residue 7 and name HB#)	6.0 4.2 0
assign	(residue 6 and name HB) (residue 7 and name HN)	6.0 4.2 0
assign	(residue 6 and name HB) (residue 8 and name HD#)	6.0 4.2 0

TABLE IV
NOES FOR STRUCTURE CALCULATION OF X4-2-1 MONOMER (continued)

assign	(residue 6 and name HG2#) (residue 7 and name HG)	6.0 4.2 0
assign	(residue 6 and name HG2#) (residue 8 and name HD#)	6.0 4.2 0
assign	(residue 6 and name HG2#) (residue 14 and name HA)	7.0 5.2 0
assign	(residue 6 and name HG2#) (residue 15 and name H	8.0 5.2 0
assign	(residue 7 and name HN) (residue 7 and name HG)	6.0 4.2 0
assign	(residue 7 and name HA) (residue 8 and name HB#)	6.0 4.2 0
assign	(residue 7 and name HA) (residue 8 and name HD#)	2.5 0.7 0
assign	(residue 7 and name HN) (residue 8 and name HD#)	6.0 4.2 0
assign	(residue 7 and name HB#) (residue 10 and name HE3)	6.0 5.2 0
assign	(residue 7 and name HB#) (residue 9 and name HD#)	6.0 4.2 0
assign	(residue 7 and name HG) (residue 9 and name HD#)	6.0 4.2 0
assign	(residue 7 and name HB#) (residue 8 and name HD#)	3.5 1.7 0
assign	(residue 7 and name HG) (residue 10 and name HE3)	7.0 5.2 0
assign	(residue 8 and name HA) (residue 9 and name HD*)	5.0 3.2 0
assign	(residue 8 and name HG#) (residue 10 and name HZ2)	6.0 4.2 0
assign	(residue 8 and name HB#) (residue 10 and name HZ2)	7.0 5.2 0
assign	(residue 8 and name HD#) (residue 9 and name HN)	6.0 4.2 0
assign	(residue 8 and name HB#) (residue 9 and name HA)	6.0 4.2 0
assign	(residue 8 and name HB#) (residue 9 and name HB#)	6.0 4.2 0
assign	(residue 8 and name HD#) (residue 11 and name HB#)	7.0 4.2 0
assign	(residue 8 and name HD#) (residue 14 and name HB#)	7.0 4.2 0
assign	(residue 8 and name HB#) (residue 11 and name HA)	6.0 4.2 0
assign	(residue 8 and name HG#) (residue 11 and name HA)	6.0 4.2 0
assign	(residue 8 and name HB#) (residue 11 and name HB#)	6.0 4.2 0
assign	(residue 8 and name HG#) (residue 11 and name HB#)	6.0 4.2 0
assign	(residue 8 and name HB#) (residue 13 and name HA)	6.0 4.2 0
assign	(residue 8 and name HD#) (residue 9 and name HD#)	7.0 5.2 0
assign	(residue 9 and name HN) (residue 9 and name HD#)	6.0 4.2 0
assign	(residue 9 and name HB#) (residue 10 and name HE3)	6.0 4.2 0
assign	(residue 9 and name HN) (residue 10 and name HB#)	6.0 4.2 0
assign	(residue 10 and name HB#) (residue 10 and name HZ2)	7.0 5.2 0
assign	(residue 10 and name HE3) (residue 11 and name HA)	6.0 4.2 0
assign	(residue 10 and name HB#) (residue 11 and name HB#)	7.0 5.2 0
assign	(residue 11 and name HB#) (residue 12 and name HB)	6.0 4.2 0
assign	(residue 12 and name HN) (residue 12 and name HB)	6.0 4.2 0
assign	(residue 12 and name HA) (residue 12 and name HB)	3.5 1.7 0
assign	(residue 12 and name HB) (residue 13 and name HN)	5.0 3.2 0
assign	(residue 12 and name HB) (residue 13 and name HA)	6.0 4.2 0
assign	(residue 12 and name HB) (residue 13 and name HB#)	6.0 4.2 0
assign	(residue 12 and name HB) (residue 14 and name HB#)	6.0 4.2 0

TABLE IV
NOES FOR STRUCTURE CALCULATION OF X4-2-1 MONOMER (continued)

assign	(residue 12 and name HB) (residue 18 and name HD1)	7.0 4.2 0
assign	(residue 12 and name HG*) (residue 13 and name HN)	7.0 4.2 0
assign	(residue 13 and name HA) (residue 14 and name HB#)	7.0 5.2 0
assign	(residue 13 and name HB#) (residue 13 and name HN)	6.0 3.5 0
assign	(residue 13 and name HB#) (residue 14 and name HB#)	5.0 3.2 0
assign	(residue 13 and name HB#) (residue 15 and name HB)	6.0 4.2 0
assign	(residue 13 and name HB#) (residue 18 and name HD1)	6.0 4.2 0
assign	(residue 14 and name HN) (residue 14 and name HB#)	6.0 4.2 0
assign	(residue 14 and name HB#) (residue 15 and name HA)	6.0 4.2 0
assign	(residue 14 and name HB#) (residue 15 and name HB)	6.0 4.2 0
assign	(residue 14 and name HB#) (residue 15 and name HN)	6.0 4.2 0
assign	(residue 14 and name HB#) (residue 17 and name HB#)	6.0 4.2 0
assign	(residue 14 and name HB#) (residue 18 and name HD1)	7.0 4.2 0
assign	(residue 14 and name HB#) (residue 18 and name HE3)	7.0 4.2 0
assign	(residue 14 and name HB#) (residue 19 and name HE#)	7.0 4.2 0
assign	(residue 15 and name HA) (residue 16 and name HB#)	7.0 5.2 0
assign	(residue 15 and name HA) (residue 18 and name HB#)	5.0 3.2 0
assign	(residue 15 and name HA) (residue 18 and name HD1)	5.0 3.2 0
assign	(residue 15 and name HA) (residue 18 and name HE3)	6.0 4.2 0
assign	(residue 15 and name HA) (residue 19 and name HD#)	6.0 4.2 0
assign	(residue 15 and name HB) (residue 15 and name HN)	6.0 4.2 0
assign	(residue 15 and name HB) (residue 16 and name HA)	5.0 3.2 0
assign	(residue 15 and name HB) (residue 16 and name HB#)	6.0 4.2 0
assign	(residue 15 and name HB) (residue 16 and name HN)	6.0 4.2 0
assign	(residue 15 and name HB) (residue 18 and name HB#)	7.0 4.2 0
assign	(residue 15 and name HB) (residue 18 and name HD1)	6.0 4.2 0
assign	(residue 15 and name HB) (residue 18 and name HZ2)	6.0 4.2 0
assign	(residue 15 and name HB) (residue 19 and name HD#)	6.0 4.2 0
assign	(residue 15 and name HB) (residue 19 and name HE#)	5.0 3.2 0
assign	(residue 15 and name HG*) (residue 19 and name HE#)	6.0 4.2 0
assign	(residue 16 and name HA) (residue 17 and name HA)	6.0 4.2 0
assign	(residue 16 and name HA) (residue 17 and name HB#)	6.0 4.2 0
assign	(residue 16 and name HB#) (residue 17 and name HB#)	6.0 4.2 0
assign	(residue 16 and name HA) (residue 18 and name HD1)	6.0 4.2 0
assign	(residue 16 and name HB#) (residue 18 and name HE#)	7.5 4.2 0
assign	(residue 16 and name HB#) (residue 19 and name HE#)	7.0 4.2 0
assign	(residue 16 and name HB#) (residue 19 and name HB#)	7.0 4.2 0
assign	(residue 16 and name HB#) (residue 20 and name HE#)	7.0 4.2 0
assign	(residue 16 and name HB#) (residue 21 and name HA#)	7.5 4.2 0
assign	(residue 17 and name HN) (residue 18 and name HN)	5.0 3.2 0

TABLE IV
NOES FOR STRUCTURE CALCULATION OF X4-2-1 MONOMER (continued)

assign	(residue 17 and name HA) (residue 18 and name HD1)	6.0 4.2 0
assign	(residue 17 and name HB#) (residue 18 and name HN)	6.0 4.2 0
assign	(residue 17 and name HB#) (residue 18 and name HA)	6.0 4.2 0
assign	(residue 17 and name HB#) (residue 18 and name HD1)	3.5 1.7 0
assign	(residue 17 and name HB#) (residue 18 and name HE#)	7.0 4.2 0
assign	(residue 17 and name HA) (residue 19 and name HE#)	6.0 4.2 0
assign	(residue 17 and name HB#) (residue 19 and name HE#)	6.0 4.2 0
assign	(residue 18 and name HE3) (residue 18 and name HA)	6.0 4.2 0
assign	(residue 18 and name HE3) (residue 18 and name HB#)	3.5 1.7 0
assign	(residue 18 and name HB#) (residue 19 and name HD#)	6.0 4.2 0
assign	(residue 18 and name HB#) (residue 19 and name HN)	7.0 5.2 0
assign	(residue 18 and name HA) (residue 19 and name HD#)	6.0 4.2 0
assign	(residue 18 and name HA) (residue 19 and name HE#)	6.0 4.2 0
assign	(residue 18 and name HB#) (residue 19 and name HE#)	7.0 4.2 0
assign	(residue 18 and name HE3) (residue 19 and name HB#)	6.0 4.2 0
assign	(residue 18 and name HE3) (residue 19 and name HA)	6.0 4.2 0
assign	(residue 18 and name HZ3) (residue 19 and name HB#)	6.0 4.2 0
assign	(residue 18 and name HD1) (residue 19 and name HE#)	6.0 4.2 0
assign	(residue 18 and name HH2) (residue 19 and name HE#)	6.0 4.2 0
assign	(residue 18 and name HE3) (residue 19 and name HE#)	6.0 4.2 0
assign	(residue 19 and name HN) (residue 19 and name HD#)	7.0 4.2 0
assign	(residue 19 and name HB#) (residue 20 and name HD#)	6.0 4.2 0
assign	(residue 19 and name HD#) (residue 21 and name HA#)	7.0 4.2 0
assign	(residue 19 and name HE#) (residue 20 and name HD#)	6.0 4.2 0
assign	(residue 19 and name HE#) (residue 21 and name HA#)	6.0 4.2 0
assign	(residue 20 and name HA) (residue 20 and name HB#)	2.5 0.7 0
assign	(residue 20 and name HA) (residue 21 and name HA#)	6.0 4.2 0
assign	(residue 20 and name HD#) (residue 21 and name HN)	7.0 5.2 0
assign	(residue 20 and name HD#) (residue 23 and name HB#)	7.0 5.2 0
assign	(residue 21 and name HN) (residue 22 and name HN)	5.0 3.2 0
assign	(residue 21 and name HA#) (residue 22 and name HA)	6.0 4.2 0
assign	(residue 21 and name HA#) (residue 22 and name HB#)	7.0 5.2 0
assign	(residue 1 and name HA) (residue 2 and name HN)	5.0 3.2 0
assign	(residue 3 and name HA) (residue 4 and name HN)	3.5 1.7 0
assign	(residue 4 and name HA) (residue 5 and name HN)	5.0 3.2 0
assign	(residue 5 and name HA) (residue 6 and name HN)	3.5 1.7 0
assign	(residue 6 and name HA) (residue 7 and name HN)	5.0 3.2 0
assign	(residue 8 and name HA) (residue 9 and name HN)	3.5 1.7 0
assign	(residue 9 and name HA) (residue 10 and name HN)	5.0 3.2 0
assign	(residue 11 and name HA) (residue 12 and name HN)	5.0 3.2 0

TABLE IV
NOES FOR STRUCTURE CALCULATION OF X4-2-1 MONOMER (continued)

assign	(residue 12 and name HA) (residue 13 and name HN)	5.0 3.2 0
assign	(residue 13 and name HA) (residue 14 and name HN)	5.0 3.2 0
assign	(residue 15 and name HA) (residue 16 and name HN)	5.0 3.2 0
assign	(residue 16 and name HA) (residue 17 and name HN)	5.0 3.2 0
assign	(residue 17 and name HA) (residue 18 and name HN)	5.0 3.2 0
assign	(residue 18 and name HA) (residue 19 and name HN)	5.0 3.2 0
assign	(residue 19 and name HA) (residue 20 and name HN)	5.0 3.2 0
assign	(residue 20 and name HA) (residue 21 and name HN)	5.0 3.2 0
assign	(residue 21 and name HA#) (residue 22 and name HN)	6.0 4.2 0
assign	(residue 22 and name HA) (residue 23 and name HN)	5.0 3.2 0

TABLE IV
NOES FOR STRUCTURE CALCULATION OF X4-2-9 MONOMER

assign	(residue 3 and name ha) (residue 4 and name hn)	3.0 1.2 0.5
assign	(residue 4 and name ha) (residue 5 and name hn)	3.0 1.2 0.5
assign	(residue 5 and name ha) (residue 6 and name hn)	3.0 1.2 0.5
assign	(residue 6 and name ha) (residue 7 and name hn)	3.5 1.7 0.0
assign	(residue 8 and name ha) (residue 9 and name hn)	3.5 1.2 0.5
assign	(residue 9 and name ha) (residue 10 and name hn)	3.0 1.2 0.5
assign	(residue 10 and name ha) (residue 11 and name hn)	3.0 1.2 0.5
assign	(residue 11 and name ha) (residue 12 and name hn)	3.0 1.2 0.5
assign	(residue 12 and name ha) (residue 13 and name hn)	2.5 0.2 0.5
assign	(residue 14 and name ha) (residue 15 and name hn)	3.0 1.2 0.5
assign	(residue 15 and name ha) (residue 16 and name hn)	2.0 0.2 0.5
assign	(residue 16 and name ha) (residue 17 and name hn)	2.0 0.2 0.5
assign	(residue 17 and name ha) (residue 18 and name hn)	3.0 1.2 0.5
assign	(residue 18 and name ha) (residue 19 and name hn)	2.5 0.2 0.5
assign	(residue 19 and name ha) (residue 20 and name hn)	3.0 1.2 0.5
assign	(residue 20 and name ha) (residue 21 and name hn)	3.0 1.2 0.5
assign	(residue 21 and name ha#) (residue 22 and name hn)	3.0 1.2 0.5
assign	(residue 22 and name ha) (residue 23 and name hn)	3.5 1.2 0.0
assign	(residue 23 and name ha) (residue 24 and name hn)	3.0 1.2 0.5
assign	(residue 6 and name hn) (residue 7 and name hn)	3.0 1.2 0.5
assign	(residue 9 and name hn) (residue 10 and name hn)	3.0 1.2 0.5
assign	(residue 10 and name hn) (residue 11 and name hn)	3.0 1.2 1.0
assign	(residue 11 and name hn) (residue 12 and name hn)	3.5 1.7 0.0
assign	(residue 12 and name hn) (residue 13 and name hn)	3.5 1.7 0.0
assign	(residue 13 and name hn) (residue 14 and name hn)	3.5 1.7 0.0
assign	(residue 14 and name hn) (residue 15 and name hn)	3.0 1.2 0.5
assign	(residue 15 and name hn) (residue 16 and name hn)	3.5 1.7 0.5
assign	(residue 16 and name hn) (residue 17 and name hn)	5.0 3.2 0.0
assign	(residue 17 and name hn) (residue 18 and name hn)	5.0 3.2 0.0
assign	(residue 18 and name hn) (residue 19 and name hn)	3.0 1.2 0.5
assign	(residue 19 and name hn) (residue 20 and name hn)	3.0 1.2 1.0
assign	(residue 20 and name hn) (residue 21 and name hn)	3.0 1.2 1.0
assign	(residue 21 and name hn) (residue 22 and name hn)	3.0 1.2 0.5
assign	(residue 22 and name hn) (residue 23 and name hn)	5.0 3.2 0.0
assign	(residue 3 and name ht1) (residue 4 and name hn)	5.0 3.2 0.0
assign	(residue 3 and name ht1) (residue 19 and name oh)	5.0 3.2 1.0
assign	(residue 3 and name ht1) (residue 22 and name ha)	5.0 3.2 1.0
assign	(residue 3 and name ha) (residue 4 and name ha)	5.0 3.2 0.0
assign	(residue 3 and name ha) (residue 19 and name oh)	5.0 3.2 1.5

TABLE IV
NOES FOR STRUCTURE CALCULATION OF X4-2-9 MONOMER (continued)

assign	(residue 3 and name ha) (residue 5 and name hd#)	5.0 3.2 0
assign	(residue 3 and name hd#) (residue 4 and name hb)	7.0 4.2 0.5
assign	(residue 3 and name hd#) (residue 5 and name hg1*)	7.0 4.2 0.0
assign	(residue 3 and name he#) (residue 5 and name hg1*)	7.0 4.2 0.0
assign	(residue 3 and name he#) (residue 5 and name hd#)	7.0 4.2 0.0
assign	(residue 4 and name hn) (residue 5 and name hn)	5.0 3.2 0.0
assign	(residue 4 and name hn) (residue 19 and name oh)	5.0 3.2 1.0
assign	(residue 4 and name hn) (residue 21 and name ha*)	7.0 5.2 0.0
assign	(residue 4 and name hn) (residue 21 and name hn)	5.0 3.2 1.5
assign	(residue 4 and name hn) (residue 22 and name hn)	5.0 3.2 1.5
assign	(residue 4 and name ha) (residue 19 and name he#)	6.0 4.2 0.0
assign	(residue 4 and name hb) (residue 5 and name hn)	3.0 1.2 0.5
assign	(residue 4 and name hg#) (residue 6 and name hg2#)	7.0 5.2 0.3
assign	(residue 5 and name hn) (residue 6 and name hg2#)	7.0 4.2 0.0
assign	(residue 5 and name hn) (residue 6 and name hn)	3.0 1.2 0.5
assign	(residue 5 and name ha) (residue 7 and name hn)	5.0 3.2 1.0
assign	(residue 5 and name hb) (residue 7 and name hn)	5.0 3.2 0.5
assign	(residue 5 and name ha) (residue 17 and name hd21)	5.0 3.2 1.0
assign	(residue 5 and name hg2#) (residue 6 and name hn)	5.5 3.2 0.0
assign	(residue 5 and name hg1#) (residue 6 and name hn)	7.0 4.2 0.0
assign	(residue 6 and name hn) (residue 6 and name hg2*)	5.0 3.2 0.0
assign	(residue 6 and name hn) (residue 7 and name hb#)	5.0 3.2 0.0
assign	(residue 6 and name hn) (residue 7 and name hg)	5.0 3.2 0.0
assign	(residue 6 and name ha) (residue 7 and name hb#)	5.0 3.2 0.0
assign	(residue 6 and name ha) (residue 7 and name hg)	5.0 3.2 0.0
assign	(residue 6 and name ha) (residue 7 and name hd#)	7.0 5.2 0.0
assign	(residue 6 and name hb) (residue 7 and name hb#)	5.0 3.2 1.5
assign	(residue 6 and name hb) (residue 7 and name hg)	5.0 4.2 1.0
assign	(residue 6 and name hg1) (residue 7 and name hn)	5.0 3.2 0.0
assign	(residue 6 and name hg1) (residue 7 and name hb#)	7.0 3.2 0.0
assign	(residue 6 and name hg2#) (residue 7 and name hn)	7.0 4.2 0.0
assign	(residue 6 and name hg2#) (residue 7 and name hg)	5.0 3.2 1.0
assign	(residue 6 and name hg2#) (residue 9 and name hz)	7.0 3.2 0.0
assign	(residue 6 and name hg2#) (residue 9 and name hd#)	7.0 3.2 0.0
assign	(residue 6 and name hg2#) (residue 9 and name he#)	7.0 3.2 0.0
assign	(residue 6 and name hg2#) (residue 9 and name hn)	5.0 3.2 1.0
assign	(residue 6 and name hg2#) (residue 10 and name hd1)	7.0 3.2 0.0
assign	(residue 6 and name ha) (residue 17 and name hd21)	5.0 3.2 1.0
assign	(residue 6 and name hb) (residue 17 and name ha)	5.0 3.2 1.0
assign	(residue 7 and name hb#) (residue 8 and name hd#)	5.0 3.2 1.0

TABLE IV
NOES FOR STRUCTURE CALCULATION OF X4-2-9 MONOMER (continued

assign	(residue 7 and name hb#) (residue 9 and name hn)	5.0 3.2 1.0
assign	(residue 7 and name hb#) (residue 9 and name hb#)	5.0 3.2 1.0
assign	(residue 7 and name hb#) (residue 9 and name hd#)	5.0 3.2 1.0
assign	(residue 7 and name hb#) (residue 9 and name he#)	5.0 3.2 1.0
assign	(residue 7 and name hb#) (residue 10 and name hb#)	7.0 3.2 0
assign	(residue 7 and name hd#) (residue 8 and name hb#)	7.0 3.2 0.5
assign	(residue 7 and name hd#) (residue 10 and name he1)	7.0 3.2 0.5
assign	(residue 7 and name hn) (residue 17 and name hd21)	6.0 3.2 0.0
assign	(residue 8 and name ha) (residue 9 and name hb#)	5.0 3.2 0.0
assign	(residue 8 and name ha) (residue 9 and name hd#)	5.0 3.2 0
assign	(residue 8 and name ha) (residue 10 and name hn)	5.0 3.2 0.0
assign	(residue 8 and name ha) (residue 10 and name ha)	5.0 3.2 0.0
assign	(residue 8 and name ha) (residue 10 and name he1)	7.0 3.2 0.0
assign	(residue 8 and name hb#) (residue 9 and name hn)	5.0 3.2 1.0
assign	(residue 8 and name hb#) (residue 9 and name hd#)	5.0 3.2 1.0
assign	(residue 8 and name hb#) (residue 10 and name hn)	5.0 3.2 1.0
assign	(residue 8 and name hb#) (residue 10 and name hd1)	5.0 3.2 1.0
assign	(residue 8 and name hb#) (residue 10 and name he1)	5.0 3.2 1.0
assign	(residue 8 and name hg#) (residue 9 and name hd#)	5.0 3.2 1.0
assign	(residue 8 and name hg#) (residue 9 and name hn)	5.0 3.2 1.0
assign	(residue 8 and name hg#) (residue 10 and name ha)	5.0 5.2 0.0
assign	(residue 8 and name hg#) (residue 10 and name hn)	7.0 5.2 0.0
assign	(residue 8 and name hg#) (residue 10 and name he1)	5.0 3.2 1.0
assign	(residue 9 and name hn) (residue 11 and name hb#)	7.0 4.2 0.0
assign	(residue 9 and name hn) (residue 10 and name he1)	7.0 5.2 0.0
assign	(residue 9 and name ha) (residue 10 and name hb#)	5.0 3.2 1.0
assign	(residue 9 and name ha) (residue 10 and name he1)	5.0 3.2 1.0
assign	(residue 9 and name hb#) (residue 10 and name hn)	3.5 1.2 0.5
assign	(residue 9 and name hd#) (residue 11 and name hb#)	5.0 3.2 1.0
assign	(residue 9 and name he#) (residue 11 and name hb#)	5.0 3.2 1.0
assign	(residue 9 and name hd#) (residue 11 and name hn)	5.0 3.2 1.0
assign	(residue 9 and name hd#) (residue 12 and name hg*)	7.0 5.2 0.0
assign	(residue 9 and name hd#) (residue 12 and name hb)	7.0 5.2 0.0
assign	(residue 10 and name hn) (residue 10 and name he1)	5.0 3.2 0.0
assign	(residue 10 and name hb#) (residue 10 and name hn)	3.0 1.2 0.5
assign	(residue 10 and name hb#) (residue 10 and name he3)	3.0 1.2 0.5
assign	(residue 10 and name hb#) (residue 11 and name hb*)	5.0 3.2 1.0
assign	(residue 10 and name hb#) (residue 12 and name hn)	5.0 3.2 1.0
assign	(residue 10 and name hb#) (residue 12 and name hg#)	5.0 3.2 1.0
assign	(residue 10 and name hd1) (residue 12 and name hn)	5.0 3.2 1.0

TABLE IV
NOES FOR STRUCTURE CALCULATION OF X4-2-9 MONOMER (continued

assign	(residue 10 and name he1) (residue 11 and name hn)	5.0 3.2 1.0
assign	(residue 10 and name he1) (residue 12 and name hg#)	7.0 5.2 0.0
assign	(residue 10 and name he3) (residue 11 and name ha)	5.0 3.2 1.0
assign	(residue 10 and name he3) (residue 11 and name hb#)	7.0 3.2 0.0
assign	(residue 10 and name he3) (residue 12 and name hg#)	5.0 3.2 1.0
assign	(residue 10 and name he3) (residue 12 and name hn)	5.0 3.2 1.0
assign	(residue 10 and name hz3) (residue 11 and name hb#)	5.0 3.2 1.0
assign	(residue 11 and name hN) (residue 13 and name hn)	5.0 3.2 1.0
assign	(residue 11 and name hb#) (residue 13 and name hn)	6.0 3.2 1.0
assign	(residue 12 and name hn) (residue 13 and name hb#)	5.0 3.2 1.0
assign	(residue 12 and name ha) (residue 14 and name hn)	5.0 3.2 0
assign	(residue 12 and name hb) (residue 13 and name hn)	3.5 1.2 0.0
assign	(residue 12 and name hb) (residue 13 and name ha)	3.0 1.2 1.5
assign	(residue 12 and name hb) (residue 13 and name hb#)	5.0 3.2 1.0
assign	(residue 12 and name hb) (residue 14 and name hb#)	5.0 3.2 1.0
assign	(residue 12 and name hb) (residue 14 and name hn)	5.0 3.2 1.0
assign	(residue 12 and name hg#) (residue 13 and name hn)	6.0 4.2 0.0
assign	(residue 13 and name hn) (residue 14 and name hb#)	6.0 3.2 1.0
assign	(residue 13 and name hn) (residue 15 and name hb)	5.0 3.2 1.0
assign	(residue 13 and name ha) (residue 14 and name hb#)	5.0 3.2 1.0
assign	(residue 13 and name ha) (residue 15 and name hn)	5.0 3.2 0.0
assign	(residue 13 and name hb#) (residue 14 and name hn)	3.0 1.2 0.5
assign	(residue 13 and name hb#) (residue 14 and name hb#)	5.0 3.2 1.5
assign	(residue 13 and name hb#) (residue 15 and name hn)	5.0 3.2 1.0
assign	(residue 14 and name ha) (residue 15 and name ha)	5.0 3.2 1.0
assign	(residue 14 and name ha) (residue 15 and name hg#)	5.0 3.2 1.0
assign	(residue 14 and name ha) (residue 16 and name ha)	5.0 3.2 1.0
assign	(residue 14 and name ha) (residue 16 and name hn)	5.0 3.2 1.0
assign	(residue 14 and name ha) (residue 16 and name hb#)	5.0 3.2 1.0
assign	(residue 14 and name hb#) (residue 15 and name hg#)	7.0 5.2 0.0
assign	(residue 14 and name hb#) (residue 16 and name hn)	7.0 5.2 0.0
assign	(residue 15 and name hn) (residue 16 and name hb#)	7.0 3.2 0.0
assign	(residue 15 and name hb) (residue 16 and name hb#)	7.0 3.2 0.0
assign	(residue 15 and name hb) (residue 17 and name hn)	5.0 3.2 1.0
assign	(residue 15 and name hb) (residue 18 and name hd1)	5.0 3.2 1.2
assign	(residue 15 and name hg#) (residue 18 and name hd1)	5.0 3.2 1.0
assign	(residue 15 and name hg#) (residue 18 and name he1)	7.0 5.2 1.0
assign	(residue 15 and name hg#) (residue 18 and name he1)	7.0 5.2 0.0
assign	(residue 15 and name hg#) (residue 18 and name hz2)	7.0 5.2 0.0
assign	(residue 15 and name hg#) (residue 18 and name hh2)	7.0 5.2 0.0

TABLE IV
NOES FOR STRUCTURE CALCULATION OF X4-2-9 MONOMER (continued

assign	(residue 15 and name hg#) (residue 19 and name he#)	7.0 5.2 0.0
assign	(residue 16 and name hn) (residue 18 and name he1)	5.0 3.2 1.5
assign	(residue 16 and name ha) (residue 17 and name hb#)	3.0 1.2 0.8
assign	(residue 16 and name hb#) (residue 17 and name hb#)	5.0 3.2 1.0
assign	(residue 16 and name ha) (residue 18 and name he1)	5.0 3.2 0.5
assign	(residue 16 and name ha) (residue 18 and name hn)	5.0 3.2 0.5
assign	(residue 16 and name hb#) (residue 18 and name hb#)	5.0 3.2 1.0
assign	(residue 16 and name hb#) (residue 18 and name hd1)	5.0 3.2 0.0
assign	(residue 16 and name hb#) (residue 18 and name hz2)	6.0 4.2 0.0
assign	(residue 16 and name hb#) (residue 18 and name he1)	7.0 5.2 0.0
assign	(residue 16 and name hb#) (residue 18 and name hn)	3.0 1.2 0.5
assign	(residue 16 and name hb#) (residue 17 and name hd#)	7.0 5.2 0.0
assign	(residue 16 and name hb#) (residue 18 and name he3)	7.0 5.2 0.0
assign	(residue 16 and name hb#) (residue 19 and name ha)	7.0 5.2 0.0
assign	(residue 16 and name hb#) (residue 19 and name hd#)	7.0 5.2 0.0
assign	(residue 16 and name hb#) (residue 20 and name hd#)	7.0 5.2 0.0
assign	(residue 17 and name hn) (residue 18 and name he1)	5.0 3.2 1.0
assign	(residue 17 and name ha) (residue 18 and name hd1)	5.0 3.2 1.0
assign	(residue 17 and name ha) (residue 18 and name he1)	5.0 3.2 0.0
assign	(residue 17 and name ha) (residue 19 and name hn)	5.0 3.2 0.0
assign	(residue 17 and name ha) (residue 19 and name hd#)	5.0 3.2 0.0
assign	(residue 17 and name hb#) (residue 19 and name hd#)	5.0 3.2 1.0
assign	(residue 17 and name hb#) (residue 20 and name hn)	5.0 3.2 1.0
assign	(residue 17 and name hb#) (residue 20 and name hd#)	5.0 3.2 1.0
assign	(residue 17 and name hd22) (residue 18 and name hn)	5.0 3.2 0.0
assign	(residue 17 and name hd22) (residue 19 and name hn)	5.0 3.2 0.0
assign	(residue 18 and name hn) (residue 18 and name he1)	5.0 3.2 1.0
assign	(residue 18 and name hn) (residue 20 and name hb#)	5.0 3.2 1.0
assign	(residue 18 and name hn) (residue 20 and name hn)	5.0 3.2 1.0
assign	(residue 18 and name ha) (residue 18 and name hd1)	3.5 1.2 0.5
assign	(residue 18 and name hb#) (residue 19 and name hd#)	5.0 3.2 1.0
assign	(residue 18 and name hb#) (residue 20 and name hd#)	5.0 3.2 1.0
assign	(residue 18 and name hb#) (residue 20 and name hn)	5.0 3.2 0.0
assign	(residue 18 and name hd1) (residue 19 and name hn)	5.0 3.2 0.0
assign	(residue 18 and name he1) (residue 19 and name hn)	5.0 3.2 1.0
assign	(residue 18 and name he1) (residue 20 and name hn)	7.0 3.2 0.0
assign	(residue 18 and name he3) (residue 19 and name hb#)	7.0 3.2 0.0
assign	(residue 18 and name he3) (residue 20 and name hn)	5.0 3.2 1.0
assign	(residue 18 and name he3) (residue 22 and name hd21)	5.0 3.2 1.0
assign	(residue 19 and name ha) (residue 19 and name he#)	6.0 4.2 0.5

TABLE IV
NOES FOR STRUCTURE CALCULATION OF X4-2-9 MONOMER (continued

assign	(residue 19 and name hb#) (residue 20 and name hn)	5.0 3.2 1.0
assign	(residue 19 and name hb#) (residue 20 and name hd#)	7.0 3.2 0.0
assign	(residue 19 and name hb#) (residue 21 and name hn)	5.0 3.2 1.0
assign	(residue 19 and name hd#) (residue 20 and name hb#)	5.0 3.2 1.0
assign	(residue 19 and name hd#) (residue 20 and name hn)	5.0 3.2 0.0
assign	(residue 19 and name hd#) (residue 21 and name ha#)	7.0 3.2 0.0
assign	(residue 19 and name he#) (residue 21 and name ha#)	7.0 3.2 0.0
assign	(residue 20 and name hn) (residue 21 and name ha#)	5.0 3.2 1.0
assign	(residue 20 and name hn) (residue 20 and name hb#)	3.0 1.2 0.5
assign	(residue 20 and name hd#) (residue 21 and name ha#)	5.0 3.2 1.0
assign	(residue 21 and name ha#) (residue 22 and name ha)	5.0 3.2 1.0
assign	(residue 21 and name ha#) (residue 22 and name hb#)	5.0 3.2 1.0
assign	(residue 21 and name ha#) (residue 22 and name hd21)	5.0 3.2 1.0
assign	(residue 21 and name ha#) (residue 23 and name hn)	5.0 3.2 1.0
assign	(residue 22 and name ha) (residue 23 and name ha)	5.0 3.2 0.0
assign	(residue 22 and name hd21) (residue 23 and name hn)	5.0 3.2 1.0
assign	(residue 22 and name hd21) (residue 24 and name hn)	5.0 3.2 1.0

TABLE VI
DYNAMIC SCATTERING RESULTS FOR PEPTIDE DERIVATIVES

Peptide	Structure	Particle hydrodynamic radii, nm* (population weight fraction)	Percentage polydispersity¶
X4-2-1	LLFVITLPFWAVDAVANWYFGNDD-OH	**6.0 (87.3%) 22.4 (12.1%)**	**6.7 16.1**
X4-2-2	LLFVITLPFWAVDAVANWYFGNKK-NH_2	**66.5 (100%)**	**68.7**
X4-2-3	LLFVITLPFWAVDAVANWYFGN-OH	**92.2 (100%)**	**19.5**
X4-2-5	LLFVITLPFWAVDAVANWYFGNDD-$(CH_2CH_2O)_{11}$-NH_2	**5.5 (100%)**	**26.2**
X4-2-6	LLFVITLPFWAVDAVANWYFGN-$(CH_2CH_2O)_{27}$-NH_2	**5.5 (99.9%)**	**8.5**
X4-2-8	LLFVITLPFWAVDAVANWYFGNDD-$(CH_2CH_2O)_{27}$-NH_2	**n/a**	
X4-2-9	AAVANWYFGNDD-$(CH_2CH_2O)_{11}$-NH_2	**11.1 (97.4%) 62.8 (2.5%)**	**16.9 19.5**
X4-2-11	LLFVITLPFWAVDAVANWYFGNDD-$(CH_2CH_2O)_{27}$-CO-NH- $(CH_2CH_2O)_{11}$-NH_2	**5.6 (99.9%)**	**16.5**

*The particle hydrodynamic radii were determined from DLS. The data presented is for 0.4 mg⁄Ml solutions of peptides in PBS containing 1.25% (v⁄v) DMSO. Dynamics 6.7.7.9 software (Wyatt Technologies) was used to calculate molecular weight from the size data. The calculation was based on a globular protein model. Comparison of the calculated apparent molecular weight with the weight of the monomer provided the apparent number of peptide molecules per particle.

¶Percentage polydispersity reflects the homogeneity of the nanoparticles. It is defined as a standard deviation of the size divided by the mean radius multiplied by 100%.

VITA

NAME Youngshim Lee

EDUCATION

Doctor of Philosophy, 2012
Department of Biochemistry and Molecular Genetics
University of Illinois at Chicago, USA

Master of Science, 2006
Department of Applied Biology & Science
Konkuk University, Seoul, Korea

Bachelor of Science, 2004
Department of Applied Biology & Science
Konkuk University, Seoul, Korea

PUBLICATIONS

The structure of monomeric components of self-assembling CXCR4 antagonists determines the architecture of resulting nanostructures.
Lee Y, Chen Y, Tarasova NI, Gaponenko V.
Nanotechnology 2011 22(50):505101

The Use of Reductive Methylation of Lysine Residues to Study Protein-Protein Interactions in High Molecular Weight Complexes by Solution NMR.
Lee Y, Abraham SJ, Gaponenko V.
Protein Interaction / Book 1, ISBN 979-953-307-577-7, InTech. in press

Structural plasticity of a transmembrane peptide allows self-assembly into biologically active nanoparticles.
Tarasov SG, Gaponenko V, Howard OM, Chen Y, Oppenheim JJ, Dyba MA, Subramaniam S**, Lee Y**, Michejda C, Tarasova NI.
Proc Natl Acad Sci U S A. 2011. 108(24):9798-803

Characterization of an O-methyltransferase from *Streptomyces avermitilis* MA-4680.
Yoon Y, Park Y, **Lee Y**, Yi YS, Jo G, Park JC, Ahn JH, Lim Y.
J Microbiol Biotechnol. 2010. 20(9):1359-66.

Complete assignments of NMR data of 13 hydroxymethoxyflavones.
Park Y, Moon BH, Yang H, **Lee Y**, Lee E, Lim Y.
Magn Reson Chem. 2007. 45(12):1072-5.

1H and 13C-NMR data of hydroxyflavone derivatives.

Park Y, Moon BH, Lee E, **Lee Y**, Yoon Y, Ahn JH, Lim Y.
Magn Reson Chem. 2007. 45(8):674-9.

Production of three O-methhylated esculetins with *Escherichia coli* expressing O-methyltransferase from poplar.
Kim BG, **Lee Y**, Hur HG, Lim Y, Ahn JH.
Biosci Biotechnol Biochem. 2006. 70(5):1269-72.

Regiospecific flavonoid 7-O-methylation with *Streptomyces avermitilis* O-methyltransferase expressed in *Escherichia coli*.
Kim BG, Jung BR, **Lee Y**, Hur HG, Lim Y, Ahn JH.
J Agric Food Chem. 2006. 54(3):823-8.

Flavonoid 3'-O-methyltransferase from rice: cDNA cloning, characterization and functional expression.
Kim BG, **Lee Y**, Hur HG, Lim Y, Ahn JH.
Phytochemistry. 2006. 67(4):387-94.

Complete assignment of (1)H and (13)C NMR data of dihydroxyflavone derivatives.
Lee Y, Moon BH, Ahn JH, Lim Y.
Magn Reson Chem. 2006. 44(1):99-101.

Multiple regiospecific methylations of a flavonoid by plant O-methyltransferases expressed in *E. coli*.
Kim BG, Shin KH, **Lee Y**, Hur HG, Lim Y, Ahn JH.
Biotechnol Lett. 2005. 27(23-24):1861-4.

Complete assignment of 1H and 13C NMR data of some flavonol derivatives.
Lee Y, Moon BH, Ahn JH, Lim Y.
Magn Reson Chem. 2005. 43(10):858-60.

Regiospecific methylation of naringenin to ponciretin by soybean O-methyltransferase expressed in *Escherichia coli*.
Kim DH, Kim BG, **Lee Y**, Ryu JY, Lim Y, Hur HG, Ahn JH.
J Biotechnol. 2005. 119(2):155-62.

Characterization of O-methyltransferase ScOMT1 cloned from *Streptomyces coelicolor A3(2)*.
Yoon Y, Yi YS, **Lee Y**, Kim S, Kim BG, Ahn JH, Lim Y.
Biochim Biophys Acta. 2005. 1730(2):85-95.

Identification of syn- and anti-anethole-2,3-epoxides in the metabolism of trans-anethole by the newly isolated bacterium *Pseudomonas putida* JYR-1.

Ryu J, Seo J, **Lee Y**, Lim Y, Ahn JH, Hur HG.
J Agric Food Chem. 2005. 53(15):5954-8